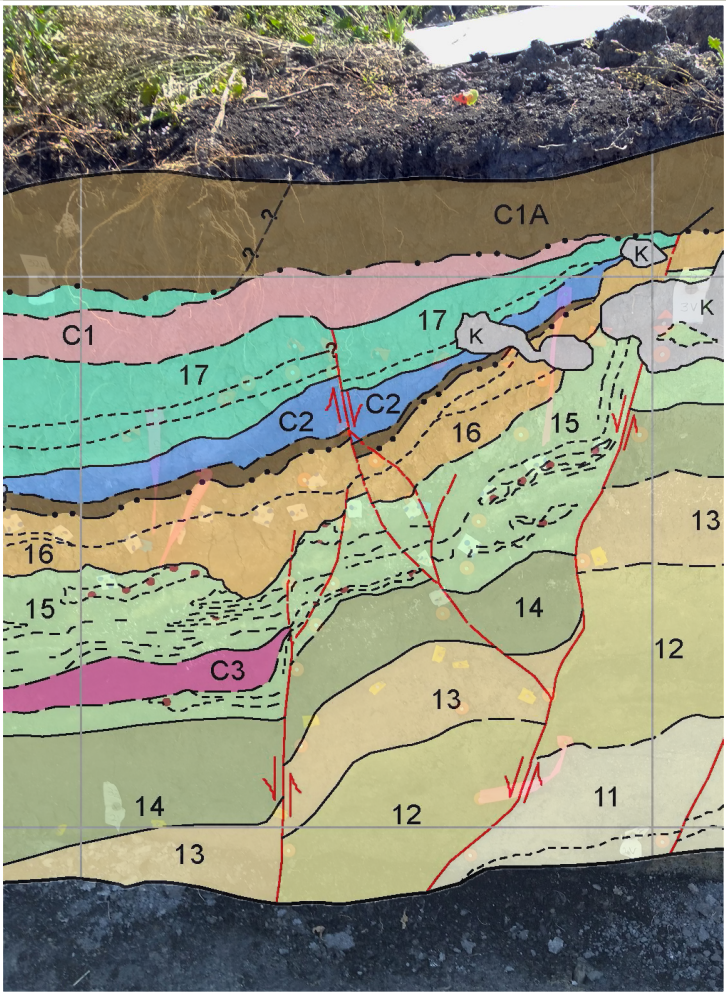


# PALEOSEISMIC INVESTIGATION OF THE TAYLORSVILLE FAULT AT THE AIRPORT EAST SITE, WEST VALLEY FAULT ZONE, SALT LAKE COUNTY, UTAH

*Michael D. Hylland, Adam I. Hiscock, Greg N. McDonald, Christopher B. DuRoss, Shannon A. Mahan, Richard W. Briggs, Stephen F. Personius, and Nadine G. Reitman*



**SPECIAL STUDY 169**  
**UTAH GEOLOGICAL SURVEY**  
UTAH DEPARTMENT OF NATURAL RESOURCES  
**2022**

*Blank pages are intentional for printing purposes.*

# PALEOSEISMIC INVESTIGATION OF THE TAYLORSVILLE FAULT AT THE AIRPORT EAST SITE, WEST VALLEY FAULT ZONE, SALT LAKE COUNTY, UTAH

by

Michael D. Hylland<sup>1</sup>, Adam I. Hiscock<sup>1</sup>, Greg N. McDonald<sup>1</sup>, Christopher B. DuRoss<sup>2</sup>,  
Shannon A. Mahan<sup>3</sup>, Richard W. Briggs<sup>2</sup>, Stephen F. Personius<sup>4</sup>, and Nadine G. Reitman<sup>2</sup>

<sup>1</sup> Utah Geological Survey, Salt Lake City, Utah

<sup>2</sup> U.S. Geological Survey, Golden, Colorado

<sup>3</sup> U.S. Geological Survey, Lakewood, Colorado

<sup>4</sup> U.S. Geological Survey, retired

**Cover image:** Trench exposure and log interpretation of the Taylorsville fault at the Airport East site (south wall of South trench; large white markers on photo indicate corners of 1-meter square grid). See plate 1 for complete trench log.

Suggested citation:

Hylland, M.D., Hiscock, A.I., McDonald, G.N., DuRoss, C.B., Mahan, S.A., Briggs, R.W., Personius, S.F., and Reitman, N.G., 2022, Paleoseismic investigation of the Taylorsville fault at the Airport East site, West Valley fault zone, Salt Lake County, Utah: Utah Geological Survey Special Study 169, 29 p., 2 plates, 7 appendices, <https://doi.org/10.34191/SS-169>.



**SPECIAL STUDY 169**  
**UTAH GEOLOGICAL SURVEY**  
UTAH DEPARTMENT OF NATURAL RESOURCES  
**2022**



**STATE OF UTAH**  
Spencer J. Cox, Governor

**DEPARTMENT OF NATURAL RESOURCES**  
Brian C. Steed, Executive Director

**UTAH GEOLOGICAL SURVEY**  
R. William Keach II, Director

**PUBLICATIONS**

contact

Natural Resources Map & Bookstore  
1594 W. North Temple  
Salt Lake City, UT 84116  
telephone: 801-537-3320  
toll-free: 1-888-UTAH MAP  
website: [utahmapstore.com](http://utahmapstore.com)  
email: [geostore@utah.gov](mailto:geostore@utah.gov)

**UTAH GEOLOGICAL SURVEY**  
contact

1594 W. North Temple, Suite 3110  
Salt Lake City, UT 84116  
telephone: 801-537-3300  
website: [geology.utah.gov](http://geology.utah.gov)

*Although this product represents the work of professional scientists, the Utah Department of Natural Resources, Utah Geological Survey, makes no warranty, expressed or implied, regarding its suitability for a particular use. The Utah Department of Natural Resources, Utah Geological Survey, shall not be liable under any circumstances for any direct, indirect, special, incidental, or consequential damages with respect to claims by users of this product.*

*The Utah Geological Survey does not endorse any products or manufacturers. Reference to any specific commercial product, process, service, or company by trade name, trademark, or otherwise, does not constitute endorsement or recommendation by the Utah Geological Survey. Any use of trade, firm, or product names is for descriptive purposes only and does not imply endorsement by the U.S. Government.*

*Research supported by the U.S. Geological Survey (USGS), Department of the Interior, under USGS award number G15AP00117.*

## FOREWORD

The Paleoseismology of Utah series makes the results of paleoseismic investigations in Utah available to geoscientists, engineers, planners, government officials, and the public. These studies provide critical information regarding paleoearthquake parameters such as earthquake timing, recurrence, displacement, slip rate, fault geometry, and segmentation, which can be used to characterize potential seismic sources and evaluate the long-term seismic hazard of Utah's Quaternary faults.

This Utah Geological Survey Special Study, number 29 in the Paleoseismology of Utah series, presents the results of a paleoseismic trench investigation conducted at the Airport East site on the Taylorsville fault of the West Valley fault zone in Salt Lake Valley, Utah. The West Valley fault zone, comprising the Taylorsville fault and subparallel Granger fault, is antithetic to the Salt Lake City segment of the Wasatch fault zone and together bound an intrabasin graben in northern Salt Lake Valley. Despite significant progress in understanding earthquake hazards along the Wasatch Front, the relation of Holocene earthquakes on the West Valley fault zone and the Salt Lake City and nearby Weber segments of the Wasatch fault zone is poorly understood.

This paleoseismic investigation provides new data on earthquake timing, recurrence, and fault displacement that add to the earthquake chronologies of the Taylorsville fault and the West Valley fault zone as a whole. The new data also provide additional insight into the seismogenic relation of the West Valley and Wasatch fault zones. The results can be summarized by two general conclusions: (1) The paleoseismic data indicate the various strands of the West Valley fault zone often do not move synchronously with each other, but rather it is more likely that different strands move during different West Valley fault zone surface-faulting earthquake events. (2) A significant correlation of mean earthquake times between the West Valley fault zone and Salt Lake City segment of the Wasatch fault zone supports the idea that, more often than not, some part of the West Valley fault zone moves in response to, and possibly synchronously with, slip on the Wasatch fault zone.

Fieldwork for this investigation was completed in 2015 and preliminary results were released in a Final Technical Report for the U.S. Geological Survey in 2017. As the current manuscript was being prepared for formal publication, Salt Lake Valley was shaken by the  $M_w$  5.7 Magna earthquake on March 18, 2020. The epicenter of this earthquake was only about 12 km west of the Airport East site. Subsequent investigations interpreted the earthquake as having resulted from slip on a low-angle part of the Warm Springs fault strand of the Salt Lake City segment of the Wasatch fault zone (see figure 3 in this report), and the University of Utah Seismograph Stations documented a distinct zone of aftershocks occurring within the West Valley fault zone. The seismicity data from the Magna earthquake lend support to the paleoseismic evidence for a kinematic relation between the West Valley fault zone and Wasatch fault zone, and together the two datasets are helping to refine models of earthquake hazard and risk in Salt Lake Valley.

*William Lund*

*Editor, Paleoseismology of Utah Series*

## PALEOSEISMOLOGY OF UTAH SERIES PUBLICATIONS

Utah Geological Survey publications released as part of the Paleoseismology of Utah series may be found online at <https://geology.utah.gov/hazards/info/paleoseismology>.

1. Fault behavior and earthquake recurrence on the Provo segment of the Wasatch fault zone at Mapleton, Utah County, Utah—Paleoseismology of Utah, Volume 1, 1991, by Lund, W.R., Schwartz, D.P., Mulvey, W.E., Budding, K.E., and Black, B.D.: Utah Geological Survey Special Study 75, 41 p.
2. Paleoseismic analysis of the Wasatch fault zone at the Brigham City trench site, Brigham City, Utah, and the Pole Patch trench site, Pleasant View, Utah—Paleoseismology of Utah, Volume 2, 1991, by Personius, S.F.: Utah Geological Survey Special Study 76, 39 p.
3. The number and timing of paleoseismic events on the Nephi and Levan segments, Wasatch fault zone, Utah—Paleoseismology of Utah, Volume 3, 1991, by Jackson, M.: Utah Geological Survey Special Study 78, 23 p., 3 plates.
4. Seismotectonics of north-central Utah and southwestern Wyoming—Paleoseismology of Utah, Volume 4, 1994, by West, M.W.: Utah Geological Survey Special Study 82, 93 p., 5 plates, scale 1:100,000.
5. Neotectonic deformation along the East Cache fault zone, Cache County, Utah—Paleoseismology of Utah, Volume 5, 1994, by McCalpin, J.P.: Utah Geological Survey Special Study 83, 37 p.
6. The Oquirrh fault zone, Tooele County, Utah—surficial geology and paleoseismicity—Paleoseismology of Utah, Volume 6, 1996, by Lund, W.R., editor: Utah Geological Survey Special Study 88, 64 p., 2 plates, scale 1:24,000.
7. Paleoseismic investigation on the Salt Lake City segment of the Wasatch fault zone at the South Fork Dry Creek and Dry Gulch sites, Salt Lake County, Utah—Paleoseismology of Utah, Volume 7, 1996, by Black, B.D., Lund, W.R., Schwartz, D.P., Gill, H.E., and Mayes, B.H.: Utah Geological Survey Special Study 92, 22 p., 1 plate.
8. Paleoseismic investigation at Rock Canyon, Provo segment, Wasatch fault zone, Utah County, Utah—Paleoseismology of Utah, Volume 8, 1998, by Lund, W.R., and Black, B.D.: Utah Geological Survey Special Study 93, 21 p., 2 plates.
9. Paleoseismic investigation of the Clarkston, Junction Hills, and Wellsville faults, West Cache fault zone, Cache County, Utah—Paleoseismology of Utah, Volume 9, 2000, by Black, B.D., Giraud, R.E., and Mayes, B.H.: Utah Geological Survey Special Study 98, 23 p., 1 plate.
10. Post-Bonneville paleoearthquake chronology of the Salt Lake City segment, Wasatch fault zone, from the 1999 “mega-trench” site—Paleoseismology of Utah, Volume 10, 2002, by McCalpin, J.P.: Utah Geological Survey Miscellaneous Publication 02-7, 38 p.
11. Post-Provo paleoearthquake chronology of the Brigham City segment, Wasatch fault zone, Utah—Paleoseismology of Utah, Volume 11, 2002, by McCalpin, J.P., and Forman, S.L.: Utah Geological Survey Miscellaneous Publication 02-9, 46 p.
12. Neotectonics of Bear Lake Valley, Utah and Idaho; a preliminary assessment—Paleoseismology of Utah, Volume 12, 2003, by McCalpin, J.P.: Utah Geological Survey Miscellaneous Publication 03-4, 43 p.
13. Holocene earthquake history of the northern Weber segment of the Wasatch fault zone, Utah—Paleoseismology of Utah, Volume 13, 2006, by Nelson, A.R., Lowe, M., Personius, S., Bradley, L., Forman, S.L., Klauk, R., and Garr, J.: Utah Geological Survey Miscellaneous Publication 05-8, 39 p., 2 plates.
14. Paleoseismic investigation and long-term slip history of the Hurricane fault in southwestern Utah—Paleoseismology of Utah, Volume 14, 2007, by Lund, W.R., Hozik, M.J., and Hatfield, S.C.: Utah Geological Survey Special Study 119, 81 p.
15. Surficial-geologic reconnaissance and scarp profiling on the Collinston and Clarkston Mountain segments of the Wasatch fault zone, Box Elder County, Utah—paleoseismic inferences, implications for adjacent segments, and issues for diffusion-equation scarp-age modeling—Paleoseismology of Utah, Volume 15, 2007, by Hylland, M.D.: Utah Geological Survey Special Study 121, 18 p.
16. Paleoseismic reconnaissance of the Sevier fault, Kane and Garfield Counties, Utah—Paleoseismology of Utah, Volume 16, 2008, by Lund, W.R., Knudsen, T.R., and Vice, G.S.: Utah Geological Survey Special Study 122, 31 p.

17. Paleoseismic investigation of the northern strand of the Nephi segment of the Wasatch fault zone at Santaquin, Utah—Paleoseismology of Utah, Volume 17, 2008, by DuRoss, C.B., McDonald, G.N., and Lund, W.R.: Utah Geological Survey Special Study 124, 33 p., 1 plate.
18. Paleoseismic investigation of the northern Weber segment of the Wasatch fault zone at Rice Creek trench site, North Ogden, Utah—Paleoseismology of Utah, Volume 18, 2009, by DuRoss, C.B., Personius, S.F., Crone, A.J., McDonald, G.N., and Lidke, D.J.: Utah Geological Survey Special Study 130, 37 p., 2 plates.
19. Late Quaternary faulting in East Canyon Valley, Northern Utah—Paleoseismology of Utah, Volume 19, 2010, by Piety, L.A., Anderson, L.W., and Ostenaar, D.A.: Utah Geological Survey Miscellaneous Publication 10-5, 40 p.
20. Compilation of U.S. Bureau of Reclamation Seismotectonic Studies in Utah, 1982–1999—Paleoseismology of Utah, Volume 20, 2011, compiled by Lund, W.R., Bowman, S.D., and Piety, L.A.: Utah Geological Survey Miscellaneous Publication 11-2, variously paginated.
21. Compilation of 1982–83 seismic safety investigation reports of eight SCS dams in southwestern Utah (Hurricane and Washington fault zones) and low-sun-angle aerial photography, Washington and Iron Counties, Utah, and Mohave County, Arizona—Paleoseismology of Utah, Volume 21, 2011, by Bowman, S.D., Young, B.W., and Unger, C.D.: Utah Geological Survey Open-File Report 583, 4 p., 2 plates, 6 DVD set.
22. Late Holocene earthquake history of the Brigham City segment of the Wasatch fault zone at the Hansen Canyon, Kotter Canyon, and Pearsons Canyon trench sites, Box Elder County, Utah—Paleoseismology of Utah, Volume 22, 2012, by DuRoss, C.B., Personius, S.F., Crone, A.J., McDonald, G.N., and Briggs, R.: Utah Geological Survey Special Study 142, 28 p., 3 plates, 5 appendices.
23. Compilation of U.S. Geological Survey National Earthquake Hazards Reduction Program Final Technical Reports for Utah—Paleoseismology of Utah, Volume 23, 2013, compiled by Bowman, S.D., and Lund, W.R.: Utah Geological Survey Miscellaneous Publication 13-3, 9 p. plus 56 reports.
24. Evaluating surface fault chronologies of graben-bounding faults in Salt Lake Valley, Utah—new paleoseismic data from the Salt Lake City segment of the Wasatch fault zone and the West Valley fault zone—Paleoseismology of Utah, Volume 24, 2014, by DuRoss, C.B., and Hylland, M.D.: Utah Geological Survey Special Study 149, 76 p., 2 plates, 14 appendices.
25. History of late Holocene earthquakes at the Willow Creek site on the Nephi segment, Wasatch fault zone, Utah—Paleoseismology of Utah, Volume 25, 2014, by Crone, A.J., Personius, S.F., DuRoss, C.B., Machette, M.N., and Mahan, S.A.: Utah Geological Survey Special Study 151, 43 p., 3 appendices.
26. Compilation of 1970s Woodward-Lundgren & Associates Wasatch fault investigation reports and low-sun-angle aerial photography, Wasatch Front and Cache Valley, Utah and Idaho—Paleoseismology of Utah, Volume 26, 2015, compiled by Bowman, S.D., Hiscock, A.I., and Unger, C.D., Utah Geological Survey Open-File Report 632, 8 p., 6 plates, 9 DVD set.
27. Geologic mapping and paleoseismic investigations of the Washington fault zone, Washington County, Utah, and Mohave County, Arizona—Paleoseismology of Utah, Volume 27, 2015, edited by Lund, W.R., Utah Geological Survey Miscellaneous Publication 15-6, 175 p.
28. Holocene surface-faulting earthquakes at the Spring Lake and North Creek sites on the Wasatch fault zone—evidence for complex rupture of the Nephi segment—Paleoseismology of Utah, Volume 28, 2017, by DuRoss, C.B., Hylland, M.D., Hiscock, A.I., Personius, S.F., Briggs, R.W., Gold, R.D., Beukelman, G.S., McDonald, G.N., Erickson, B.A., McKean, A.P., Angster, S.J., King, R., Crone, A.J., and Mahan, S.A.: Utah Geological Survey Special Study 159, 44 p., 4 plates, 12 appendices.
29. Paleoseismic investigation of the Taylorsville fault at the Airport East site, West Valley fault zone, Salt Lake County, Utah—Paleoseismology of Utah, Volume 29, 2022, by Hylland, M.D., Hiscock, A.I., McDonald, G.N., DuRoss, C.B., Mahan, S.A., Briggs, R.W., Personius, S.F., and Reitman, N.G.: Utah Geological Survey Special Study 169, 29 p., 2 plates, 7 appendices.

## ABBREVIATIONS, ACRONYMS, AND SYMBOLS USED IN THIS REPORT

AMRT	apparent mean residence time
AMS	accelerator mass spectrometry
AMSL	above mean sea level (datum)
B.P.	before present (where present = 1950 CE)
<sup>14</sup> C	carbon-14 (radiocarbon)
cal yr B.P.	calibrated years before present
CE	Common Era
GNSS	Global Navigation Satellite System
GPS	Global Positioning System
ka	kiloannum (thousand years ago)
km	kilometer(s)
kyr	kilo years (thousands of years)
lidar	light detection and ranging
M	earthquake magnitude (generic)
M <sub>w</sub>	earthquake moment magnitude
m	meter(s)
mm/yr	millimeters per year
NOSAMS	National Ocean Sciences Accelerator Mass Spectrometry
OSL	optically stimulated luminescence
PDF	probability density function
SfM	structure-from-motion
SLCS	Salt Lake City segment of the Wasatch fault zone
σ	standard deviation (sigma)
UGRC	Utah Geospatial Resource Center
UGS	Utah Geological Survey
USGS	U.S. Geological Survey
VRS	virtual reference station
WVFZ	West Valley fault zone
yr	year(s)



## CONTENTS

FOREWORD .....	iv
PALEOSEISMOLOGY OF UTAH SERIES PUBLICATIONS.....	v
ABBREVIATIONS, ACRONYMS, AND SYMBOLS USED IN THIS REPORT .....	vii
ABSTRACT.....	1
INTRODUCTION .....	1
Purpose and Scope.....	1
Geologic Setting .....	2
Previous Paleoseismic Research on the West Valley Fault Zone .....	3
OVERVIEW AND METHODS.....	5
Trench Investigation .....	5
Numerical Dating.....	8
Radiocarbon Dating.....	8
Luminescence Dating.....	8
OxCal Modeling Methods .....	8
AIRPORT EAST TRENCH SITE .....	9
Surface Faulting and Geology .....	9
Taylorsville Fault Scarp and Surface Offset.....	9
Trench Stratigraphy and Structure.....	9
Wetland and Fluvial Channel Deposits .....	9
Fluvial Overbank, Marsh, and Lacustrine Deposits.....	11
Scarp-Derived Colluvium and Related Deposits.....	12
Taylorsville Fault.....	13
Paleoseismology of the Airport East Site .....	15
Chronology of Surface-Faulting Earthquakes.....	15
Earthquake Recurrence and Fault Slip Rate.....	15
PALEOSEISMOLOGY OF THE WEST VALLEY FAULT ZONE.....	19
Correlation of Earthquakes .....	19
Earthquake Recurrence and Fault Slip Rate.....	19
COMPARISON OF EARTHQUAKE CHRONOLOGIES FOR THE WEST VALLEY FAULT ZONE AND NEARBY SEGMENTS OF THE WASATCH FAULT ZONE.....	22
SUMMARY AND CONCLUSIONS.....	23
ACKNOWLEDGMENTS .....	25
REFERENCES .....	25
APPENDICES .....	30
Appendix A—Description of Stratigraphic Units Exposed in Trenches at the Airport East Site.....	31
Appendix B—Description of Soil Units in Trenches at the Airport East Site.....	32
Appendix C—Description of Scarp-Derived Colluvium and Related Deposits in Trenches at the Airport East Site.....	33
Appendix D—Processing and Analysis of Radiocarbon Sample Material from the Airport East Site by PaleoResearch Institute .....	34
Appendix E—Summary of Radiocarbon Dating at the Airport East Site.....	58
Appendix F—Summary of Luminescence Dating at the Airport East Site .....	59
Appendix G—OxCal Model for the Taylorsville Fault at the Airport East Site.....	60

## FIGURES

Figure 1. Location of West Valley fault zone and other nearby faults .....	2
Figure 2. Location of Airport East trench site and other paleoseismic investigation sites on the West Valley fault zone .....	3
Figure 3. Inferred subsurface geometry of the Wasatch–West Valley fault system.....	4
Figure 4. Overview of the Airport East site and vicinity .....	6
Figure 5. Lidar hillshade detail of the Airport East site.....	7
Figure 6. Panoramic photograph of the Airport East site .....	7
Figure 7. Scarp profiles, Airport East site.....	10
Figure 8. Liquefaction-induced sand dike in the North trench.....	11
Figure 9. Fault-zone exposure in the south wall of the South trench, showing deposits of scarp-derived colluvium.....	13

Figure 10. OxCal model for the Airport East site.....	16
Figure 11. Chronostratigraphic summary for the Airport East site, showing timing of earthquakes AE1, AE2, AE3, and LE1.....	17
Figure 12. Comparison of surface-faulting chronologies for the Granger and Taylorsville faults.....	20
Figure 13. Comparison of surface-faulting chronologies for the West Valley fault zone and Salt Lake City and Weber segments of the Wasatch fault zone .....	24

## TABLES

Table 1. Vertical displacement data for the Taylorsville fault, Airport East site.....	14
Table 2. Summary of earthquake timing and displacement data, Airport East site .....	17
Table 3. Chronology and recurrence of surface-faulting earthquakes, Airport East site .....	18
Table 4. Paleoseismic (closed-interval) slip rates at the Airport East site .....	18
Table 5. Geologic (open-interval) slip rates at the Airport East site.....	18
Table 6. Chronology and recurrence of surface-faulting earthquakes, Taylorsville fault.....	21
Table 7. Chronology and recurrence of surface-faulting earthquakes, West Valley fault zone .....	21
Table 8. Comparison of earthquake times on the West Valley fault zone and Salt Lake City and Weber segments of the Wasatch fault zone .....	23

## PLATES

- Plate 1. Stratigraphic and structural relations in the South trench at the Airport East trench site
- Plate 2. Stratigraphic and structural relations in the North trench at the Airport East trench site

# PALEOSEISMIC INVESTIGATION OF THE TAYLORSVILLE FAULT AT THE AIRPORT EAST SITE, WEST VALLEY FAULT ZONE, SALT LAKE COUNTY, UTAH

by Michael D. Hylland, Adam I. Hiscock, Greg N. McDonald, Christopher B. DuRoss, Shannon A. Mahan,  
Richard W. Briggs, Stephen F. Personius, and Nadine G. Reitman

## ABSTRACT

The West Valley fault zone (WVFZ) and Salt Lake City segment (SLCS) of the Wasatch fault zone comprise Holocene-active normal faults that bound an intrabasin graben in northern Salt Lake Valley, Utah. Both fault zones have evidence of recurrent Holocene surface-faulting earthquakes. A topic of recent research is the seismogenic relation of the antithetic (subsidiary) WVFZ to the Wasatch fault zone—specifically, to what degree are WVFZ earthquakes independent of slip on the SLCS, or other adjacent segments, of the Wasatch fault zone. To improve paleoseismic data for the WVFZ and better understand the seismogenic relation between the WVFZ and Wasatch fault zone, we conducted a fault-trench investigation at the Airport East site, developed new earthquake recurrence and fault slip-rate estimates for the WVFZ, and compared WVFZ earthquake timing data with data from the Wasatch fault zone.

The Airport East site is near the northern end of the easternmost traces of the WVFZ, collectively referred to as the Taylorsville fault. At this site, we excavated two parallel trenches across a small (~0.5-m high) east-facing fault scarp. Shallow groundwater severely limited trench depth, and we were able to expose deposits only as old as mid-Holocene. However, the late Holocene section contained evidence for three surface-faulting earthquakes on the Taylorsville fault, as well as earthquake-related deformation (liquefaction and folding) from a fourth earthquake that was likely sourced elsewhere. Based on OxCal modeling of radiocarbon and optically stimulated luminescence ages, the most recent earthquake, AE1, occurred at  $0.4 \pm 0.2$  ka (mean modeled time  $\pm 2\sigma$ ), earthquake AE2 occurred at  $0.6 \pm 0.2$  ka, and earthquake AE3 occurred at  $2.0 \pm 0.3$  ka. Timing data from the Airport East site indicate the liquefaction and folding event (LE1) occurred at  $5.1 \pm 0.3$  ka. Net vertical displacement across the fault is 0.6–1.1 m, and calculations of mean per-event displacement range from 0.20 to 0.37 m. Inter-event recurrence intervals for the Taylorsville fault at the Airport East site vary from 200 to 1400 yr, and the mean late Holocene (post-2 ka) recurrence interval is 800 yr. Paleoseismic (closed-interval) slip rates range from 0.23 to 1.4 mm/yr, and geologic (open-interval) slip rates range from 0.1–0.2 mm/yr over the past ~5000 yr to 0.2–0.4 mm/yr over the past ~2500 yr.

Combining our new Airport East data with previous paleoseismic data for the WVFZ shows that during individual late Holocene earthquakes, surface faulting has occurred on either the Taylorsville or Granger fault, but not both faults at the same time (at least not on the parts of the faults that have been trenched). However, five mid- to late Holocene WVFZ earthquakes have mean modeled times that are either very similar or identical to mean modeled times of SLCS and Weber-segment earthquakes, and temporal correlations of two additional late Pleistocene WVFZ earthquakes with SLCS earthquakes cannot be ruled out. When comparing the earthquake chronologies of the WVFZ and Wasatch fault zone, our new data lend support to the idea that, more often than not, some part of the WVFZ moves in response to, and possibly synchronously with, slip on the Wasatch fault zone.

## INTRODUCTION

### Purpose and Scope

The West Valley fault zone (WVFZ) comprises intrabasin faults in the hanging wall of the Wasatch fault zone in the northern part of Salt Lake Valley (figure 1). Despite trending through part of the most urbanized area of Utah and having evidence of recurrent Holocene surface-faulting earthquakes, relatively few detailed paleoseismic investigations have been completed on the WVFZ, and so its faulting behavior is not well understood. The WVFZ is spatially distributed; the two subparallel main strands, along with their associated subsidiary strands, are known as the Granger fault (western strands) and Taylorsville fault (eastern strands) (figure 2). Very few of the numerous strands of the WVFZ have had detailed investigations to characterize per-event timing and displacement of surface-faulting earthquakes, and prior to this investigation, almost no per-event timing and displacement data existed for the Taylorsville fault. Sparse and poorly constrained earthquake timing and displacement data preclude determining robust recurrence-interval and slip-rate estimates for the Taylorsville fault and WVFZ as a whole and limit a clear understanding of the seismogenic relation between the WVFZ and Wasatch fault zone.

To better characterize the earthquake chronology and permanent displacements for the Taylorsville fault and WVFZ as a whole, as well as improve our understanding of the kinematic relation between the WVFZ and Wasatch fault zone, the Utah Geological Survey (UGS), with assistance from the U.S. Geological Survey (USGS), conducted a paleoseismic fault-trench investigation at a site near the northern end of the Taylorsville fault (Airport East site; figures 1 and 2). The investigation included (1) detailed topographic and geologic mapping of the trench site, (2) scarp profiling, (3) excavating

two trenches, (4) logging the trench-wall exposures in detail, (5) sampling organic remains and fine-grained detrital sediment for radiocarbon and luminescence dating, respectively, (6) developing probabilistic models of earthquake times using OxCal modeling software, and (7) determining earthquake chronologies, vertical displacement, recurrence, and fault slip rate. This report presents the data and results from the investigation, contributing to a more accurate assessment of earthquake hazard in the central Wasatch Front.

## Geologic Setting

Salt Lake Valley occupies one of several north-south trending basins at the eastern margin of the actively extending Basin and Range Province. The Wasatch Range and Oquirrh Mountains bound the valley on the east and west, respectively; Great Salt Lake lies to the north, and the east-west trending Traverse Mountains separate Salt Lake Valley from Utah Valley to the south. Structurally, Salt Lake Valley is on the hanging wall of the Wasatch fault zone, which comprises a major, west-dipping, range-bounding normal fault that forms the boundary between the Wasatch Range to the east and numerous structural basins to the west.

The Wasatch fault zone is the longest active normal-slip fault in the western United States and the most active fault in Utah. Extending 350 km from southern Idaho to central Utah, the Wasatch fault zone comprises 10 segments, each of which is generally considered to be seismogenically independent (Swan and others, 1980; Schwartz and Coppersmith, 1984; Machette and others, 1992; Wheeler and Krystinik, 1992; DuRoss and others, 2016a). The Salt Lake City segment (SLCS), one of the five central segments of the Wasatch fault zone having evidence of repeated Holocene earthquakes (Machette and others, 1992), generally forms the eastern margin of Salt Lake Valley. Adjacent segments to the north and south are the Weber and Provo segments, respectively (figure 1). Since the mid-Holocene (~6 ka), surface-faulting earthquakes on the central segments of the Wasatch fault zone have occurred on average every 700–2700 yr, and mean vertical slip rates (closed-interval) range from about 1.3 to 2.3 mm/yr (DuRoss and others, 2016b).

A variety of geologic and geophysical data provide evidence for the northeastern part of Salt Lake Valley being a structural graben bounded by the SLCS on the east and the WVFZ on the west (e.g., Marsell and Threet, 1960; Cook and Berg, 1961; Marine and Price, 1964; Arnow and Mattick, 1968; Zoback, 1983; Keaton and others, 1987; DuRoss and Hylland, 2015). The WVFZ consists of intrabasin normal faults within an area 16 km long by 1–6 km wide in the northern part of the valley (figure 2). Strands of the WVFZ lie 4 to 10 km west of the SLCS. WVFZ scarps are typically about 0.5–1.5 m high, but have a maximum height of 6 m near the southern end of the Granger fault (Hylland and others, 2014). Scarps on the Granger fault face east, and scarps on the Taylorsville fault face both east and west. Collectively,

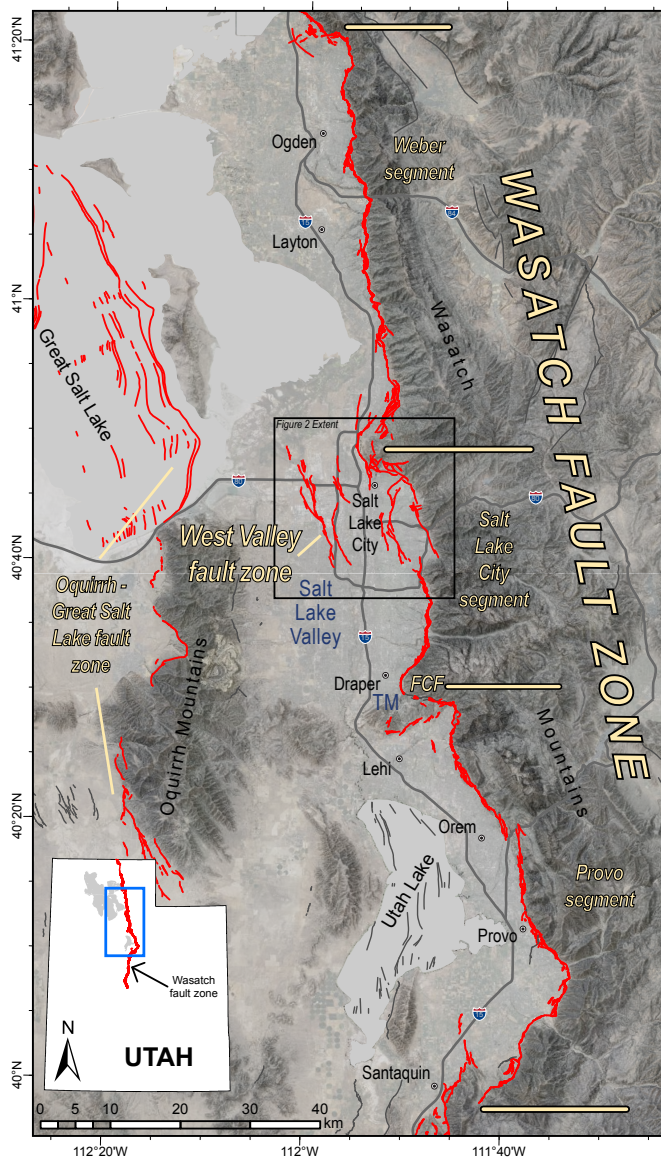


**Figure 1.** Relation of the West Valley fault zone with the Wasatch fault zone and other Quaternary-active faults along the eastern margin of the Basin and Range Province in northern Utah. The West Valley fault zone, Oquirrh–Great Salt Lake fault zone, and Salt Lake City and adjacent segments of the Wasatch fault zone are shown in red; other Quaternary faults are shown in light gray. Fault traces from Utah Geologic Hazards Portal (<https://geology.utah.gov/apps/hazards/>). FCF, Fort Canyon fault; TM, Traverse Mountains. Base is combined lidar hillshade image (UGRC, 2014a) and aerial imagery (UGRC, 2018).

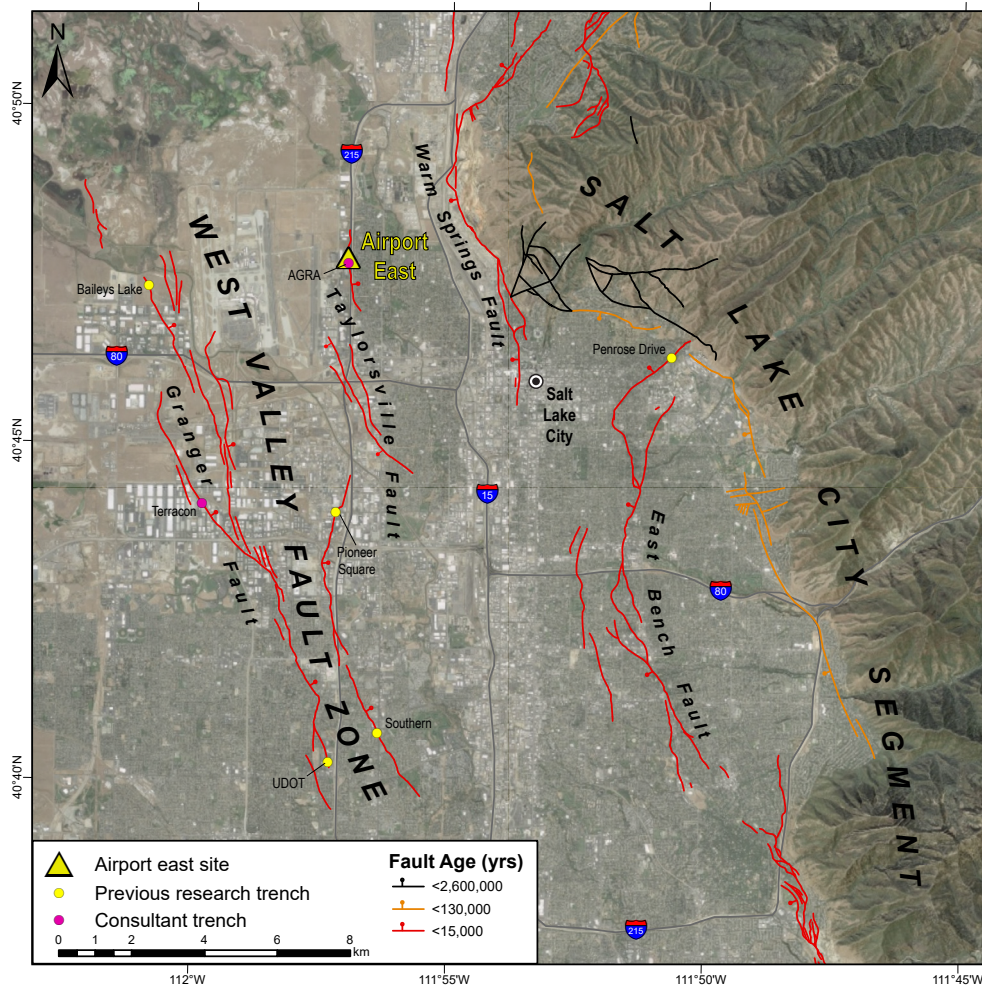


**Figure 2.** Location of the Airport East trench site (yellow triangle; this study), previous paleoseismic research trenches on the West Valley fault zone (Keaton and others, 1987; Keaton and Currey, 1989; Hylland and others, 2014) and Salt Lake City segment of the Wasatch fault zone (DuRoss and others, 2014), and consultant trenches on the West Valley fault zone that have yielded earthquake timing data (see Hylland and others, 2014, appendix H). Fault traces from Utah Geologic Hazards Portal (<https://geology.utah.gov/apps/hazards/>). Aerial imagery base from UGRC (2018).

the WVfZ is an antithetic structure to the Wasatch fault zone, with the Wasatch fault zone acting as the primary or controlling fault (DuRoss and Hylland, 2015; see also Bruhn and Schultz, 1996) (figure 3).

Quaternary basin-fill deposits extend to a depth of about 400 m beneath the floor of northern Salt Lake Valley (McKean and Hylland, 2019b). These deposits include lacustrine sediments that accumulated in pluvial lakes that intermittently occupied this part of the Great Basin during the Pleistocene, including four relatively deep lakes since 780 ka (Oviatt and others, 1999). The most recent and largest of these lakes was Lake Bonneville (Gilbert, 1890; Oviatt and Shroder, 2016), which occupied the Bonneville basin between 30 and 13 ka (Oviatt, 2015). Highstand deposits of Lake Bonneville (~18 ka) are present along the margins of Salt Lake Valley up to an elevation of about 1585 m. On the floor of northern Salt Lake Valley, the Lake Bonneville deposits are overlain by a sequence of Holocene lacustrine, alluvial, marsh, and loess deposits, including (1) marl and sandy shorezone deposits as-

sociated with the Gilbert-episode lake (11.6 ka; Hylland and others, 2012, 2014; Oviatt, 2014), (2) sand and silt deposited in Jordan River channels, floodplains, terraces, and deltas (Van Horn, 1982; Personius and Scott, 1992; McKean, 2014; McKean and Hylland, 2019b), and (3) oolitic sand and mud deposits associated with highstands of saline, terminal Great Salt Lake (McKean and Hylland, 2019b).

### Previous Paleoseismic Research on the West Valley Fault Zone

Previous paleoseismic investigations have documented multiple post-Bonneville highstand surface-faulting earthquakes on the WVfZ, but until recently timing and displacement data for individual earthquakes have been sparse and poorly constrained. Investigations by Keaton and others (1987) and Keaton and Currey (1989), involving mostly borehole exploration with some geomorphic mapping and limited trenching, established long-term (140 kyr) cumulative displacements and

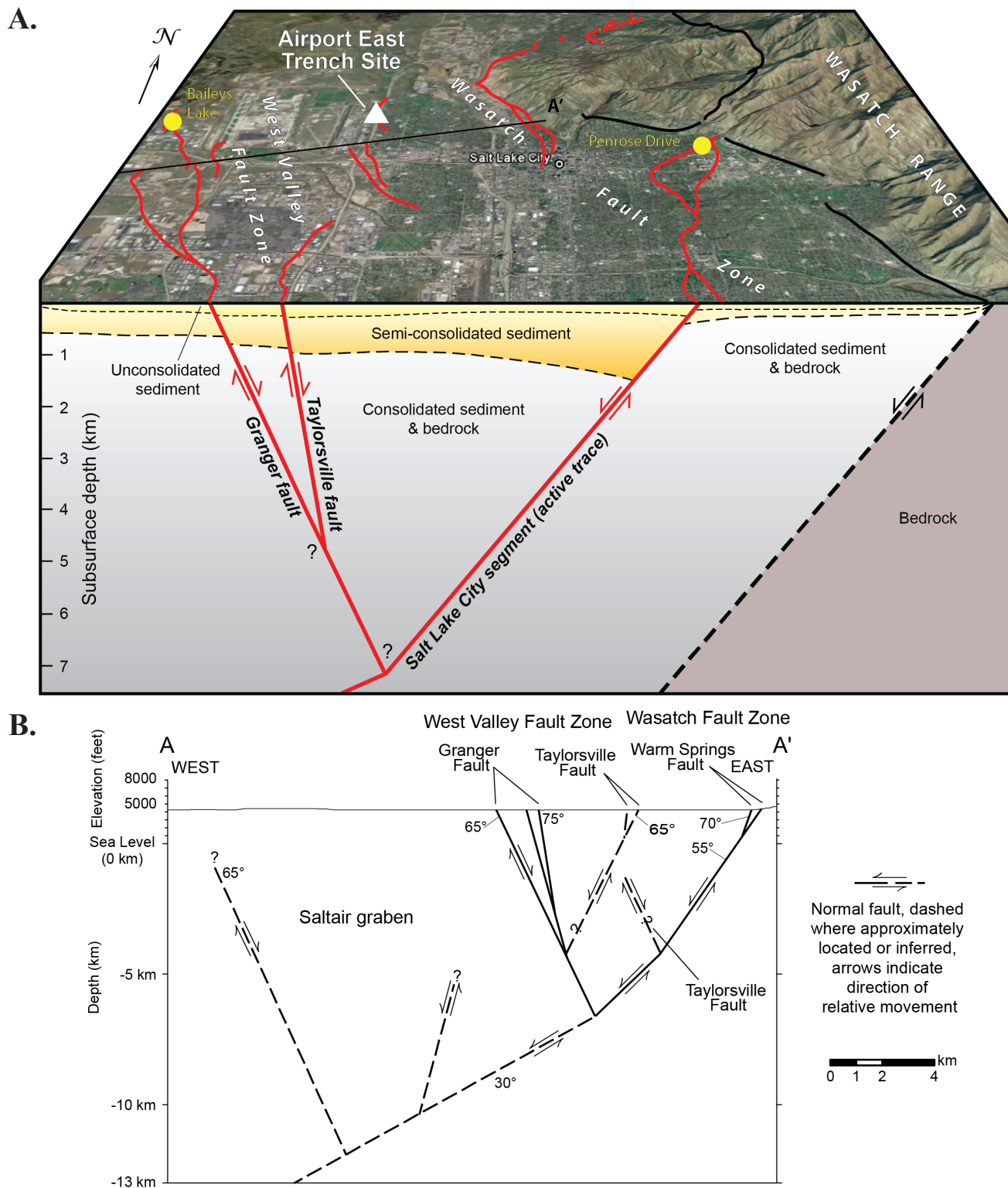


**Figure 3.** (A) Schematic diagram illustrating the generalized inferred subsurface geometry of the Wasatch–West Valley fault system (after Hylland and others, 2014), based largely on figure 1 of Bruhn and Schultz (1996). The West Valley fault zone is antithetic to the west-dipping Salt Lake City segment (primary fault), forming an intrabasin graben in northern Salt Lake Valley. Baileys Lake and Penrose Drive sites were investigated in a recent paleoseismic study (DuRoss and Hylland, 2014, 2015). Holocene fault traces shown in red, older fault traces shown in black. Line of section south of Airport East site indicates extent of approximately the eastern half of cross section A-A' shown on 3B. Map scale varies, no vertical exaggeration implied. Aerial imagery from UGRC (2018). (B) Cross section illustrating proposed structural model for the Wasatch–West Valley fault system in the vicinity of the Airport East site (after Kleber and others, 2021). This cross section was created using seismicity data from the 18 March 2020  $M_w$  5.7 Magna, Utah, earthquake, summarized in Pang and others (2020). The Magna earthquake was interpreted as having resulted from slip on a low-angle part of the Salt Lake City segment (Warm Springs fault), indicating a listric subsurface geometry (Pang and others, 2020; Kleber and others, 2021).

slip rates for the WVFZ, but were unable to obtain well-constrained earthquake timing and per-event displacement data. Cumulative vertical displacements include 0.7–3 m offset of “post-Bonneville” (<12 ka) deposits, 5–7 m offset of Bonneville lake-cycle deposits (12–28 ka), and 13–14 m offset of a paleosol developed on Cutler Dam (pre-Bonneville) lake-cycle deposits ( $60 \pm 20$  ka). Slip rates determined by these two investigations include 0.03–0.5 mm/yr for the Granger fault over various time intervals within the past 140 kyr, 0.1–0.2 mm/yr for the Taylorsville fault since 12 ka, and 0.5–0.6 mm/yr for the entire WVFZ since 13 ka.

Hylland and others (2014) obtained data for four surface-faulting earthquakes at the Baileys Lake site near the north end of the Granger fault (figure 2). These earthquakes occurred at  $15.7 \pm 3.4$  ka ( $2\sigma$ ),  $13.0 \pm 1.1$  ka,  $12.3 \pm 1.1$  ka, and  $5.5 \pm 0.8$  ka, and mean per-event vertical displacement at the Baileys Lake site is  $0.5 \pm 0.1$  m. The timing and displacement data yield slip rates of 0.09–0.12 mm/yr (post-Bonneville highstand) and 0.06–0.09 mm/yr (Holocene) (Hylland and others, 2014). Based on the similarity of earthquake times with SLCS earthquakes and considering kinematic and geometric models of the WVFZ-SLCS fault system, synchronous or triggered-slip rupture of the WVFZ with the SLCS seems likely (Hylland and others, 2014; DuRoss and Hylland, 2015). However, because of the distributed nature of WVFZ strands, multiple per-event displacement measurements tied to specific earthquake times from different parts of the WVFZ are needed to rigorously evaluate slip rates, net tectonic displacement across the WVFZ, and kinematic interaction with the SLCS.

At the time of the present investigation, only a single, poorly constrained earthquake timing estimate existed for the Taylorsville fault. This estimate came from a geotechnical fault setback study conducted by AGRA Earth and Environmental in September 1997 at a site near the northern end of the Taylorsville fault (figure 2). Radiocarbon age results from two bulk-soil samples collected by UGS geologists—one from “crack-fill sediment” and one from sag pond sediment beneath a possible colluvial wedge—were averaged to yield an age of 2200 cal yr B.P., interpreted to approximate the time of the surface-faulting earthquake (Solomon, 1998; see also Hylland and others, 2014). Interestingly, this timing coincides with the timing of the penultimate surface-faulting earthquake on the SLCS (~2.2 ka; DuRoss and others, 2014, 2016a, 2016b), indicating possible synchronous faulting. However, the stratigraphic context and relation of the soil ages at the AGRA site to the timing of surface faulting is not well understood due to the very limited time frame available to interpret the trench exposure. Also, uncertainty in earthquake timing is broad (and poorly constrained) because the soil ages were apparent mean residence time (AMRT) radiocarbon ages. AMRT ages are problematic in that they are composite ages that reflect the total age distribution of carbon in the sampled soil (Machette and others, 1992).

Like the timing data, existing per-event displacement data for the Taylorsville fault are also sparse and poorly constrained.

Prior to the present investigation, per-event displacement estimates on the Taylorsville fault had been published for just two earthquakes: one at the AGRA geotechnical site discussed above (0.5–0.7 m; Solomon, 1998; see also Hylland and others, 2014) and one at the Pioneer Industrial Park (1.2–1.5 m; Keaton and others, 1987) about 7 km south of the AGRA site (figure 2). The displacement estimate from the AGRA site compares favorably with the mean per-event displacement documented at the Baileys Lake site on the Granger fault ( $0.5 \pm 0.1$  m). The larger displacement estimate of Keaton and others (1987), which was based on cross-cutting geomorphic relations and a single vertical displacement measurement in a trench exposure, is from near the middle of the WVFZ, whereas the Baileys Lake and AGRA sites are near the northern end of the mapped traces of the WVFZ. Displacement may decrease to the north, and/or a displacement of 1.2–1.5 m may be more representative of maximum displacement for the WVFZ than average displacement (Hylland and others, 2014).

GCS Geoscience excavated three fault trenches in the vicinity of our Airport East site in August 2014 as part of a pre-development fault setback study (figure 4), and we were given the opportunity to observe the exposures. Although this investigation did not produce any quantitative earthquake timing data, it showed the variability in near-surface expression of fault slip (discrete shear versus monoclinical folding) over relatively short distances along the strike of the fault, and this proved very useful in making the final decision for the location of our trenches.

## OVERVIEW AND METHODS

### Trench Investigation

We identified potential trench sites using (1) fault-trace and surficial-geologic mapping by Keaton and others (1987), Personius and Scott (1992), and McKean (2014); (2) interpretation of 1937 (Agricultural Adjustment Administration; scale 1:20,000) and 1958 (Soil Conservation Service; scale 1:10,000) stereo aerial photographs; (3) interpretation of 1-m-posting lidar data (2011) for Salt Lake Valley (<https://geology.utah.gov/map-pub/data-databases/lidar/>); and (4) field reconnaissance. Discussions and analyses of WVFZ and SLCS paleoseismic data by the Utah Quaternary Fault Parameters Working Group (<https://geology.utah.gov/hazards/info/workshops/working-groups/q-faults/>) helped guide our decisions regarding trench-site locations. Of the few possible trench sites on the Taylorsville fault, we selected the Airport East site as our preferred site because of the relatively undisturbed nature of the fault scarp, as well as the availability of existing data from previous fault-setback investigations by consultants.

The Airport East site is east of the Salt Lake City International Airport, between 2200 West Street and Interstate 215 (figures 2 and 4). The site is on a large parcel of commercial property; a commercial building was under construction on the western

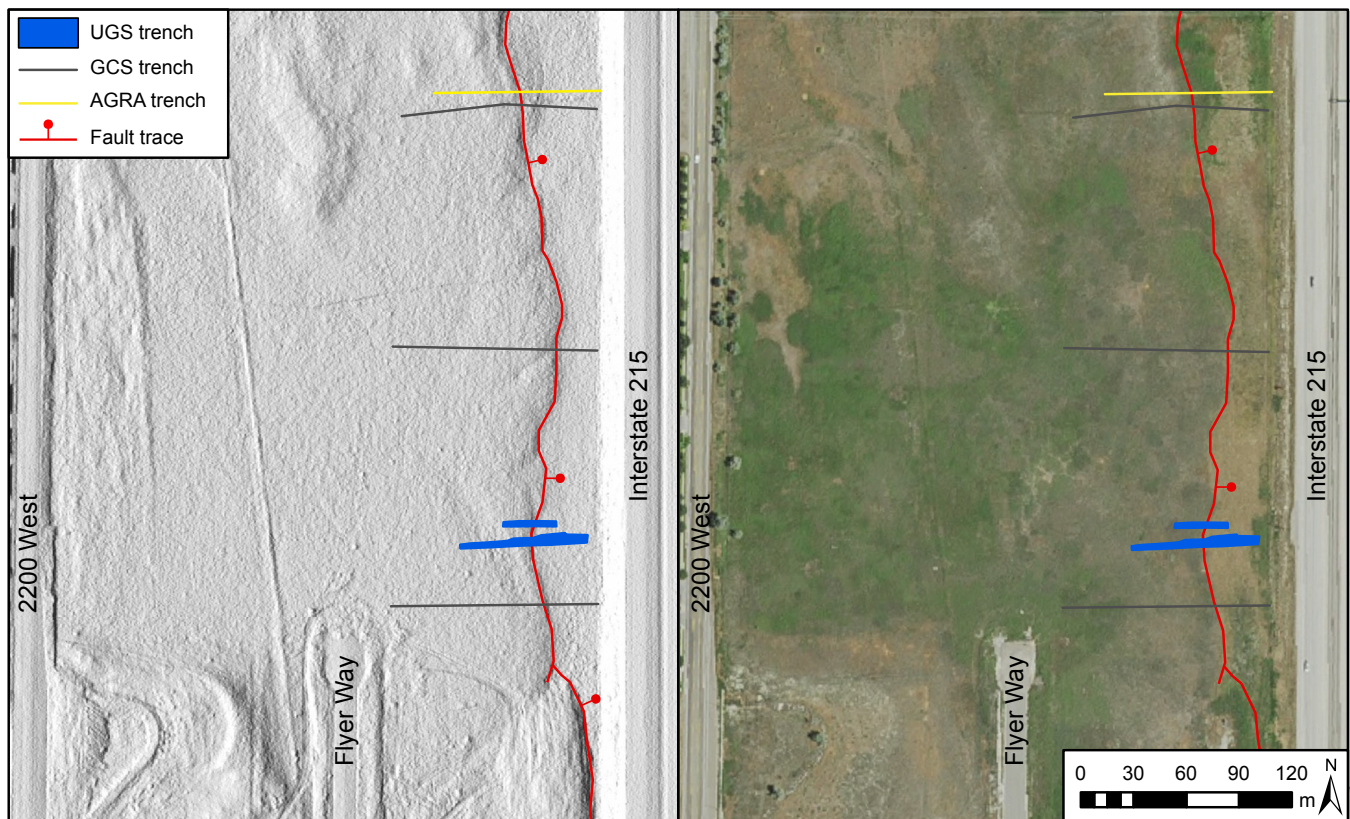


**Figure 4.** Overview of the Airport East site and vicinity; lidar hillshade image (left; UGRC, 2014a) and orthophoto (right; UGRC, 2014b). AGRA trench (approximate location) was excavated in September 1997, GCS trenches were excavated in August 2014. Lidar: 2013–14, 0.5-m posting, hillshade illumination from the west. Image center point coordinates:  $40.796491^{\circ}$  N,  $111.951518^{\circ}$  W.

half of the parcel at the time of our investigation. The parcel is generally flat and vegetated with grass and scattered low bushes. The site is underlain by fine-grained Holocene fluvial, lacustrine, and deltaic deposits (Miller, 1980; McKean, 2014). A single north-trending, east-facing fault scarp  $\sim 0.5$  m high crosses the site (figure 4). Extensive fill obscures the scarp on the parcel immediately south of the Airport East site, but the scarp appears to be relatively unmodified across the Airport East site. We measured two scarp profiles at the site using VRS GNSS surveying equipment (figure 5).

We excavated two parallel trenches across the fault scarp at the Airport East site in August–September 2015 using a track-mounted hydraulic excavator, to expose fault-related sediments and document vertical displacement on the Taylorsville fault. The trenches consisted of the 73-m-long South trench, and about 10 m to the north, the 30-m-long North trench (figures 5 and 6). Because the site is on the floor of the Great Salt Lake basin, shallow groundwater was a logistical concern for trenching. For planning purposes, we installed three piezometers at the site—one on the footwall (AE-FW1) and two on the hanging wall (AE-HW1 and HW2) of the fault—for groundwater monitoring. Piezometer AE-HW1 was equipped with an hourly monitoring sensor, and AE-FW1 and AE-HW2 were monitored on a monthly basis for six months prior to trenching (data available at <https://apps.geology.utah.gov/gwdp/>). Maximum depth to groundwater ranged from 1.5 m below the

ground surface to nearly at the ground surface on the hanging wall, and 1–2 m below the ground surface on the footwall. To maximize trench safety and workability, we excavated the trench floors at about the depth of the water table along most of the length of the trenches and deepened the east (hanging-wall) ends of the trenches to form sumps from which we pumped accumulated water using two portable trash pumps. The shallow groundwater levels at the site were a major limiting factor in how deep the trenches could be excavated.

We used a hand auger to drill two shallow boreholes in the floor of the South trench, one on the hanging wall and one on the footwall and each within about 3 m of the fault zone (plate 1). The boreholes were drilled to investigate stratigraphic units beneath those exposed in the trench walls, providing additional data to calculate net tectonic displacement across the fault zone as well as determine whether the stratigraphy exhibited any differential displacements. The boreholes also provided opportunity to sample material conducive to radiocarbon or luminescence dating, broadening the chronostratigraphic context of fault activity at the site.

To map the trench-wall exposures, we constructed a 1-meter square grid using a total station instrument (Trimble TTS 500) to project points to an average, vertical plane parallel to the trench walls. We then took approximately 700 photographs of the south wall of the South trench and 350 photographs of

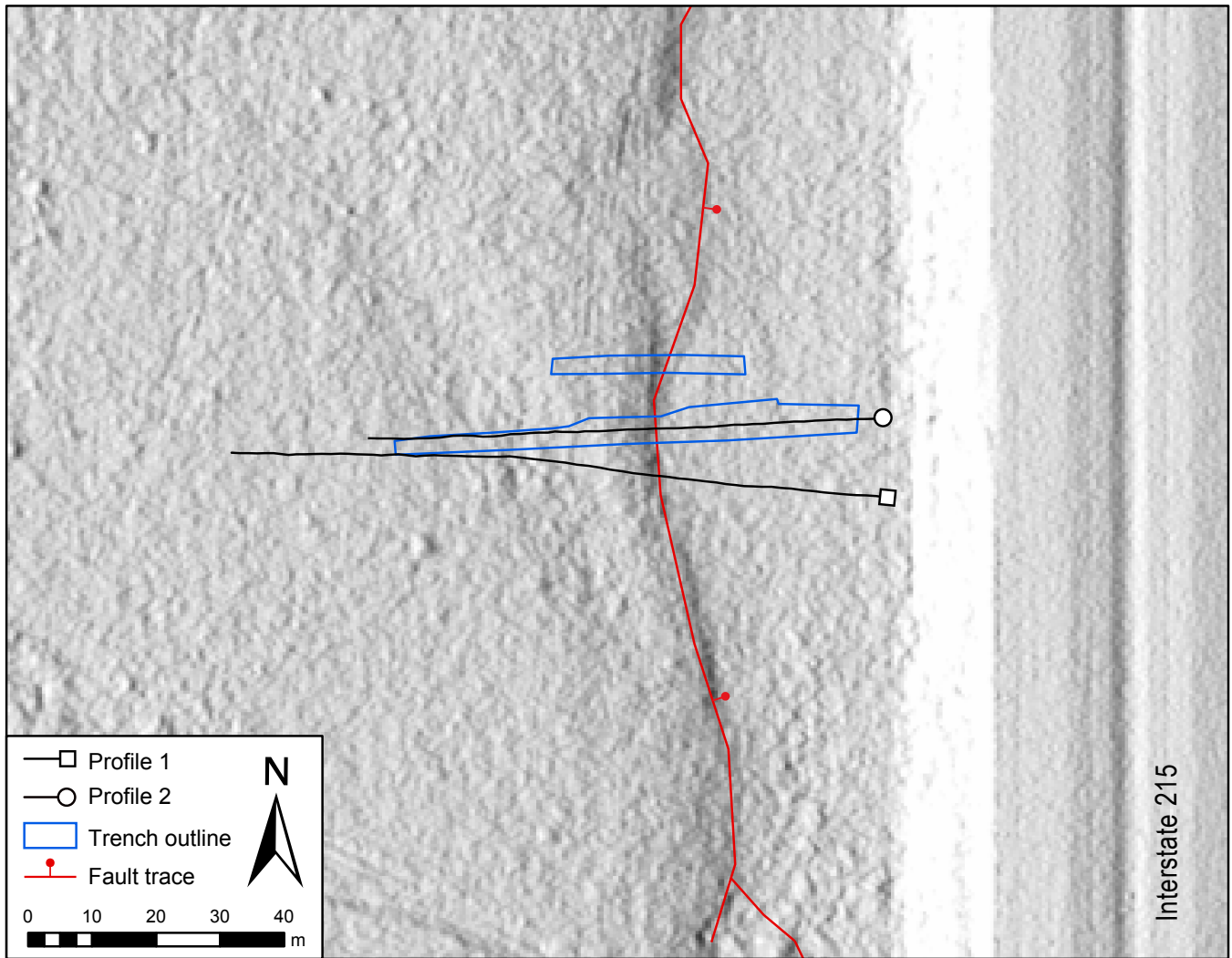


**Figure 5.** Lidar hillshade (UGRC, 2014a) detail of the Airport East site. Scarp profiles shown on figure 7. Lidar: 2013–14, 0.5-m posting, hillshade illumination from the west. Image center point coordinates: 40.795630° N, 111.950332° W.



**Figure 6.** Panoramic photograph of Airport East site, looking southwest into South trench. North trench visible on right.

the south wall of the North trench and created photomosaics using the structure-from-motion (SfM) method with Agisoft Photoscan Professional (version 1.0.4) software (Reitman and others, 2015). The fine-grained nature of the exposed deposits and the fine detail visible on the photomosaics allowed us to map stratigraphic contacts and structure on clear acetate overlays using the photomosaics as a base. Plates 1 and 2 show logs and photomosaics of the exposures, using a common arbitrary coordinate system for both trenches, referenced herein using horizontal (h-) and vertical (v-) meter marks. Stratigraphic units and pedogenic soils are described in appendices A through C and summarized on plates 1 and 2.

## Numerical Dating

### Radiocarbon Dating

We sampled fluvial, marsh, and scarp-colluvial deposits as well as buried soil A horizon sediment for accelerator mass spectrometry (AMS) radiocarbon ( $^{14}\text{C}$ ) dating to estimate deposit and soil ages and provide limits on the timing of paleoearthquakes (appendices D and E). For discussions of common sources of uncertainty in radiocarbon dating and paleoseismic investigations, see Trumbore (2000), Nelson and others (2006), and DuRoss and others (2011). We collected 11 bulk-soil samples, 10 discrete charcoal samples, and 1 wood-fragment sample, for a total of 22 samples. PaleoResearch Institute (Golden, Colorado) separated discrete charcoal fragments from the bulk-soil samples, and also attempted to identify the separated fragments to increase the likelihood of dating locally derived charcoal (e.g., phreatophytes) rather than non-local (detrital) charcoal (e.g., conifer species transported from the basin margins). Locally derived charcoal fragments are more likely burned in-place or very near the location where they are sampled, and therefore are less likely to have an inherited, older age (Puseman and Cummings, 2005). We combined individual fragments from each original sample, favoring seed and stem material, into 14 composite charcoal samples for AMS dating (appendix E; see also Hylland and others, 2022).

The 14 charcoal samples were dated by the National Ocean Sciences Accelerator Mass Spectrometry (NOSAMS) Facility of the Woods Hole Oceanographic Institution (Woods Hole, Massachusetts). We calendar-calibrated the  $^{14}\text{C}$  ages using the IntCal13 terrestrial calibration curve (Reimer and others, 2013) applied in OxCal calibration software (version 4.2.4, Bronk Ramsey, 1995, 2001, 2009; Bronk Ramsey and Lee, 2013). In our text discussions, the radiocarbon age results are generally reported as the mean rounded to the nearest century in thousands of calendar years B.P. (i.e., before 1950 CE) and two-sigma ( $2\sigma$ ) uncertainty.

### Luminescence Dating

We collected three samples to estimate burial ages of sandy or silty lacustrine and alluvial sediment using optically stim-

ulated luminescence (OSL) dating (appendix F). OSL has been used successfully in recent Wasatch Front paleoseismic investigations to supplement  $^{14}\text{C}$  dating (e.g., DuRoss and Hylland, 2014; see also Gray and others [2015] for a broader discussion of OSL applied to paleoseismic research). However, certain conditions can affect the accuracy of OSL ages, so OSL results should be compared to other dating results whenever possible. If the sediment's exposure to sunlight before final deposition was not long enough (e.g., because of rapid deposition, a short travel path, or filtered light in turbid water) to fully reset the luminescence signal, the sediment may retain an inherited signal (Forman and others, 1991; Duller, 2008) and OSL dating will produce an overestimated (maximum) age for the deposit. Conversely, if the luminescence signal becomes saturated, where the signal does not increase despite continued exposure of the sediment to radiation, OSL dating will produce an underestimated (minimum) age for the deposit (Duller, 2008).

Luminescence dating consisted of OSL ages on quartz grains (quartz OSL). The samples were processed at the USGS Luminescence Dating Laboratory (Lakewood, Colorado). For samples collected from the trench walls, background radiation from potassium, uranium, and thorium was measured in the field using a portable gamma-ray spectrometer. For a sample collected from a hand-auger hole in the trench floor, background radiation was measured in the laboratory using an accompanying bulk sample. Sample moisture content for all samples was measured in the laboratory. To estimate the water saturation history of the samples, which is critical to obtaining accurate OSL ages (see Hylland and others, 2012), we used the saturated moisture content with a correction factor representing the relative amount of time the sediment was likely saturated due to a shallow water table. The correction factor was estimated using the Great Salt Lake hydrograph of Murchison (1989) as a proxy for fluctuations in groundwater levels. Appendix F (see also Hylland and others, 2022) presents the OSL ages as the mean and one-sigma uncertainty rounded to the nearest decade; where discussed in the text, however, the error is doubled ( $2\sigma$  rounded to the nearest century) for continuity with the calendar-calibrated radiocarbon ages and the modeling of earthquake times using OxCal. In discussing the OSL ages, we report the ages in thousands of calendar years before the sample processing date (2016) and did not adjust for the 66-year difference in the processing date versus the reference standard for  $^{14}\text{C}$  (1950 CE). This difference is minor compared to the large OSL age uncertainties (400–2000 yr at  $2\sigma$ ) and is accounted for in OxCal modeling of earthquake times.

### OxCal Modeling Methods

To evaluate earthquake timing and associated uncertainties, we used OxCal radiocarbon calibration and analysis software (version 4.2.4; Bronk Ramsey, 1995, 2001, 2009; Bronk Ramsey and Lee, 2013). OxCal probabilistically models the

timing of undated events (such as earthquakes) by weighting the time distributions of chronological constraints (e.g., radiocarbon and luminescence ages and historical constraints) included in a stratigraphic model (Bronk Ramsey, 2008). OxCal generates a probability density function (PDF) for each event in the model—i.e., the likelihood that an earthquake occurred at a particular time—using the chronologic and stratigraphic constraints and a Markov-chain Monte Carlo sampling method (Bronk Ramsey, 2008). For more detailed discussions of the application of OxCal modeling to paleoseismic data, see Lienkaemper and Bronk Ramsey (2009) and DuRoss and others (2011).

The OxCal depositional model for the Airport East site (appendix G) uses stratigraphic ordering information, radiocarbon and OSL ages, and a historical constraint that no large surface-faulting earthquakes ( $\geq M \sim 6.5$ ) have occurred since 1847, to define the time distributions of paleoearthquakes at the site. Where necessary, we removed numerical-age outliers using geologic judgment (knowledge of sediments, soils, and sample contexts), the degree of inconsistency with other ages in the model for comparable deposits (e.g., stratigraphically inverted ages), and an agreement index between the original (unmodeled) and modeled numerical ages (Bronk Ramsey, 1995, 2008). We report earthquake time ranges as the mean and two-sigma uncertainty in thousands of calendar years B.P. rounded to the nearest century.

## AIRPORT EAST TRENCH SITE

### Surface Faulting and Geology

The Airport East site is near the northern end of the Taylorsville fault, and is crossed by a single east-facing, north-south trending scarp. The nearly flat site lies at an elevation of about 1284 m (AMSL), the same elevation as that of Great Salt Lake's historical highstand, reached in the late 1860s to early 1870s and again in 1986–87. The site is about 3 m lower than the 1287 m elevation of the late Holocene highstand of Great Salt Lake (Currey and others, 1988; Murchison, 1989); this highstand occurred during one or more lake expansions sometime between about 1.3 and 4.8 ka (Currey and others, 1988; Murchison, 1989; Miller and others, 2005).

Geologic deposits at the Airport East site include mid- to late Holocene fine-grained wetland, paludal (marsh), lacustrine, deltaic, and fluvial sediments, mostly associated with the Jordan River. The modern Jordan River channel lies 1 km east of the Airport East site. However, the river channel has migrated eastward in Holocene time, possibly in response to tectonic tilting and subsidence associated with normal faulting along the SLCS (Keaton, 1987; McKean and Hylland, 2019a). At the Baileys Lake trench site on the Granger fault 5 km west of the Airport East site, a Jordan River paleochannel cuts the fault scarp, where paleoseismic data indicate the most recent

surface faulting occurred at  $5.5 \pm 0.8$  ka (Hylland and others, 2014); therefore, the Jordan River paleochannel in the Baileys Lake area was abandoned sometime after 5.5 ka.

### Taylorsville Fault Scarp and Surface Offset

The fault scarp that crosses the Airport East site is a relatively short, semi-arcuate strand that is part of an en echelon series of scarps that make up the northern half of the Taylorsville fault (figure 2). The geomorphically subtle, east-facing scarp has 0.4 to 0.5 m of vertical surface offset based on projections of the upper and lower ground surfaces along two east-west-trending profiles (figure 7). However, the surficial deposits on the hanging wall are younger than the surficial deposits on the footwall, so the measured surface offset across the scarp is less than the net vertical displacement across the fault zone (see Taylorsville Fault section below). Both the north and south ends of the scarp are crossed by the Interstate 215 highway embankment.

### Trench Stratigraphy and Structure

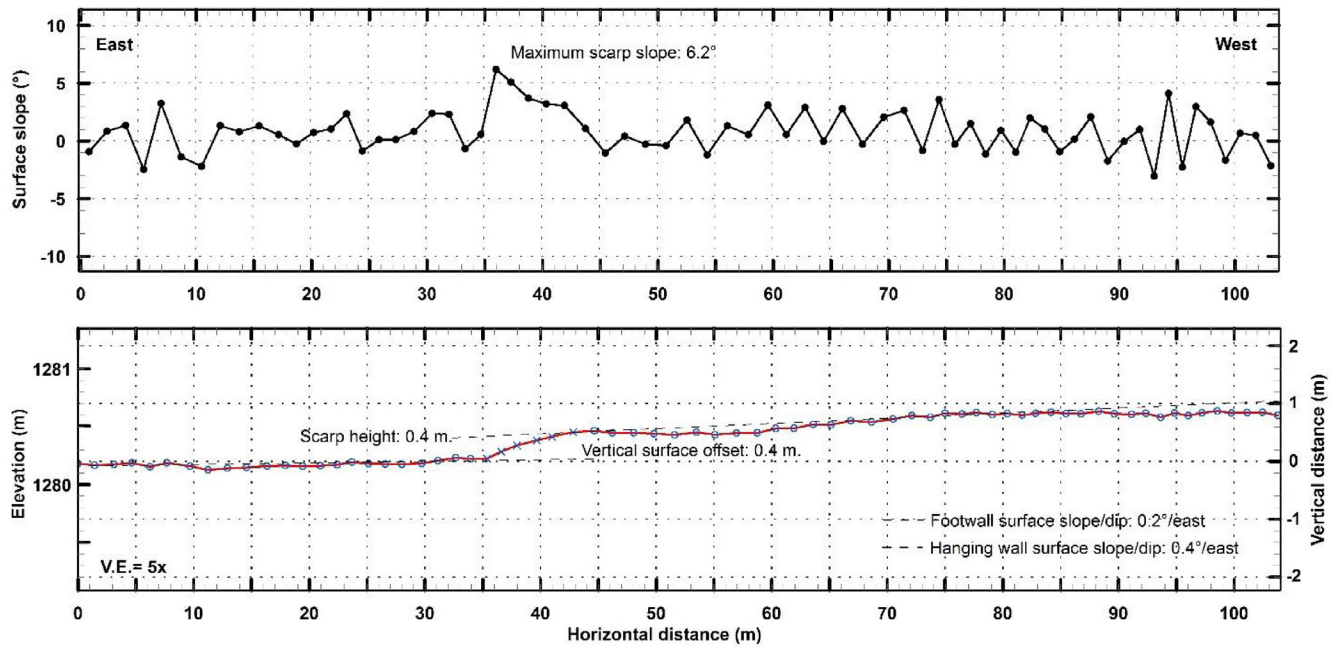
The deposits exposed by our trenches at the Airport East site are dominated by fine-grained wetland, marsh, and fluvial overbank sediments, with minor lacustrine interbeds and scarp-derived colluvium. We also encountered sandy fluvial channel sediments in hand-auger holes in the floor of the South trench. See plates 1 and 2 for logs and photomosaics of the exposed stratigraphy, and appendices A and C for descriptions of the stratigraphic units.

### Wetland and Fluvial Channel Deposits

A distinctive silty clay (unit 11) was present at the base of the footwall exposures. The grayish brown clay contains two thin (5–10 cm), dark, seemingly organic-rich layers that indicate the unit is deformed in broad, open folds (wavelength approximately several meters). A bulk sample from one of the dark layers returned no charred floral remains for radiocarbon dating. However, silt from this unit yielded an OSL age of  $4.3 \pm 0.5$  ka. The silt was obtained from sample AE-N-L3 (discussed further below), which targeted a thin sand dike exposed in the North trench (plate 2); the silt represents in situ unit 11 sediment adjacent to the injected sand. We interpret unit 11 as a sequence of wetland deposits based on the clayey sediment and abundant gastropod (*Lymnaea*) shells.

Underlying unit 11, we encountered dark gray, fine, mica-rich quartz sand (unit 10) in our auger holes. In the hanging wall of the South trench (h-30, v-0.8), we advanced the auger 90 cm into the sand before sloughing of the saturated sand prevented us from augering deeper (bottom of hole was 3 m below the trench floor). The sand coarsened with depth, becoming medium grained at the bottom of the hole. Compressed, lignified root fragments recovered from the bottom of the hole yielded an age of  $6.3 \pm 0.1$  ka (AE-S-RC23), and an OSL sample of

### Scarp Profile 1



### Scarp Profile 2

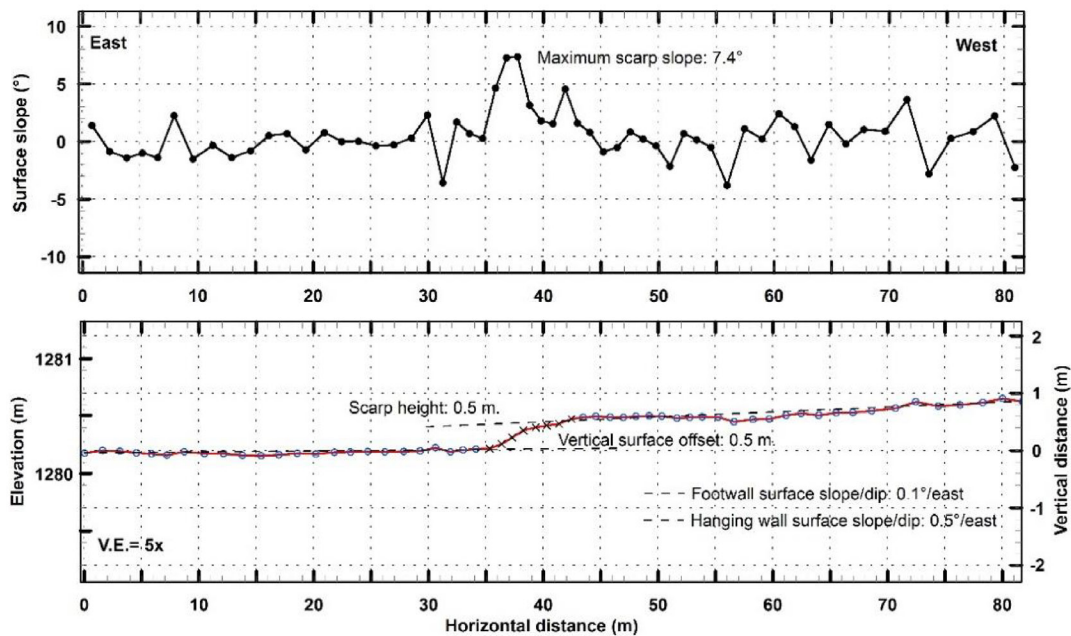


**Figure 7.** Scarp profiles and surface slope plots across the Airport East site; profile locations shown on figure 5. Profile points measured using high-precision GPS. Elevation is relative to mean sea level, vertical distance is relative to minimum surface elevation along each profile. Scarp height is the vertical distance between the intersections of the maximum scarp slope with the upper and lower surface-slope projections. Vertical exaggeration = 5x.

the sand collected from an auger hole in the footwall of the South trench (h-36, v-1.45) yielded an age of  $5.0 \pm 0.5$  ka (AE-S-L1). We interpret the sand as fluvial channel deposits, possibly correlative with the “young lacustrine and deltaic deposits” mapped in the area by McKean (2014).

In both the South and North trenches, we observed several sand dikes that had been injected upward into unit 11 (figure 8), likely as the result of liquefaction during strong ground shaking. We did not observe any of the sand dikes extending into any deposits overlying unit 11. The source and depth of the injected sand are unknown; however, the sand from a dike in the North trench yielded an OSL age of  $12.8 \pm 2.0$  ka (AE-N-L3), indicating that the sand originated as lacustrine sand deposited near or at the end of the regressive phase of Lake Bonneville (~14–13 ka; Oviatt, 2015).

### Fluvial Overbank, Marsh, and Lacustrine Deposits

We interpret units 12, 13, and 14 to be a mixture of fluvial and marsh sediments deposited on the Jordan River floodplain. All three units consist of very dark grayish brown to dark gray clayey silt and contain abundant gastropod (*Lymnaea*)

shells, stonewort (*Chara*), bulrush (*Scirpus*), and unidentified ostracodes (see appendix D). Unit 12 overlies an angular unconformity, and the base of unit 12 contains rip-up clasts of the underlying grayish brown clay of unit 11. Two charcoal samples from the top (AE-S-RC15) and middle (AE-S-RC20) of unit 12 each yielded an age of  $4.9 \pm 0.1$  ka. Locally, we observed weak soil development at the top of unit 12 (e.g., South trench, between h-47.3 and h-49.3; plate 1). Unit 13 conformably overlies and is texturally similar to unit 12, but has a slightly lighter color, and unit 14 conformably overlies unit 13 and is very similar to unit 12 in color and texture. Charcoal from unit 14 yielded an age of  $2.7 \pm 0.2$  ka (AE-S-RC1).

Unit 15 is a distinctive package of black silty clay containing thin, light yellowish brown silt and fine sand interbeds. The black silty clay is organic rich; organic remains included bulrush (*Scirpus*), gastropod (*Lymnaea*) shells, and unidentified ostracodes and bone fragments (see appendix D), indicating marsh deposition. Charcoal yielded ages of  $2.3 \pm 0.1$  ka (AE-S-RC2a) from the bottom of unit 15 and  $1.1 \pm 0.1$  ka (AE-S-RC6a) from the top of the unit. This age range indicates deposition during the late Holocene highstand of Great Salt Lake based on timing data reported by Currey and oth-

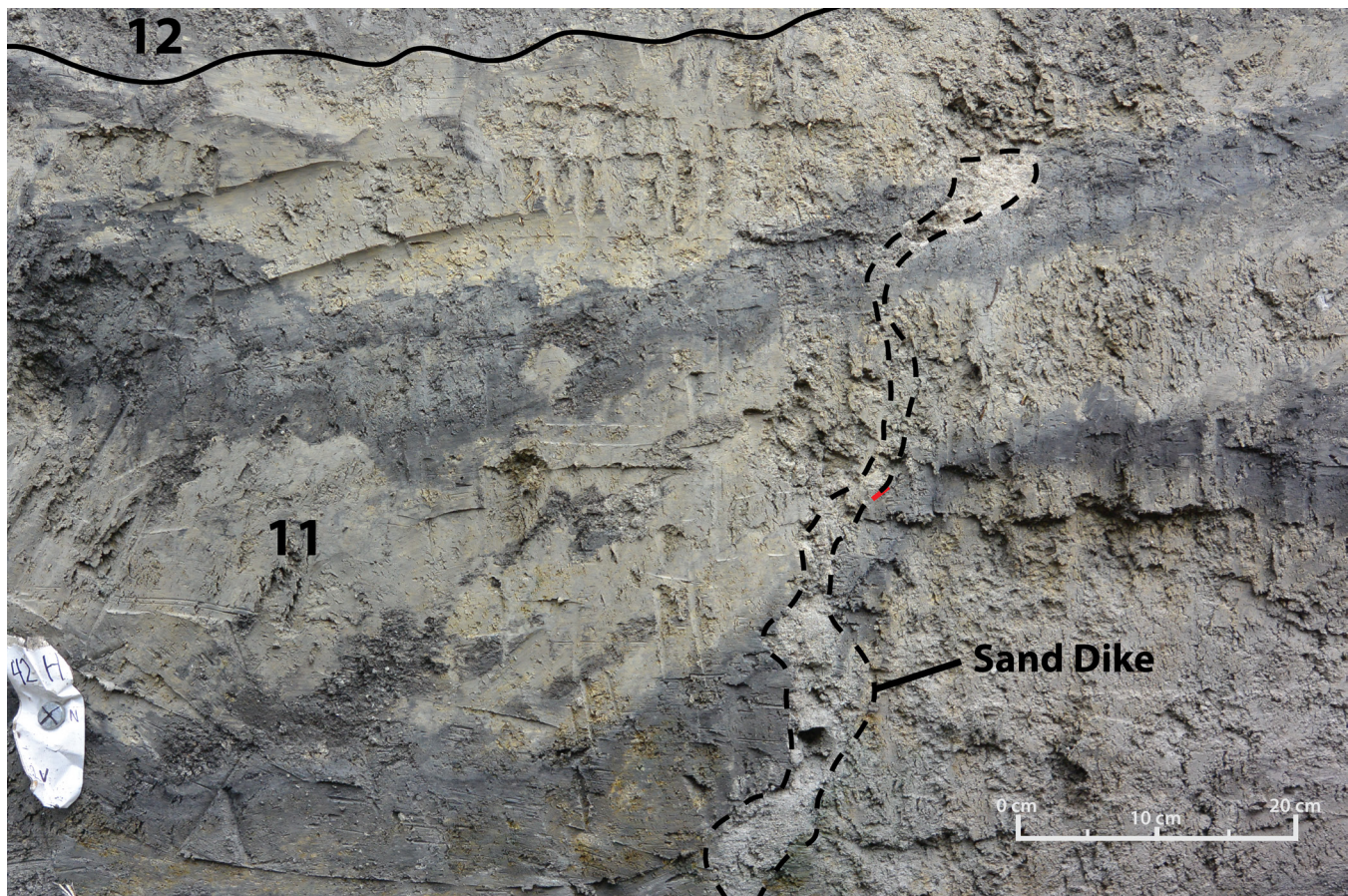


**Figure 8.** Liquefaction-induced sand dike in the North trench (at approximately grid line h-42.5, v-2.2). This and other sand dikes observed do not extend above unit 11 (see plates 1 and 2). A local “sag,” presumably formed as the result of localized subsidence over an area of evacuated liquefied sand, is evident from the folded dark marker beds within unit 11. Contact between units 11 and 12 indicated by solid black line.

ers (1988), Murchison (1989), and Miller and others (2005). The light yellowish brown silt and fine sand within unit 15 comprises three thin (<7 cm), discontinuous, but laterally persistent, interbeds. Microscopic examination of samples from these interbeds revealed the silt and fine sand is dominantly quartz, and the samples contained abundant clear crystal blades that X-ray diffraction identified as gypsum (Peter Nielsen, UGS, written communication, 2015). We interpret the thin interbeds as transgressive lacustrine sands deposited within the marsh deposits as Great Salt Lake episodically expanded across the site during the late Holocene highstand. The uppermost interbed yielded an OSL age of  $1.9 \pm 0.4$  ka (AE-S-L2); although this age falls within the age range of the late Holocene highstand, it appears somewhat old relative to the  $1.1 \pm 0.1$  ka age at the top of unit 15. This can perhaps be explained by the luminescence signal not being completely reset during this final depositional event (i.e., filtered light in turbid water), so that the sample retained an inherited age associated with earlier transport and deposition of the sediment into the lake. This interpretation is consistent with the relatively high scatter value (39%) associated with sample AE-S-L2 (see appendix F).

Unit 16 conformably overlies the unit 15 marsh deposits and consists of gray clay capped by a weakly developed pedogenic soil. Organic remains in the clay include bulrush (*Scirpus*), cattail (*Typha*), stonewort (*Chara*), gastropod (*Lymnaea*) shells, and unidentified ostracodes (see appendix D), indicating wetland or shallow lake deposition. Two charcoal samples (AE-S-RC7a and AE-S-RC8a) each yielded an age of  $0.8 \pm 0.1$  ka. Unit 16 appears to be similar to surficial “young lacustrine deposits” mapped in the area by McKean (2014), which include two nearby historical lakes mentioned by Van Horn (1982): Hot Springs Lake (1869) at Becks Hot Springs about 3.5 km northeast of the Airport East site, and Smith Lake (1906) south of the Salt Lake City International Airport about 4 km southwest of the Airport East site.

The youngest deposits (unit 17), present only in the hanging walls of the trenches, consist of dark gray silt and silty clay capped by the modern soil. The lower part of the unit (17a) has a 2-cm-thick burn layer at its top. Organic remains in unit 17 include bulrush (*Scirpus*) and gastropod (*Lymnaea*) shells. Charcoal yielded ages of  $0.5 \pm 0.01$  ka (AE-S-RC11) and  $0.4 \pm 0.1$  ka (AE-S-RC12a). These deposits, which we interpret as fluvial overbank and marsh deposits, likely correlate with the “young stream deposits, undivided” map unit of McKean (2014), which are widespread across the present Jordan River floodplain.

The South trench shows that the entire stratigraphic section exposed in the footwall of the Taylorsville fault is broadly warped (plate 1), likely as the result of slip on the fault. Also, unit contacts and interbeds show evidence of local soft-sediment deformation, likely the response of wet sediment to strong ground shaking.

## Scarp-Derived Colluvium and Related Deposits

We identified three separate lens- or wedge-shaped, organic-rich sedimentary deposits—oldest to youngest, units C3 to C1, herein generally referred to as “wedge” deposits—on the hanging wall of the Taylorsville fault (figure 9; plates 1 and 2; appendix C). These deposits are thin (~10 cm) and of limited lateral extent (<2 m horizontally) and are distinct from sedimentary units 11–17 and pedogenic units 16A and 17A, which are thicker (tens of centimeters) and substantially more laterally extensive (tens of meters). Several observations suggest that these wedge deposits are related to surface-faulting earthquakes on the Taylorsville fault. First, these deposits are restricted to the fault hanging wall, are thickest at what at the time of deposition would have been the base of the fault scarp, thin toward the former scarp crest, and pinch out away from the fault, all consistent with a scarp-derived colluvial origin. Second, units C1 and C2 are deposited on pedogenic units (a burn horizon within unit 17 and soil horizon 16A, respectively), suggesting rapid deposition. Third, upward fault terminations and differential stratigraphic thickening of associated deposits suggest a tectonic origin. For example, unit 15, which contains unit C3, exhibits stratigraphic growth on the hanging wall of the fault. At the western end of unit C3, basal interbeds within unit 15 (below C3) are clearly faulted, whereas the uppermost interbeds (above C3) appear to have draped the former scarp (before being faulted by a later rupture). Many faults clearly expressed within units 12–16 terminate below the uppermost parts of unit 16 and unit 16A and thus predate unit C2. Finally, units C2 and overlying unit 17 are clearly offset by a fault splay which then terminates below unfaulted unit C1.

Unit C3 is an organic-rich subunit of the unit 15 marsh deposits. This wedge likely contains a component of colluvial sediment eroded from the scarp, but primarily comprises marsh deposits that thicken adjacent to the fault. Unit C3 formed in response to down-to-the-east slip along a fault trace about 0.5 m east of the main Taylorsville fault trace. Unit C3 is itself offset by subsidiary faults active in a subsequent faulting event. The C3 wedge extends over a horizontal distance of about 1.4 m and attains a maximum thickness of about 10 cm in the South trench. Charcoal from the base of the C3 wedge yielded an age of  $1.8 \pm 0.1$  ka (AE-S-RC4a).

Unit C2 is an organic-rich deposit of clayey colluvial sediment derived from unit 16. Unit C2 accumulated on the hanging wall of the main Taylorsville fault trace and overlies the paleosol developed on unit 16. The C2 wedge extends over a horizontal distance of about 1.5 m and attains a maximum thickness of about 12 cm in the South trench. At that location, unit C2 is offset down-to-the-west by a subsidiary fault that is antithetic to the main Taylorsville fault trace. Charcoal from the C2 colluvium yielded an age of  $0.5 \pm 0.04$  ka (AE-S-RC10a).

Unit C1 is an organic-rich, silty colluvial deposit that was difficult to differentiate from unit 17b and is partly obscured by

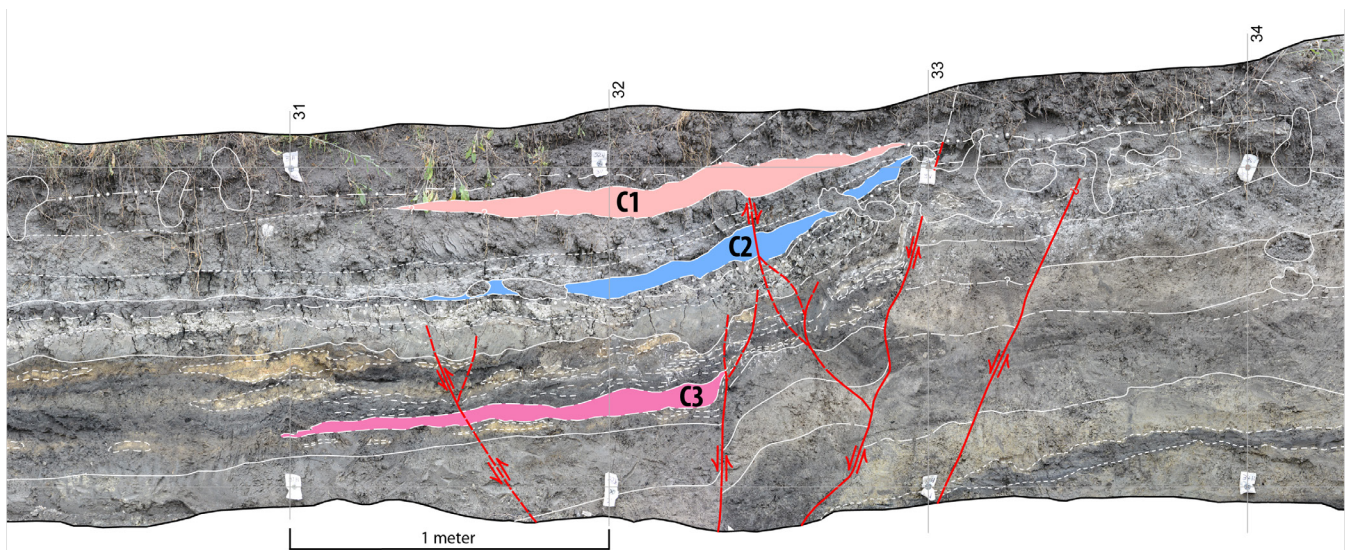


**Figure 9.** Fault-zone exposure in the south wall of the South trench, showing thin, wedge-shaped units of scarp-derived colluvium and related deposits (C1, C2, and C3) associated with the three most recent surface-faulting earthquakes (AE1, AE2, and AE3) at the Airport East site. Fault traces shown in red, other contacts shown in white. Grid line spacing is 1 meter. See plate 1 for trench log details.

modern soil development. The wedge was largely identified by its extremely loose texture and the upward termination of a fault (the fault that cuts unit C2) at its base. The C1 wedge accumulated on the hanging wall of the main Taylorsville fault trace, extends over a horizontal distance of about 1.6 m, and attains a maximum thickness of about 10 cm in the South trench. Charcoal from the C1 colluvium yielded ages of  $0.2 \pm 0.2$  ka (AE-S-RC17a) and  $0.5 \pm 0.01$  ka (AE-S-RC17b).

### Taylorsville Fault

In the South trench, the Taylorsville fault comprises three east-dipping fault traces, several subsidiary antithetic traces, and a fault-related monoclinical fold in a deformation zone about 4 m wide (between h-30.5 and h-34.5; plate 1, figure 9). The main fault trace dips about  $40^{\circ}$ – $75^{\circ}$  E. and is traceable upward into the modern soil. Offset of the contacts between units 12 through 15 indicates 27 cm of vertical displacement on this fault trace. We were unable to determine if differential displacements exist across the main fault trace because of (1) a lack of identifiable strata younger than unit 16 in the footwall, (2) complex deformation of units 15 and 16 in the fault zone, and (3) krotovinas (infilled animal burrows) in the fault zone. However, given that the C3 wedge is not adjacent to the main fault trace, this fault trace apparently underwent no surface-faulting displacement during the earthquake responsible for C3 wedge formation. The position of both younger colluvial wedges adjacent to the main fault trace indicates surface faulting displacement on this fault trace during the earthquakes responsible for both C2 and C1 wedge formation. Also, a mean vertical displacement of 13.5 cm (27 cm divided by two events) is very similar to the maximum thicknesses of units C2 (12 cm) and C1 (10 cm).

The two other east-dipping fault traces exposed in the South trench include a subsidiary trace about 0.4 m west of the main

fault trace, and a subsidiary trace about 0.5 m east of the main fault trace (plate 1). The western subsidiary trace is subparallel to the main fault trace and shows about 4 cm of vertical displacement of contacts between units 11 through 15. This fault trace appears to terminate within unit 15, so it is possible that this fault trace moved during the surface-faulting earthquake responsible for C3 wedge development. However, movement of this fault trace during either, or both, of the two younger surface-faulting events cannot be ruled out. The eastern subsidiary fault trace was apparently responsible for formation of the C3 wedge. This fault trace has a near-vertical orientation below unit C3 and shows about 7 to 10 cm of displacement of contacts between units 13 through 15. A splay of this fault trace offsets the C3 wedge, indicating reactivation and upward extension of this fault trace during a subsequent faulting event.

In the South trench, several antithetic fault traces having an average dip of  $58^{\circ}$  W. are present in the hanging wall of the main Taylorsville fault trace (plate 1). The most significant of these is an antithetic splay off of the main Taylorsville fault trace. This splay cuts units 13 through 17 and terminates at the base of the C1 colluvial wedge, so it formed during the earthquake responsible for C1 wedge formation. This splay shows about 2 cm of down-to-the-west vertical displacement.

The geometry of faulting in the North trench is generally similar to that in the South trench. However, displacement is more evenly distributed across the various fault traces (plate 2). Also, monoclinical folding in the North trench accounts for a larger component of the net vertical displacement across the fault zone than it does in the South trench. Both synthetic (east-dipping) and antithetic fault traces in the North trench have dips in the range of  $70^{\circ}$ – $84^{\circ}$ . Similar to the South trench, the C3 wedge in the North trench is cut by faults, but the C2 wedge is not. Also, we identified no clear fault terminations at the bases of the three wedge units in the North trench.

To calculate total net vertical displacement across the Taylorsville fault at the Airport East site, we measured the vertical offset between footwall and hanging-wall projections of the contact between units 14 and 15. This contact, which dates to about 2.5 ka based on bracketing radiocarbon ages, was well exposed on the footwall and hanging wall in both the South and North trenches and predates the oldest identified wedge deposit (unit C3). Away from the fault-related monoclinical folding, hanging-wall strata are flat to slightly east dipping at approximately  $1^\circ$  (plates 1 and 2). The footwall strata are broadly folded, which adds uncertainty in the net vertical displacement calculation but does not affect the result in a significant way. Near the fault in the South trench (h-34.5, plate 1), the elevation of the unit 14–15 contact is at v-3.0; the elevation of this contact is also at v-3.0 near the west end of the trench (h-68.5), indicating no net vertical offset of strata across 34 m of the footwall. In other words, all of the net vertical displacement at the site takes place within the 4-m-wide deformation zone at the fault. If the v-3.0 elevation is assumed to represent an “undisplaced” unit 14–15 contact footwall reference elevation, then the vertical offset measured to the projected hanging-wall contact at h-33.5 in the South trench is 1.1 m. We also estimated an “undisplaced” unit 14–15 contact reference elevation by averaging the highest (v-3.1) and lowest (v-2.4) elevations of the contact observed in the South trench footwall. Using a footwall reference elevation of h-2.75, the vertical offset measured to the projected hanging-wall contact at h-33.5 in the South trench is 0.8 m. Taking into consideration the uncertainty in determining the average dip as well as

the appropriate reference elevation of the unit 14–15 contact in the footwall, stratigraphic offset of the unit 14–15 contact in both the South and North trenches indicates total net vertical displacement of  $0.9 \pm 0.2$  m (table 1).

We also used projections of the subsurface contact between units 10 and 11 encountered in hand-auger boreholes in the floor of the South trench to calculate total net vertical displacement across the fault, as well as determine if any differential displacement exists between pre- and post-unit 14 strata. Taking into consideration the uncertainty in determining the precise location of the contact, we estimate the total net vertical displacement is  $0.8 \pm 0.2$  m (table 1). Because of the overlap between this value and the displacement values determined from the unit 14–15 contact, no strong evidence for differential displacement exists. This indicates that the liquefaction features at the Airport East site are likely the result of ground shaking triggered by slip on a fault elsewhere in the region, rather than being associated with Taylorsville-fault slip at the site. Combining the results of the unit 14–15 contact offset and the unit 10–11 contact offset, the calculated range of total net vertical displacement across the Taylorsville fault at the Airport East site is 0.6–1.1 m (table 1).

To estimate per-event vertical displacements, we applied two methods: (1) dividing total net vertical displacement by the number of documented surface-faulting earthquakes (i.e., number of earthquake-related wedge deposits), and (2) using wedge-deposit thickness as a proxy for fault displacement

**Table 1.** Vertical displacement data for the Taylorsville fault, Airport East site.

<b>Net Vertical Displacement:</b>					
	<b>Total (m)</b>		<b>Mean Per-Event<sup>1</sup> (m)</b>		
Post-unit 14 (South trench)	0.9 ± 0.2		0.30 ± 0.07		
Post-unit 14 (North trench)	0.9 ± 0.2		0.30 ± 0.07		
Post-unit 10 (South trench)	0.8 ± 0.2		0.27 ± 0.07		
RANGE	0.6–1.1		0.20–0.37		

<b>Wedge-Deposit Thickness:</b>					
<b>Wedge<sup>2</sup></b>	<b>Max. Thickness<sup>3</sup> (m)</b>	<b>Percent Total Thickness</b>	<b>Per-Event Displacement</b>		
			<b>2x Max. Thickness<sup>4</sup> (m)</b>	<b>Apportioned<sup>5</sup> (0.6 m total displacement) (m)</b>	<b>Apportioned<sup>5</sup> (1.1 m total displacement) (m)</b>
C1	0.10	31%	0.20	0.19	0.34
C2	0.12	38%	0.24	0.23	0.42
C3	0.10	31%	0.20	0.19	0.34
TOTAL	0.32	100%	0.64		
RANGE			0.20–0.24 (mean = 0.22)	0.19–0.42 (mean = 0.30)	

<sup>1</sup> Net vertical displacement divided by three events (earthquakes AE1, AE2, and AE3).

<sup>2</sup> Wedge deposits correspond to earthquakes as follows: C1 = AE1, C2 = AE2, C3 = AE3.

<sup>3</sup> Maximum wedge-deposit thickness as measured in the Airport East trenches.

<sup>4</sup> Double wedge-deposit thickness used as proxy for vertical displacement (e.g., Ostenaar, 1984; McCalpin and others, 1994).

<sup>5</sup> Apportioned per-event vertical displacement based on ratio (percentage) of individual maximum wedge thickness to total maximum thickness of all wedges applied to total net displacement range (e.g., Nelson and others, 2006).

(see DuRoss, 2008). Dividing the range of total net displacement discussed in the preceding paragraph (0.6–1.1 m) by three yields a mean per-event vertical displacement range of 0.20–0.37 m (table 1). As described above and summarized in table 1, maximum thickness of wedge units C1, C2, and C3 is 0.10 to 0.12 m. Doubling these thicknesses to provide a proxy for fault displacement (e.g., Ostenaar, 1984; McCauley and others, 1994) yields per-event displacements of 0.20 to 0.24 m (table 1). Finally, using wedge-deposit thickness to apportion total displacement among individual events (e.g., Nelson and others, 2006) yields per-event displacements of 0.19–0.23 m (using a total displacement value of 0.6 m) and 0.34–0.42 m (using a total displacement value of 1.1 m) (table 1). Considering all the data, calculations of mean late Holocene per-event vertical displacement on the Taylorsville fault at the Airport East site range from 0.20 to 0.37 m.

## Paleoseismology of the Airport East Site

### Chronology of Surface-Faulting Earthquakes

At the Airport East site, three surface-faulting earthquakes (designated AE1 through AE3) associated with movement on the Taylorsville fault have occurred in the late Holocene. We observed evidence of four paleoearthquakes in the trench exposures, but the earliest earthquake (which we designate as LE1 [“liquefaction event 1”]) cannot be directly attributed to slip on the Taylorsville fault at the Airport East site. The other three earthquakes produced stratigraphic offsets that can be directly tied to discrete fault traces, as well as associated scarp-derived colluvium and related deposits, in the trench exposures. OxCal modeling of the earthquake times is presented in appendix G, and the results are shown on figures 10 and 11 and in table 2.

The earliest earthquake documented in the Airport East trenches, earthquake LE1, occurred at  $5.1 \pm 0.3$  ka. Evidence for earthquake LE1 consists of ground deformation (relatively small-scale folding and soft-sediment deformation), presumably the result of strong ground shaking, that affected unit 11 but not deposits overlying unit 11. Therefore, the unconformable contact between units 11 and 12 (i.e., the former ground surface at the time of unit 11 deposition, subsequently modified by the pre-unit 12 unconformity) represents the event horizon associated with this earthquake. Evidence for liquefaction during this earthquake includes sand dikes that were injected upward no higher than unit 11 (figure 8), and spatially associated “sags” that presumably formed as the result of localized subsidence over areas of evacuated liquefied sand (e.g., see plate 2, h-36 and h-42). We were unable to excavate the trenches deep enough to expose the unit 11–12 contact in the hanging wall of the fault zone, so the presence of scarp-derived colluvium associated with this event horizon is unknown. We cannot directly tie earthquake LE1 to movement on the Taylorsville fault, and it is possible (likely?) that the ground deformation at the Airport East site was produced

by ground shaking from a large earthquake triggered by slip on some other nearby fault (see discussion in the Taylorsville Fault section above). The timing of this earthquake is constrained by an OSL age of  $5.0 \pm 0.5$  ka (AE-S-L1) from near the top of unit 10 providing a maximum limit, and a charcoal age of  $4.9 \pm 0.1$  ka (AE-S-RC15 and AE-S-RC20) from the top of unit 12 providing a minimum limit.

Earthquake AE3 occurred at  $2.0 \pm 0.3$  ka, which was during the late Holocene highstand of Great Salt Lake (Currey and others, 1988; Murchison, 1989; Miller and others, 2005). This earthquake is based on fault offset of units 12 through 15 east of the main Taylorsville fault trace, differential displacement within unit 15, and the wedge of thickened marsh deposits (unit C3) on the hanging wall adjacent to the fault. A charcoal age of  $2.3 \pm 0.1$  ka (AE-S-RC2a) from the base of unit 15 provides a close maximum limit on the earthquake time, and a charcoal age of  $1.8 \pm 0.1$  ka (AE-S-RC4a) from the unit C3 wedge deposits provides a minimum limit. The timing of the earthquake within the span of the late Holocene highstand of Great Salt Lake implies deposition of the unit C3 wedge in shallow surface water during episodic lake expansions associated with the highstand.

Earthquake AE2 occurred at  $0.6 \pm 0.2$  ka and is based on the thin wedge of scarp-derived colluvium (unit C2) that directly overlies the paleosol developed on unit 16. A charcoal age of  $0.8 \pm 0.1$  ka (AE-S-RC8a) from the paleosol provides a close maximum limit on the earthquake time, and a charcoal age of  $0.5 \pm 0.04$  ka (AE-S-RC10a) from the unit C2 wedge deposits provides a minimum limit.

Earthquake AE1 occurred at  $0.4 \pm 0.2$  ka and is based on the thin wedge of scarp-derived colluvium (unit C1) within unit 17, and the antithetic fault trace that cuts the unit C2 wedge and terminates at the base of the unit C1 wedge. A charcoal age of  $0.5 \pm 0.1$  ka (AE-S-RC11) from the base of unit 17b provides a maximum limit on the earthquake time, and a charcoal age of  $0.2 \pm 0.2$  ka (AE-S-RC17a) from the unit C1 wedge deposits provides a minimum limit. We prefer the  $0.2 \pm 0.2$  ka age as a minimum limit on earthquake timing rather than the  $0.5 \pm 0.01$  ka age from sample AE-S-RC17b, given that ages of  $\sim 0.5$  ka were also obtained from stratigraphically lower deposits, including the C2 wedge deposits.

### Earthquake Recurrence and Fault Slip Rate

We calculated recurrence intervals between individual Airport East surface-faulting earthquakes (inter-event recurrence) and over several earthquake cycles (mean recurrence). Using the mean earthquake times, inter-event recurrence intervals for the Taylorsville fault at the Airport East site vary from 200 yr for the AE2–AE1 interval to 1400 yr for the AE3–AE2 interval (table 3). We also calculated inter-event recurrence for the LE1–AE3 interval (3100 yr). However, as discussed above, earthquake LE1 cannot be directly attributed to slip on

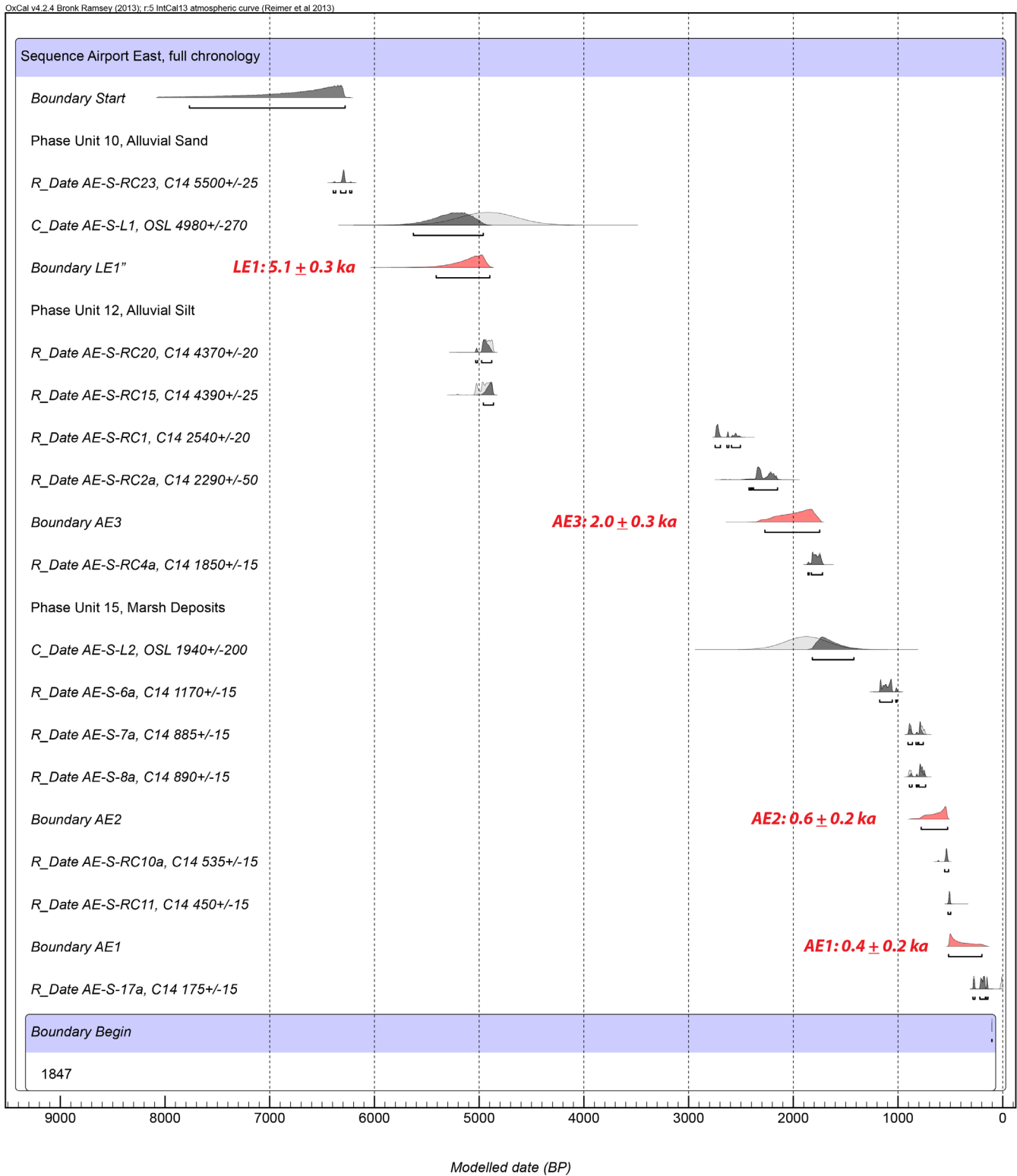


**Figure 10.** OxCal model for the Airport East site, showing stratigraphic ordering of radiocarbon and luminescence ages (appendices E and F) and probability density functions (PDFs) for the timing of earthquakes AE1–AE3 and LE1 (red). Appendix G presents a summary table of the model output. The model includes **C\_Date** for luminescence ages, **R\_Date** for radiocarbon ages, **Phase** for groups of ages where the relative stratigraphic ordering is unknown, and **Boundary** for undated events (e.g., earthquakes); see DuRoss and others (2011) for a general discussion of OxCal modeling applied to paleoseismic studies. Model constructed using OxCal version 4.2.4 (Bronk Ramsey and Lee, 2013) and the IntCal13 terrestrial radiocarbon calibration curve (Reimer and others, 2013). Brackets below PDFs indicate 2σ time ranges.

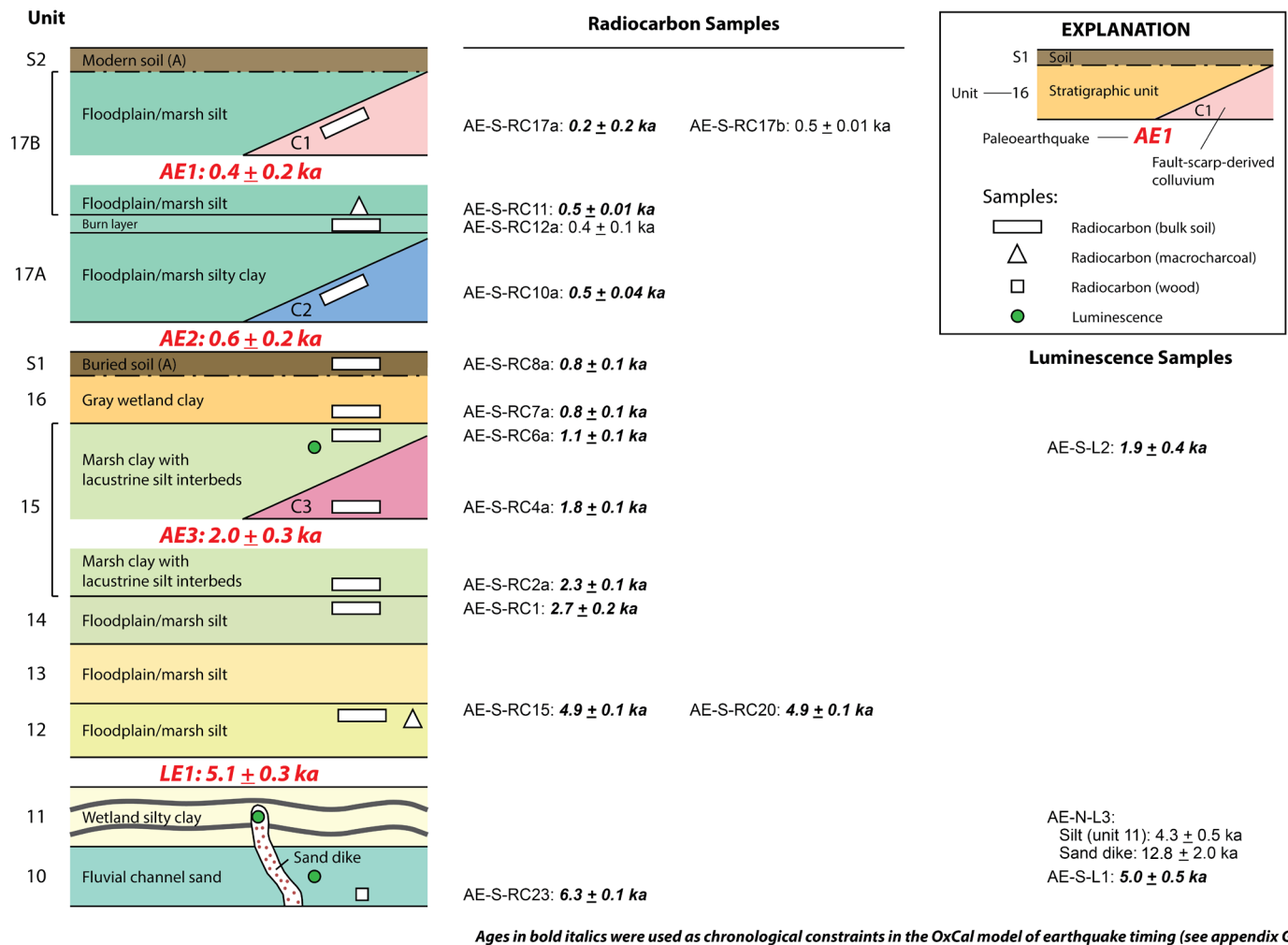


**Figure 11.** Chronostratigraphic summary for the Airport East site, showing timing of earthquakes AE1 through LE1 as modeled in OxCal (see figure 10 and appendix G). Earthquake times and all numerical ages are reported with  $2\sigma$  uncertainty. Refer to appendices E (radiocarbon ages) and F (luminescence ages) for details.

**Table 2.** Summary of earthquake timing and displacement data, Airport East site.

Event <sup>1</sup>	Mean <sup>2</sup> (ka)	$\pm 2\sigma^2$ (kyr)	5% <sup>2</sup> (ka)	95% <sup>2</sup> (ka)	Displacement <sup>3</sup> (m)	Unit <sup>4</sup>
AE1	0.39	0.20	0.20	0.52	0.28 (0.19–0.37)	C1
AE2	0.63	0.16	0.53	0.78	0.32 (0.23–0.42)	C2
AE3	1.98	0.29	1.75	2.27	0.28 (0.19–0.37)	C3
LE1 <sup>5</sup>	5.09	0.26	4.90	5.36	—	—

<sup>1</sup> Earthquake identified at the Airport East site and modeled in OxCal (figure 10; appendix G).

<sup>2</sup> Mean earthquake times,  $2\sigma$  ranges, and 5th–95th percentile ranges based on the OxCal model (appendix G).

<sup>3</sup> Per-event vertical displacement (mean and range); range based on average displacement and wedge-deposit thickness data (see table 1).

<sup>4</sup> Trench-log unit for scarp-derived colluvium and related deposits (wedge deposits) corresponding to the individual earthquakes (plates 1 and 2; appendix C).

<sup>5</sup> Earthquake LE1 cannot be directly attributed to movement on the Taylorsville fault at the Airport East site (i.e., deformation at the Airport East site is likely the result of shaking from an earthquake on an unknown source).

the Taylorsville fault, so this recurrence interval may not be a valid parameter for Taylorsville-fault earthquakes. Using the two intervals between AE3 and AE1, the mean late Holocene (post-2 ka) recurrence interval for the Taylorsville fault at the Airport East site is 800 yr (table 3).

We calculated both paleoseismic (closed-interval) and geologic (open-interval) slip rates for the Taylorsville fault at the Airport East site. Paleoseismic slip rates are 1.4 mm/yr using the vertical displacement of AE1 and the elapsed time between AE2 and AE1, 0.23 mm/yr using the vertical displacement of AE2 and the elapsed time between AE3 and AE2, and 0.37 mm/yr using the combined vertical displacement of AE2 and AE1 and the elapsed time between AE3 and AE1 (table 4). Geologic (average) slip rates range from 0.1–0.2 mm/yr over

the past ~5000 yr (post-unit 10 time) to 0.2–0.4 mm/yr over the past ~2500 yr (post-unit 14 time) (table 5).

When considering these recurrence intervals and slip rates, it is important to keep in mind the spatial and temporal limitations of the data. These recurrence intervals and slip rates are only applicable to the Airport East site, and they only relate to surface-faulting earthquake activity over the past ~5000 yr (with most of the data associated with earthquakes occurring since ~2.5 ka). As discussed further below, these data need to be considered within the context of the Taylorsville fault being part of a more extensive, distributed fault zone, one where the paleoseismic record is relatively short and incomplete, and where fault parameters for a given site on a given strand may differ markedly from other sites on other strands.

**Table 3.** Chronology and recurrence of surface-faulting earthquakes, Airport East site.

Airport East Earthquake	Earthquake Time (ka)	Chronology <sup>1</sup> (ka)	Inter-event RI <sup>2</sup> (kyr)
AE1	0.4 ± 0.2	<b>0.4</b> (0.2–0.6)	–
AE2	0.6 ± 0.2	<b>0.6</b> (0.4–0.8)	AE2–AE1: <b>0.2</b> (0–0.6)
AE3	2.0 ± 0.3	<b>2.0</b> (1.7–2.3)	AE3–AE2: <b>1.4</b> (0.9–1.9)
LE1 <sup>3</sup>	5.1 ± 0.3	5.1 (4.8–5.4)	LE1–AE3: 3.1 (2.5–3.7)

Interval	Elapsed Time (kyr)	Number of Intervals	Mean RI <sup>4</sup> (kyr)	Notes
AE3–AE1	1.6	2	0.8	–
LE1–AE1	4.7	3	1.6	LE1 may not be a Taylorsville fault event

<sup>1</sup> Chronology for the Airport East site based on mean earthquake times and 2σ ranges (bold where relation of earthquake to the Taylorsville fault is certain).

<sup>2</sup> Recurrence interval (RI) calculated from mean earthquake times (bold where relation of earthquake to the Taylorsville fault is certain), with minimum and maximum recurrence intervals calculated from 2σ ranges of earthquake times; RI=0 results from overlapping 2σ ranges.

<sup>3</sup> Earthquake LE1 cannot be directly attributed to movement on the Taylorsville fault at the Airport East site (i.e., deformation at the Airport East site is likely the result of shaking from an earthquake on an unknown source).

<sup>4</sup> Recurrence interval calculated from elapsed time between earthquakes (based on mean earthquake times) divided by number of inter-event time intervals.

**Table 4.** Paleoseismic (closed-interval) slip rates at the Airport East site.

Interval <sup>1</sup>	Displacement <sup>2</sup> (m)	Elapsed Time <sup>3</sup> (kyr)	Slip Rate <sup>4</sup> (mm/yr)
AE2–AE1	0.28 (0.19–0.37)	0.2	1.4 (1.0–1.8)
AE3–AE2	0.32 (0.23–0.42)	1.4	0.23 (0.16–0.30)
AE3–AE1	0.60 (0.42–0.79)	1.6	0.37 (0.26–0.49)

<sup>1</sup> Closed interval between indicated earthquakes.

<sup>2</sup> Vertical displacement (mean and range) between indicated earthquakes (data from table 2).

<sup>3</sup> Elapsed time between indicated earthquakes, based on mean earthquake times (table 3).

<sup>4</sup> Vertical slip rate (displacement divided by elapsed time; mean and range).

**Table 5.** Geologic (open-interval) slip rates at the Airport East site.

Displacement <sup>1</sup> (m)	Elapsed Time (kyr)	Average Slip Rate <sup>2</sup> (mm/yr)
0.6–1.1	~2.5 <sup>3</sup>	0.2–0.4
0.6–1.1	~5.0 <sup>4</sup>	0.1–0.2

<sup>1</sup> Cumulative vertical displacement for earthquakes AE1, AE2, and AE3 (data from table 1).

<sup>2</sup> Average vertical slip rate (displacement divided by elapsed time).

<sup>3</sup> Post-unit 14.

<sup>4</sup> Post-unit 10.

## PALEOSEISMOLOGY OF THE WEST VALLEY FAULT ZONE

### Correlation of Earthquakes

Presently available fault-trench data document at least eight surface-faulting earthquakes on the WVFZ— three on the Taylorsville fault and five (or more) on the Granger fault— since the time of the Lake Bonneville highstand around 18 ka. On the Taylorsville fault, three surface-faulting earthquakes have been documented at the Airport East site (AE1, AE2, and AE3; this study) and one earthquake has been documented at the nearby AGRA site (figure 2; also see Hylland and others, 2014, appendix H). Timing of the earthquake at the AGRA site ( $2.2 \pm 0.2$  ka) is very similar to the timing of Airport East earthquake AE3 ( $2.0 \pm 0.3$  ka), and we consider it likely that surface faulting at the two sites occurred during the same earthquake. A fourth earthquake at the Airport East site (LE1; this study), evident from liquefaction features and ground deformation, probably did not result from slip on the Taylorsville fault at the Airport East site. On the Granger fault, four (or more) surface-faulting earthquakes have been documented at the Baileys Lake site (BL1, BL2, BL3, and BL4; Hylland and others, 2014), and a fifth earthquake was documented in a consultant trench (Terracon site; see Hylland and others, 2014, appendix H).

When comparing the mean earthquake times of Taylorsville-fault earthquakes AE1, AE2, and AE3 with timing of the single latest Holocene earthquake on the Granger fault (documented at the Terracon site), no correlation of earthquakes is readily apparent (figure 12). As noted by Hylland and others (2014), large uncertainty exists in the timing of the Terracon earthquake due to the short duration of the study (precluding detailed logging) and the nature of the radiocarbon ages (AMRT ages from bulk-soil samples) used to constrain earthquake timing. Although the two-sigma uncertainties of the Terracon-earthquake timing overlap with those of earthquakes AE2 and AE3, the mean age of the Terracon earthquake differs by 700–800 yr from the mean ages of earthquakes AE2 and AE3. Thus, the current data do not present a compelling case for the Granger-fault earthquake at the Terracon site occurring at the same time as an earthquake on the Taylorsville fault.

As described above, radiocarbon and OSL ages constrain the timing of LE1 at the Airport East site to  $5.1 \pm 0.3$  ka. Earthquake BL1 at the Baileys Lake site on the Granger fault has roughly similar timing:  $5.5 \pm 0.8$  ka (Hylland and others, 2014). Given the similar mean times and overlapping two-sigma uncertainties, a correlation between the surface-faulting earthquake at the Baileys Lake site and the liquefaction event at the Airport East site seems reasonable. If one assumes that the deformation at both sites resulted from the same earthquake, the average of the modeled mean times for LE1 and BL1 (5.3 ka) may best represent the mean time of the earthquake.

### Earthquake Recurrence and Fault Slip Rate

Current paleoseismic data for the Taylorsville fault yield inter-event recurrence intervals for surface-faulting earthquakes ranging from 200 to 1500 yr, and a mean recurrence of 800 yr (table 6). By comparison, inter-event recurrence intervals for surface-faulting earthquakes on the Granger fault range from 700 to 6800 yr, and mean recurrence for different time periods ranges from 3600 to 5400 yr (Hylland and others, 2014). The time periods over which these recurrence intervals apply differ markedly; the Granger-fault chronology spans 15,700 yr, whereas the Taylorsville-fault chronology only spans 2100 yr. Also, the wide range (order-of-magnitude difference) in inter-event recurrence on both the Granger and Taylorsville faults likely reflects differences in surface-faulting activity on different strands of the faults as well as incomplete earthquake chronologies.

For the WVFZ as a whole, the eight surface-faulting earthquakes for which timing data exist yield inter-event recurrence intervals ranging from 200 to 7000 yr and mean recurrence over different time periods ranging from 500 to 2400 yr (table 7). Previously, mean recurrence estimates for the WVFZ calculated from individual earthquake timing data ranged from 2000 to 3600 yr (Hylland and others, 2014). The shorter recurrence intervals reported in this study result from the addition of the two most recent Taylorsville-fault earthquakes (AE1 and AE2) to the WVFZ earthquake chronology. Although we present recurrence data for the WVFZ as a whole, we reiterate that the WVFZ is a distributed fault system comprising numerous individual strands, and that substantial gaps likely remain in the earthquake chronology. Nevertheless, the limited paleoseismic data currently available do not support a model of synchronous ruptures on the various individual strands of the fault zone, but rather suggest movement of different strands of the fault zone during WVFZ surface-faulting earthquake events.

Earthquake timing and displacement data from the Airport East site yield geologic slip rates of 0.1–0.2 mm/yr (post-5 ka) and 0.2–0.4 mm/yr (post-2.5 ka) for this part of the Taylorsville fault. By comparison, data from the Baileys Lake site on the Granger fault yielded geologic slip rates of 0.09–0.12 mm/yr (post-18 ka) and 0.06–0.09 mm/yr (post-12 ka) (Hylland and others, 2014). Scarps on the Granger fault are typically higher than scarps on deposits of similar age along the Taylorsville fault, and the likely subsurface geometry of the Granger and Taylorsville faults (figure 3) suggests that slip on the Taylorsville fault should be subordinate to and of a smaller magnitude than slip on the Granger fault. The substantially higher slip rates on the Taylorsville fault clearly stem from the short chronology of the Taylorsville fault (~2000 yr) versus the longer chronology of the Granger fault (~16,000 yr), and the occurrence of three surface-faulting earthquakes within the past ~2000 yr on the Taylorsville fault versus only one earthquake in the same time period on the Granger fault.

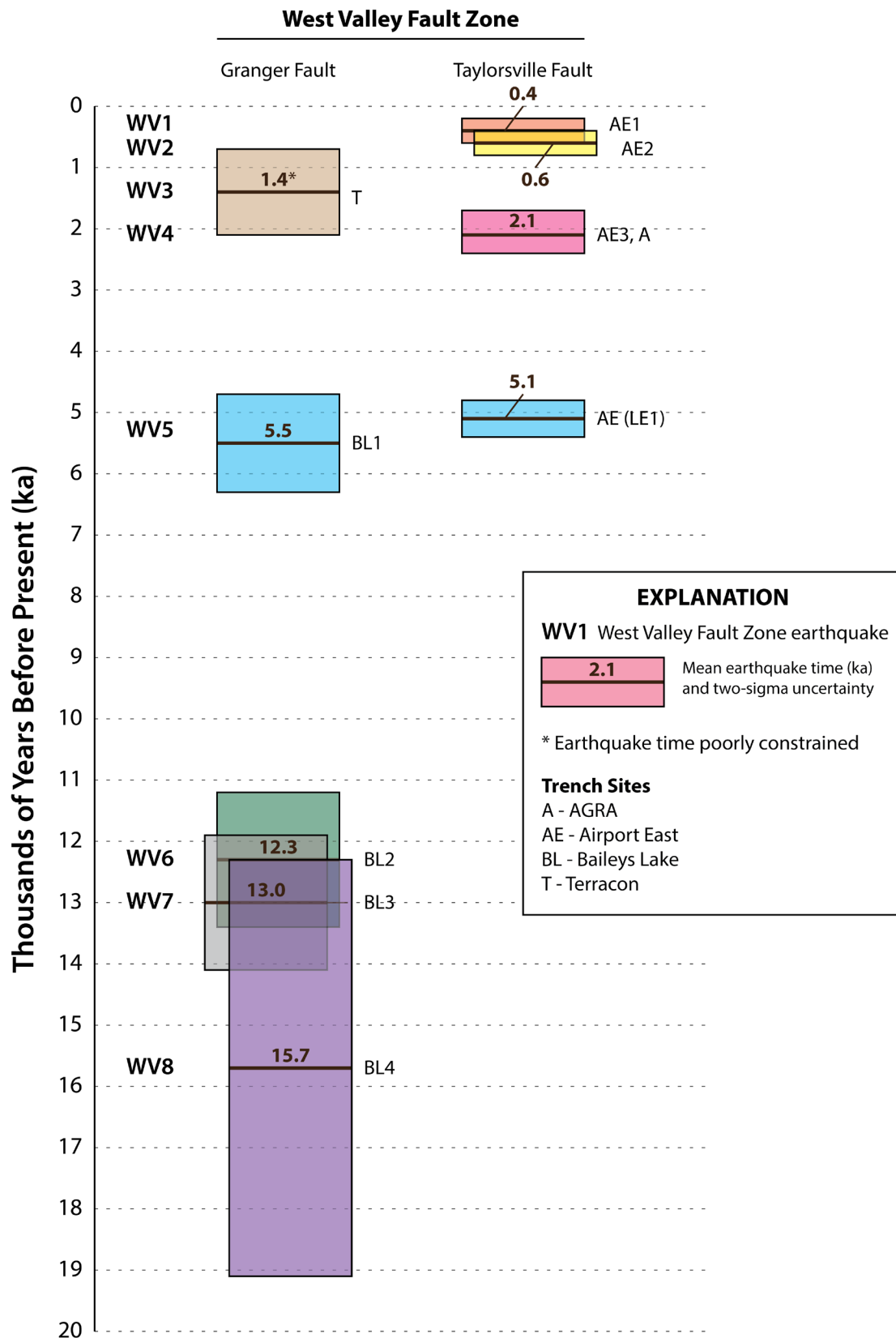


**Figure 12.** Comparison of surface-faulting chronologies for the Granger and Taylorsville faults. Note that the time of earthquake WV3 is based on a single limiting age (see discussion in text, and Hylland and others [2014], appendix H). Potentially correlative earthquakes are indicated by similar colors. Based on similarity of mean times and 2σ uncertainties, only earthquakes BL1 on the Granger fault and LE1 on the Taylorsville fault are potentially correlative. Sources of earthquake timing information: Granger fault—DuRoss and Hylland (2015); Taylorsville fault—this study.

**Table 6.** Chronology and recurrence of surface-faulting earthquakes, Taylorsville fault.

Taylorsville Fault Earthquake	Airport East Site (ka)	AGRA Site <sup>1</sup> (ka)	Chronology <sup>2</sup> (ka)	Inter-event RI <sup>3</sup> (kyr)
T1	0.4 ± 0.2	–	<b>0.4</b> (0.2–0.6)	–
T2	0.6 ± 0.2	–	<b>0.6</b> (0.4–0.8)	T2–T1: <b>0.2</b> (0–0.6)
T3	2.0 ± 0.3	2.2 ± 0.2	<b>2.1</b> (1.7–2.4)	T3–T2: <b>1.5</b> (0.9–2.0)
T4 <sup>4</sup>	5.1 ± 0.3	–	5.1 (4.8–5.4)	T4–T3: 3.0 (2.4–3.7)

Interval	Elapsed Time (kyr)	Number of Intervals	Mean RI <sup>5</sup> (kyr)	Notes
T3–T1	1.7	2	0.8	–
T4–T1	4.7	3	1.6	T4 likely not a Taylorsville fault event

<sup>1</sup> Earthquake time from Solomon (1998) and Hylland and others (2014, appendix H); see figure 2 for site location.

<sup>2</sup> Chronology for the Taylorsville fault based on mean earthquake times and 2σ ranges (bold where relation of earthquake to the Taylorsville fault is certain).

<sup>3</sup> Recurrence interval (RI) calculated from mean earthquake times (bold where relation of earthquake to the Taylorsville fault is certain), with minimum and maximum recurrence intervals calculated from 2σ ranges of earthquake times; RI=0 results from overlapping 2σ ranges.

<sup>4</sup> Earthquake T4 cannot be directly attributed to movement on the Taylorsville fault (i.e., deformation observed at the Airport East site is likely the result of shaking from an earthquake on an unknown source).

<sup>5</sup> Recurrence interval calculated from elapsed time between earthquakes (based on mean earthquake times) divided by number of inter-event time intervals.

**Table 7.** Chronology and recurrence of surface-faulting earthquakes, West Valley fault zone.

WVZF Earthquake	Granger Fault (ka)	Taylorsville Fault (ka)	Chronology <sup>1</sup> (ka)	Inter-event RI <sup>2</sup> (kyr)
WV1	–	0.4 ± 0.2 (AE1)	<b>0.4</b> (0.2–0.6)	–
WV2	–	0.6 ± 0.2 (AE2)	<b>0.6</b> (0.4–0.8)	WV2–WV1: <b>0.2</b> (0–0.6)
WV3 <sup>3</sup>	1.4 ± 0.7 (Terracon)	–	<b>1.4</b> (0.7–2.1)	WV3–WV2: <b>0.8</b> (0.1–1.7)
WV4	–	2.1 +0.3/-0.4 (AE3, AGRA)	<b>2.1</b> (1.7–2.4)	WV4–WV3: <b>0.7</b> (0.4–1.7)
WV5 <sup>4</sup>	5.5 ± 0.8 (BL1)	5.1 ± 0.3 (LE1) <sup>5</sup>	<b>5.3</b> (4.7–6.3)	WV5–WV4: <b>3.2</b> (2.3–4.6)
WV6	12.3 ± 1.1 (BL2)	–	<b>12.3</b> (11.2–13.4)	WV6–WV5: <b>7.0</b> (4.9–8.7)
WV7	13.0 ± 1.1 (BL3)	–	<b>13.0</b> (11.9–14.1)	WV7–WV6: <b>0.7</b> (0–2.9)
WV8	15.7 ± 3.4 (BL4)	–	<b>15.7</b> (12.3–19.1)	WV8–WV7: <b>2.7</b> (0–7.2)

Interval	Elapsed Time (kyr)	Number of Intervals	Mean RI <sup>6</sup> (kyr)	Notes
WV3–WV1	1.0	2	0.5	late Holocene (<2 ka)
WV4–WV1	1.7	3	0.6	late Holocene (<3 ka)
WV5–WV1	4.9	4	1.2	mid-Holocene (<6 ka)
WV6–WV1	11.9	5	2.4	latest Pleistocene–Holocene (<13 ka)
WV7–WV1	12.6	6	2.1	post-Provo shoreline (<14 ka)
WV8–WV1	15.3	7	2.2	post-Bonneville highstand (<18 ka)

<sup>1</sup> Chronology for the West Valley fault zone based on mean earthquake times and 2σ ranges; Granger fault timing from DuRoss and Hylland (2015).

<sup>2</sup> Recurrence interval (RI) calculated from mean earthquake times, with minimum and maximum recurrence intervals calculated from 2σ ranges of earthquake times; RI=0 results from overlapping 2σ ranges.

<sup>3</sup> Earthquake time poorly constrained; see Hylland and others (2014, appendix H); see figure 2 for site location.

<sup>4</sup> Timing of earthquake WV5 in the “Chronology” column assumes that the deformation observed at the Airport East site (LE1) was synchronous with the Granger fault earthquake documented at the Baileys Lake site (BL1).

<sup>5</sup> Likely not a surface-faulting earthquake at the Airport East site, but timing of deformation used to refine timing of earthquake WV5.

<sup>6</sup> Recurrence interval calculated from elapsed time between earthquakes (based on mean earthquake times) divided by number of inter-event time intervals.

The distributed nature of faulting within the WVFZ, the presence of both east- and west-facing scarps along the Taylorsville fault, and the relatively incomplete earthquake record make it difficult to estimate slip rates for the WVFZ as a whole and evaluate changes in slip rate over time using existing paleoseismic data. Keaton and others (1987) used qualitative interpretations of lacustrine stratigraphy from borehole data and very limited trench data to estimate an average Holocene slip rate of 0.5–0.6 mm/yr. Although no numerical ages were available to constrain this slip rate (see discussion in Hylland and others [2012] regarding challenges in interpreting Lake Bonneville stratigraphy in the absence of numerical age control), it remains the best available slip-rate estimate for the WVFZ as a whole.

### COMPARISON OF EARTHQUAKE CHRONOLOGIES FOR THE WEST VALLEY FAULT ZONE AND NEARBY SEGMENTS OF THE WASATCH FAULT ZONE

The structural and kinematic relations of antithetic fault pairs constitute an important topic of recent research in Utah, especially the potential for one fault to be truncated at depth by the other fault, and the degree of seismogenic dependence of the antithetic fault (i.e., the potential for synchronous or triggered slip versus independent rupture) (e.g., Lund, 2012; Working Group on Utah Earthquake Probabilities, 2016). In particular, considerable effort has been made to collect per-event timing and displacement data from the WVFZ to improve the WVFZ chronology and evaluate the seismogenic relation between the WVFZ and Wasatch fault zone (Hylland and others, 2014; DuRoss and Hylland, 2015; this study).

As noted by Hylland and others (2014) and DuRoss and Hylland (2015), uncertainties in paleoseismic earthquake timing data preclude confident determinations of prehistoric synchronous rupture on the primary and antithetic faults of a graben-forming fault system. Also, the incomplete WVFZ chronology complicates direct comparison with the more complete earthquake record of the Wasatch fault zone. Still, a comparison of WVFZ and Wasatch fault zone chronologies can provide insight into whether an earthquake on the WVFZ may have been, or clearly was not, synchronous with or triggered by a large earthquake on the nearby Wasatch fault zone, and can show to what degree earthquakes on the WVFZ may be linked to fault activity on the Wasatch fault zone. The SLCS and Weber segment of the Wasatch fault zone are of particular interest when comparing earthquake chronologies with the WVFZ, given the proximity of the antithetic WVFZ to those two primary faults (see figure 1).

Several WVFZ earthquakes overlap temporally with earthquakes on the SLCS and Weber segment, and thus may be correlative (table 8; figure 13). Although the most recent WVFZ earthquake WV1 ( $0.4 \pm 0.2$  ka) is younger than the

most recent surface-faulting earthquakes identified on the Weber segment ( $\sim 0.6$  ka) and north-central SLCS ( $\sim 1.3$  ka; DuRoss and Hylland, 2015), WV1 overlaps temporally with the most recent earthquake identified on the southernmost SLCS (earthquake S1,  $\sim 0.4$  ka, Corner Canyon site; DuRoss and others, 2018). Earthquake WV1 could be evidence of a separate event from earthquake S1, but we consider it more likely that WV1 was either triggered by that earthquake or represents a northern continuation of that fault rupture. This latter scenario would require that the  $\sim 0.4$  ka rupture occurred along a subsidiary and likely unmapped trace of the SLCS as no ruptures younger than 1 ka have been identified in SLCS paleoseismic investigations north of Corner Canyon.

WVFZ earthquakes WV2 to WV5 also have similar timing to earthquakes identified along the SLCS and Weber segment (table 8; figure 13). Earthquake WV2 ( $0.6 \pm 0.2$  ka), documented at the Airport East site on the Taylorsville fault, has an identical mean modeled time as the most recent surface-faulting earthquake on the Weber segment (earthquake W1,  $0.6 \pm 0.1$  ka; DuRoss and others, 2016a, 2016b). Earthquake WV3 ( $1.4 \pm 0.7$  ka), documented at the Terracon site on the Granger fault, has similar timing to earthquakes S2 on the SLCS ( $1.3 \pm 0.2$  ka; DuRoss and Hylland, 2015; DuRoss and others, 2016a, 2016b) and W2 on the Weber segment ( $1.1 \pm 0.6$  ka; DuRoss and others, 2016a, 2016b). Incidentally, in their analysis of possible multi-segment ruptures on the central Wasatch fault zone, DuRoss and others (2016b) included a combined S2–W2 earthquake at  $1.2 \pm 0.5$  ka in their multi-segment rupture model. A third WVFZ earthquake with intriguing timing is WV4 ( $2.1 +0.3/-0.4$  ka), documented at the Airport East and AGRA sites on the Taylorsville fault, which has very similar timing to earthquake S3 on the SLCS ( $2.2 \pm 0.2$  ka; DuRoss and Hylland, 2015; DuRoss and others, 2016a, 2016b). Earthquake WV5 ( $5.3 +1.0/-0.6$  ka), documented at the Baileys Lake site on the Granger fault and Airport East site on the Taylorsville fault, has an identical mean modeled time as earthquake S5 on the SLCS ( $5.3 \pm 0.2$  ka; DuRoss and Hylland, 2015; DuRoss and others, 2016a, 2016b). Lastly, two other WVFZ earthquakes—WV6 and WV8—have roughly similar mean times and two-sigma uncertainty ranges that overlap with those of earthquakes S9 and S10, respectively; however, the timing constraints are far too poor to correlate these earthquakes with a high level of confidence.

We highlight similarities of the WVFZ paleoearthquake chronology with the timing of SLCS and Weber-segment earthquakes because of the proximity of these two Wasatch fault zone segments to the WVFZ, and their likely subsurface structural association. However, it is interesting to note that earthquakes on several more distant faults also share similar timing to earthquakes WV1 ( $0.4 \pm 0.2$  ka) and WV2 ( $0.6 \pm 0.2$  ka). Earthquake WV1 overlaps temporally with the most recent surface-faulting earthquake identified on the Fort Canyon fault ( $\sim 0.3$  ka; Toké and others, 2021), which crosses the Traverse Mountains salient in the segment boundary zone be-

tween the SLCS and Provo segment of the Wasatch fault zone to the south, as well as with the most recent earthquake on the northernmost Provo segment ( $\sim 0.4$  ka; Bennett and others, 2018). Earthquake WV2 overlaps temporally with the penultimate surface-faulting earthquake on the Provo segment ( $0.6 \pm 0.05$  ka; DuRoss and others, 2016a, 2016b) as well as with the most recent earthquake on the Antelope Island segment of the Oquirrh–Great Salt Lake fault zone ( $0.6 \pm 0.2$  ka; Dinter and Pechmann, 2005) (figure 1). Our data are inadequate to evaluate the potential for WVFZ earthquakes to be triggered by earthquakes on these relatively distant and kinematically independent faults, but the similarity of the earthquake times is intriguing. However, movement of the WVFZ as the result of a possible kinematic association with the Weber segment (i.e., subsidiary fault–primary fault structural relation) seems plausible, especially given the possibility of a combined SLCS–Weber-segment rupture.

## SUMMARY AND CONCLUSIONS

Our paleoseismic investigation at the Airport East site provides new data that add to the earthquake chronologies of the Taylorsville fault and WVFZ as a whole, thus improving our understanding of the patterns of WVFZ earthquake recurrence and fault displacement and providing additional insight

into the seismogenic relation of the WVFZ and Wasatch fault zone. Our trenching revealed evidence for three late Holocene surface-faulting earthquakes on the Taylorsville fault, as well as earthquake-related deformation (liquefaction and folding) from a fourth earthquake likely sourced elsewhere.

Timing of the three surface-faulting earthquakes at the Airport East site, based on OxCal modeling of constraining radiocarbon and OSL ages, is as follows: AE1,  $0.4 \pm 0.2$  ka (mean modeled time  $\pm 2\sigma$ ); AE2,  $0.6 \pm 0.2$  ka; AE3,  $2.0 \pm 0.3$  ka. Net vertical displacement across the fault is 0.6 to 1.1 m, and calculations of mean per-event displacement range from 0.20 to 0.37 m. Inter-event recurrence intervals for the Taylorsville fault at the Airport East site vary from 200 to 1400 yr, and the mean late Holocene (post-2 ka) recurrence interval is 800 yr. Paleoseismic (closed-interval) slip rates range from 0.23 to 1.4 mm/yr, and geologic (open-interval) slip rates range from 0.1–0.2 mm/yr over the past  $\sim 5000$  yr to 0.2–0.4 mm/yr over the past  $\sim 2500$  yr. Although these data provide insight into surface-faulting earthquake activity on the Taylorsville fault at the Airport East site, they warrant consideration within the context of the Taylorsville fault being part of a more extensive, distributed fault zone comprising multiple strands. The paleoseismic record for the WVFZ is relatively short and incomplete, and fault parameters for a given site on a given strand may differ markedly from other

**Table 8.** Comparison of earthquake times on the West Valley fault zone (WVFZ) and Salt Lake City (SLCS) and Weber (WS) segments of the Wasatch fault zone.

WVFZ Chronology <sup>1</sup>			SLCS Chronology <sup>2</sup>			WS Chronology <sup>3</sup>		
Earthquake	Mean (ka)	2 $\sigma$ Range (ka)	Earthquake	Mean (ka)	2 $\sigma$ Range (ka)	Earthquake	Mean (ka)	2 $\sigma$ Range (ka)
WV1	0.4	0.2–0.6	S1	0.4	0.3–0.5	–	–	–
WV2	0.6	0.4–0.8	–	–	–	W1	0.6	0.5–0.7
WV3 <sup>4</sup>	1.4	0.7–2.1	S2	1.3	1.1–1.5	W2	1.1	0.5–1.7
WV4	2.1	1.7–2.4	S3	2.2	2.0–2.4	–	–	–
–	–	–	–	–	–	W3	3.1	2.8–3.4
–	–	–	S4	4.1	3.9–4.3	–	–	–
–	–	–	–	–	–	W4	4.5	4.2–4.8
WV5	5.3	4.7–6.3	S5	5.3	5.1–5.5	–	–	–
–	–	–	–	–	–	W5	5.9	5.4–6.4
–	–	–	S6	7.7	7.3–8.1	–	–	–
–	–	–	S7	9.5	9.2–9.8	–	–	–
–	–	–	S8	10.9	10.7–11.1	–	–	–
WV6	12.3	11.2–13.4	S9 <sup>5</sup>	11.6	11.4–13.8	–	–	–
WV7	13.0	11.9–14.1	–	–	–	–	–	–
WV8	15.7	12.3–19.1	S10 <sup>5</sup>	17.5	14.6–17.9	–	–	–

<sup>1</sup> Mean times and two-sigma ranges from DuRoss and Hylland (2015) and this study. Colors indicate potential correlation with earthquakes on the Salt Lake City segment and/or Weber segment, and correspond to colors on figure 13.

<sup>2</sup> Mean times and two-sigma ranges from DuRoss and Hylland (2015), DuRoss and others (2016a, 2016b, 2018).

<sup>3</sup> Mean times and two-sigma ranges from DuRoss and others (2016a, 2016b).

<sup>4</sup> Earthquake time poorly constrained; see Hylland and others (2014, appendix H).

<sup>5</sup> Earthquake times for S9 and S10 are reported as the mode and 5th–95th percentile range.

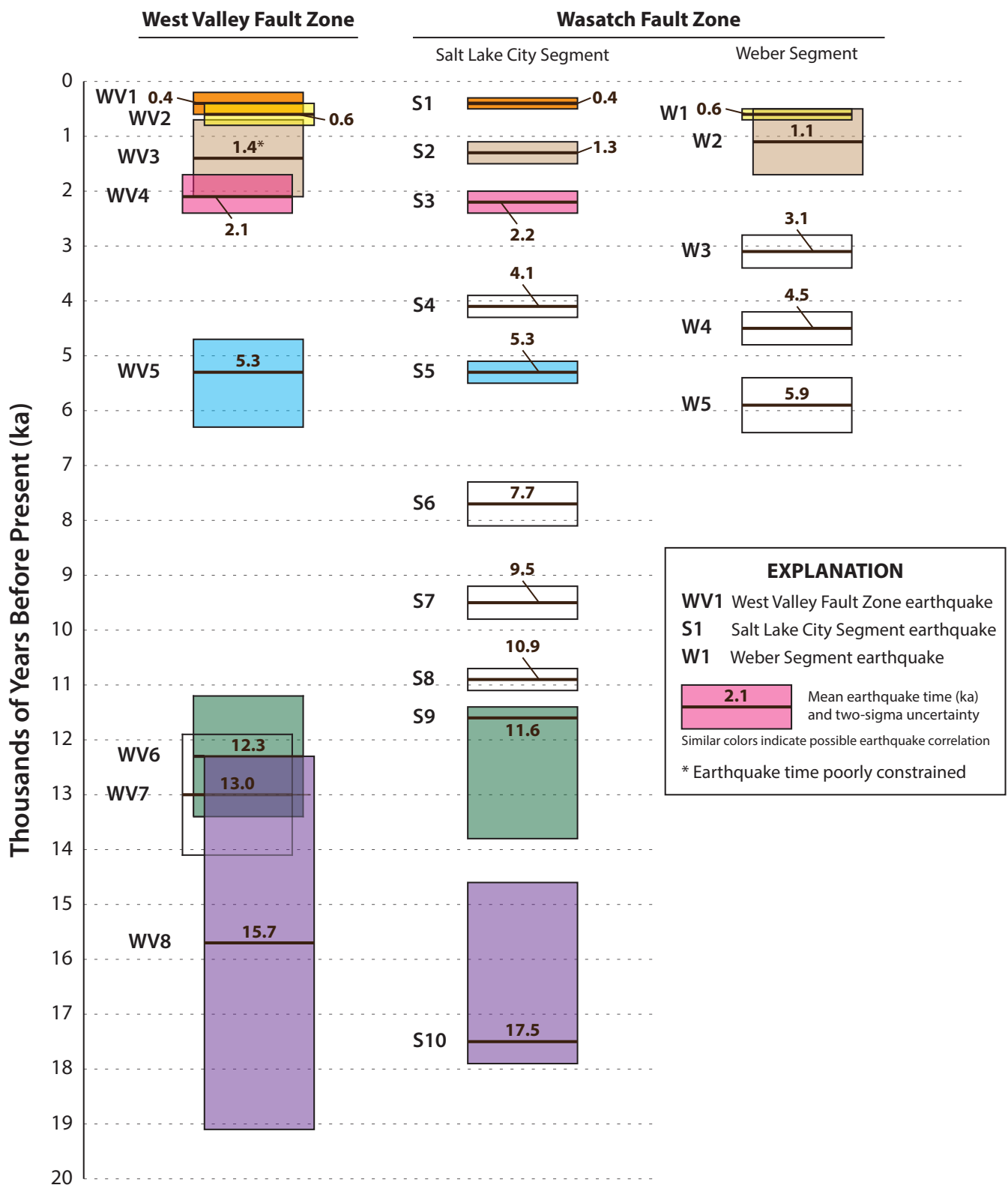


**Figure 13.** Comparison of surface-faulting chronologies for the West Valley fault zone and Salt Lake City and Weber segments of the Wasatch fault zone. Note that the time of earthquake WV3 is based on a single limiting age (see discussion in text, and Hylland and others [2014], appendix H). Potentially correlative earthquakes are indicated by similar colors. Sources of earthquake timing information: West Valley fault zone—DuRoss and Hylland (2015), this study; Salt Lake City segment— DuRoss and Hylland (2015), DuRoss and others (2016a, 2016b, 2018); Weber segment— DuRoss and others (2016a, 2016b).

sites on other strands. Inter-event surface-faulting recurrence and paleoseismic slip rate determinations from the Airport East site (this study) and the Baileys Lake site on the Granger fault (Hylland and others, 2014) highlight the variability. In our opinion, the relatively longer-term (i.e., multiple event-based) paleoseismic slip rates, and even the geologic slip rates, are more appropriate for characterizing fault activity on the Taylorsville and Granger faults than any of the paleoseismic slip rates defined by only a single inter-event time interval (particularly the AE2–AE1 interval, which results in what would seem to be an anomalously high slip rate [1.4 mm/yr] for the Taylorsville fault). Finally, the average Holocene slip rate of 0.5–0.6 mm/yr determined by Keaton and others (1987) remains the best available slip-rate estimate applicable to the WVFZ as a whole.

Combining our new Airport East data with previous paleoseismic data for the Taylorsville and Granger faults shows that in late Holocene time, the trenched fault strands have moved independently of each other. Of the paleoearthquakes identified so far, the only earthquake times that potentially correlate are the liquefaction and folding event at the Airport East site on the Taylorsville fault (LE1;  $5.1 \pm 0.3$  ka) and the most recent surface-faulting earthquake at the Baileys Lake site on the Granger fault (BL1;  $5.5 \pm 0.8$  ka). Fault relations at the Airport East site indicate that the liquefaction and folding likely were not generated by fault movement at the site, but more likely resulted from ground shaking triggered by the Granger fault rupture (and possible synchronous movement on the SLCS of the Wasatch fault; see following paragraph). The current paleoseismic data for the WVFZ support the idea that different strands within the distributed fault zone move at different times, but the paleoseismic record remains incomplete.

Our new data lend support to previous work (Hylland and others, 2014; DuRoss and Hylland, 2015) indicating that, more often than not, some part of the WVFZ moves in response to, and possibly synchronously with, slip on the Wasatch fault zone. Currently, five WVFZ earthquakes have mean modeled times that are either very similar (WV3–S2 and WV4–S3) or identical (WV1–S1, WV2–W1, and WV5–S5) to mean modeled times of SLCS and Weber-segment earthquakes, and correlations of two additional WVFZ earthquakes with SLCS earthquakes cannot be ruled out (WV6–S9 and WV8–S10). If indeed seven of eight WVFZ earthquakes were synchronous (coseismic) with earthquakes on the Wasatch fault zone, the ratio of independent to coseismic WVFZ ruptures (0.125:0.875) would not differ substantially from the ratio of independent to coseismic ruptures (0.25:0.75) used by the Working Group on Utah Earthquake Probabilities (2016) in their WVFZ rupture model. However, the temporal resolution of paleoseismic data does not allow for clear differentiation between synchronous rupture and triggered slip (i.e., slip on the antithetic fault occurring at some time after, but as a direct consequence of, slip on the primary fault).

Substantial gaps likely remain in the WVFZ chronology, especially in the middle to early Holocene earthquake record, and extensive urbanization and shallow groundwater along the fault zone severely limit opportunities for future paleoseismic research. Also, significant uncertainty remains related to the relative proportion of WVFZ earthquakes produced by synchronous rupture with the Wasatch fault zone, triggered slip, or independent fault movement. Nevertheless, the current paleoseismic dataset provides important insights into the variability of activity of individual fault strands across the WVFZ, and the likely kinematic relation of the WVFZ and SLCS.

## ACKNOWLEDGMENTS

This paleoseismic investigation of the Taylorsville fault was funded by the Utah Geological Survey and U.S. Geological Survey, National Earthquake Hazards Reduction Program, award no. G15AP00117. Gregg Beukelman, Ben Erickson, Rich Giraud, Colin Jensen, and Adam McKean (UGS) assisted with the fieldwork, and McKean shared valuable information from his surficial geologic mapping in the area. We are grateful to Greg Schlenker (GCS Geoscience) for inviting us to observe his fault trenches near our Airport East site in August 2014, and to Todd Nielson (Skyline Contractors) for his careful and diligent trench excavation. We thank Pacific Landing, Inc. and David Kuhn (Kuhn Project Management, LLC) for granting permission and facilitating access to trench the site. Lori Steadman (UGS) helped prepare some of the illustrations, John Good (UGS) prepared the manuscript for publication, and reviews by Susan Olig (Olig Seismic Geology, Inc.), Bill Lund (UGS, emeritus), and Steve Bowman and Stephanie Carney (UGS) strengthened the report.

## REFERENCES

- Arnou, T., and Mattick, R.E., 1968, Thickness of valley fill in the Jordan Valley east of the Great Salt Lake, Utah: U.S. Geological Survey Professional Paper 600-B, p. B79–B82, <https://doi.org/10.3133/pp600B>.
- Bennett, S.E.K., DuRoss, C.B., Gold, R.D., Briggs, R.W., Personius, S.F., Reitman, N.G., Devore, J.R., Hiscock, A.I., Mahan, S.A., Gray, H.J., Gunnarson, S., Stephenson, W.J., Pettinger, E., and Odum, J.K., 2018, Paleoseismic results from the Alpine site, Wasatch fault zone—timing and displacement data for six Holocene earthquakes at the Salt Lake City–Provo segment boundary: Bulletin of the Seismological Society of America, v. 108, no. 6, p. 3202–3224, <https://doi.org/10.1785/0120160358>.
- Birkeland, P.W., Machette, M.N., and Haller, K.M., 1991, Soils as tool for applied Quaternary geology: Utah Geological and Mineral Survey Miscellaneous Publication 91-3, 63 p., <https://doi.org/10.34191/MP-91-3>.

- Bronk Ramsey, C., 1995, Radiocarbon calibration and analysis of stratigraphy—the OxCal program: *Radiocarbon*, v. 37, no. 2, p. 425–430.
- Bronk Ramsey, C., 2001, Development of the radiocarbon program OxCal: *Radiocarbon*, v. 43, no. 2a, p. 355–363.
- Bronk Ramsey, C., 2008, Depositional models for chronological records: *Quaternary Science Reviews*, v. 27, no. 1-2, p. 42–60.
- Bronk Ramsey, C., 2009, Bayesian analysis of radiocarbon dates: *Radiocarbon*, v. 51, no. 1, p. 337–360.
- Bronk Ramsey, C., and Lee, S., 2013, Recent and planned developments of the program OxCal: *Radiocarbon*, v. 55, no. 2–3, p. 720–730, [https://doi.org/10.2458/azu\\_js\\_rc.55.16215](https://doi.org/10.2458/azu_js_rc.55.16215).
- Bruhn, R.L., and Schultz, R.A., 1996, Geometry and slip distribution in normal fault systems—implications for mechanics and fault-related hazards: *Journal of Geophysical Research*, v. 101, no. B2, p. 3401–3412.
- Cook, K.L., and Berg, J.W., Jr., 1961, Regional gravity survey along the central and southern Wasatch Front, Utah: U.S. Geological Survey Professional Paper 316-E, p. 75–89, 1 plate, <https://doi.org/10.3133/pp316E>.
- Currey, D.R., Berry, M.S., Douglass, G.E., Merola, J.A., Murchison, S.B., Ridd, M.K., Atwood, G., Bills, B.G., and Lambrechts, J.R., 1988, The highest Holocene stage of Great Salt Lake, Utah [abs.]: *Geological Society of America Abstracts with Programs*, v. 20, no. 6, p. 411.
- Dinter, D.A., and Pechmann, J.C., 2005, Segmentation and Holocene displacement history of the Great Salt Lake fault, Utah, *in* Lund, W.R., editor, Basin and Range Province Seismic Hazards Summit II: Utah Geological Survey Miscellaneous Publication 05-2, p. 82–86, <https://doi.org/10.34191/MP-05-2>.
- Duller, G.A.T., 2008, Luminescence dating—guidelines on using luminescence dating in archaeology: Swindon, United Kingdom, English Heritage Publishing, 43 p.
- DuRoss, C.B., 2008, Holocene vertical displacement on the central segments of the Wasatch fault zone, Utah: *Bulletin of the Seismological Society of America*, v. 98, no. 6, p. 2918–2933, <https://doi.org/10.1785/0120080119>.
- DuRoss, C.B., Bennett, S.E.K., Briggs, R.W., Personius, S.F., Gold, R.D., Reitman, N.G., Hiscock, A.I., and Mahan, S.A., 2018, Combining conflicting Bayesian models to develop paleoseismic records—an example from the Wasatch fault zone, Utah: *Bulletin of the Seismological Society of America*, v. 108, no. 6, p. 3180–3201, <https://doi.org/10.1785/0120170302>.
- DuRoss, C.B., and Hylland, M.D., 2014, Evaluating surface faulting chronologies of graben-bounding faults in Salt Lake Valley, Utah—new paleoseismic data from the Salt Lake City segment of the Wasatch fault zone and the West Valley fault zone—Paleoseismology of Utah, Volume 24: Utah Geological Survey Special Study 149, 76 p., 14 appendices, 2 plates, <https://doi.org/10.34191/SS-149>.
- DuRoss, C.B., and Hylland, M.D., 2015, Synchronous ruptures along a major graben-forming fault system—Wasatch and West Valley fault zones, Utah: *Bulletin of the Seismological Society of America*, v. 105, no. 1, p. 14–37, <https://doi.org/10.1785/0120140064>.
- DuRoss, C.B., Hylland, M.D., McDonald, G.N., Crone, A.J., Personius, S.F., Gold, R.D., and Mahan, S.A., 2014, Holocene and latest Pleistocene paleoseismology of the Salt Lake City segment of the Wasatch fault zone, Utah, at the Penrose Drive trench site, *in* DuRoss, C.B., and Hylland, M.D., Evaluating surface faulting chronologies of graben-bounding faults in Salt Lake Valley, Utah—new paleoseismic data from the Salt Lake City segment of the Wasatch fault zone and the West Valley fault zone—Paleoseismology of Utah, Volume 24: Utah Geological Survey Special Study 149, p. 1–39, 6 appendices, 1 plate, <https://doi.org/10.34191/SS-149>.
- DuRoss, C.B., Personius, S.F., Crone, A.J., Olig, S.S., Hylland, M.D., Lund, W.R., and Schwartz, D.P., 2016a, Fault segmentation—new concepts from the Wasatch fault zone, Utah, USA: *Journal of Geophysical Research – Solid Earth*, v. 121, 27 p., <https://doi.org/10.1002/2015JB012519>.
- DuRoss, C.B., Personius, S.F., Crone, A.J., Olig, S.S., Hylland, M.D., Lund, W.R., and Schwartz, D.P., 2016b, Holocene paleoseismology of the central segments of the Wasatch fault zone—Appendix B, *in* Working Group on Utah Earthquake Probabilities (WGUEP), Earthquake probabilities for the Wasatch Front region in Utah, Idaho, and Wyoming: Utah Geological Survey Miscellaneous Publication 16-3, p. B1–B70, <https://doi.org/10.34191/MP-16-3>.
- DuRoss, C.B., Personius, S.F., Crone, A.J., Olig, S.S., and Lund, W.R., 2011, Integration of paleoseismic data from multiple sites to develop an objective earthquake chronology—application to the Weber segment of the Wasatch fault zone: *Bulletin of the Seismological Society of America*, v. 101, no. 6, p. 2765–2781, <https://doi.org/10.1785/0120110102>.
- Forman, S.L., Nelson, A.R., and McCalpin, J.P., 1991, Thermoluminescence dating of fault-scarp-derived colluvium—deciphering the timing of earthquakes on the Weber segment of the Wasatch fault zone, north-central Utah: *Journal of Geophysical Research*, v. 96, no. B1, p. 595–605.
- Gilbert, G.K., 1890, Lake Bonneville: U.S. Geological Survey Monograph 1, 438 p.
- Gray, H.J., Mahan, S.A., Rittenour, T., and Nelson, M.S., 2015, Guide to luminescence dating techniques and their application for paleoseismic research, *in* Lund, W.R., editor, Proceedings volume, Basin and Range Province Seismic Hazards Summit III: Utah Geological Survey Miscellaneous Publication 15-5, invited paper, 18 p., <https://doi.org/10.34191/MP-15-5>.

- Hylland, M.D., DuRoss, C.B., McDonald, G.N., Olig, S.S., Oviatt, C.G., Mahan, S.A., Crone, A.J., and Personius, S.F., 2012, Basin-floor Lake Bonneville stratigraphic section as revealed in paleoseismic trenches at the Baileys Lake site, West Valley fault zone, Utah, *in* Hylland, M.D., and Harty, K.M., editors, Selected topics in engineering and environmental geology in Utah: Utah Geological Association Publication 41, p. 175–193.
- Hylland, M.D., DuRoss, C.B., McDonald, G.N., Olig, S.S., Oviatt, C.G., Mahan, S.A., Crone, A.J., and Personius, S.F., 2014, Late Quaternary paleoseismology of the West Valley fault zone—insights from the Baileys Lake trench site, *in* DuRoss, C.B., and Hylland, M.D., Evaluating surface faulting chronologies of graben-bounding faults in Salt Lake Valley, Utah—new paleoseismic data from the Salt Lake City segment of the Wasatch fault zone and the West Valley fault zone—Paleoseismology of Utah, Volume 24: Utah Geological Survey Special Study 149, p. 41–76, 8 appendices, 1 plate, <https://doi.org/10.34191/SS-149>.
- Hylland, M.D., Hiscock, A.I., McDonald, G.N., DuRoss, C.B., Mahan, S.A., Briggs, R.W., Personius, S.F., and Reitman, N.G., 2022, Geochronological data for Airport East trench site, West Valley fault zone, Utah: U.S. Geological Survey data release, <https://doi.org/10.5066/P9K-GEWFY>.
- Keaton, J.R., 1987, Potential consequences of earthquake-induced regional tectonic deformation along the Wasatch Front, north-central Utah, *in* McCalpin, J., editor, Proceedings of the 23rd Symposium on Engineering Geology and Soils Engineering: Boise, Idaho Department of Transportation, p. 19–34.
- Keaton, J.R., and Currey, D.R., 1989, Earthquake hazard evaluation of the West Valley fault zone in the Salt Lake City urban area, Utah: Salt Lake City, Dames & Moore, Final Technical Report prepared for U.S. Geological Survey, contract no. 14-08-0001-G1397, 69 p. (Subsequently published in 1993 as Utah Geological Survey Contract Report 93-7, <https://doi.org/10.34191/CR-93-7>.)
- Keaton, J.R., Currey, D.R., and Olig, S.J., 1987, Paleoseismicity and earthquake hazards evaluation of the West Valley fault zone, Salt Lake City urban area, Utah: Salt Lake City, Dames & Moore and University of Utah Department of Geography, Final Technical Report prepared for U.S. Geological Survey, contract no. 14-08-0001-22048, 55 p. + 33 p. appendix. (Subsequently published in 1993 as Utah Geological Survey Contract Report 93-8, <https://doi.org/10.34191/CR-93-8>.)
- Kleber, E.J., McKean, A.P., Hiscock, A.I., Hylland, M.D., Hardwick, C.L., McDonald, G.N., Anderson, Z.W., Bowman, S.D., Willis, G.C., and Erickson, B.A., 2021, Geologic setting, ground effects, and proposed structural model for the 18 March 2020  $M_w$  5.7 Magna, Utah, earthquake: Seismological Research Letters, v. 92, no. 2A, p. 710–724, <https://doi.org/10.1785/0220200331>.
- Lienkaemper, J.J., and Bronk Ramsey, C., 2009, OxCal—versatile tool for developing paleoearthquake chronologies—a primer: Seismological Research Letters, v. 80, no. 3, p. 431–434.
- Lund, W.R., editor, 2012, Basin and Range Province Working Group II—recommendations to the U.S. Geological Survey National Seismic Hazard Mapping Program for the 2014 update of the National Seismic Hazard Maps: Utah Geological Survey Open-File Report 591, 17 p, <https://doi.org/10.34191/OFR-591>.
- Machette, M.N., Personius, S.F., and Nelson, A.R., 1992, Paleoseismology of the Wasatch fault zone—a summary of recent investigations, interpretations, and conclusions, *in* Gori, P.L., and Hays, W.W., editors, Assessment of regional earthquake hazards and risk along the Wasatch Front, Utah: U.S. Geological Survey Professional Paper 1500-A-J, p. A1–A71.
- Marine, I.W., and Price, D., 1964, Geology and ground-water resources of the Jordan Valley, Utah: Utah Geological and Mineralogical Survey Water-Resources Bulletin 7, 68 p., <https://doi.org/10.34191/WRB-7>.
- Marsell, R.E., and Threet, R.L., 1960, Geologic map of Salt Lake County, Utah, *in* Crawford, A.L., compiler and editor, Geology of Salt Lake County: Utah Geological and Mineralogical Survey Bulletin 69 [published in 1964], <https://doi.org/10.34191/B-69>.
- McCalpin, J.P., Forman, S.L., and Lowe, M., 1994, Reevaluation of Holocene faulting at the Kaysville site, Weber segment of the Wasatch fault zone, Utah: Tectonics, v. 13, no. 1, p. 1–16.
- McKean, A.P., 2014, Interim geologic map of the Salt Lake City North quadrangle, Davis and Salt Lake Counties, Utah: Unpublished Utah Geological Survey contract deliverable prepared for the U.S. Geological Survey, USGS STATEMAP award no. G13AC00169, 40 p. scale 1:24,000.
- McKean, A.P., and Hylland, M.D., 2019a, Post-Lake Bonneville migration of the Jordan River, Salt Lake Valley, Utah [poster], *in* Lund, W.R., McKean, A.P., and Bowman, S.D., editors, Proceedings volume—2018 Lake Bonneville Geologic Conference and Short Course, October 3–6, 2018: Utah Geological Survey Miscellaneous Publication 170, <https://doi.org/10.34191/MP-170>.
- McKean, A.P., and Hylland, M.D., 2019b, Geologic map of the Baileys Lake quadrangle, Salt Lake and Davis Counties, Utah: Utah Geological Survey Map 281DM, 28 p., 2 plates, scale 1:24,000, <https://doi.org/10.34191/M-281DM>.
- Miller, D.M., Oviatt, C.G., Dudash, S.L., and McGeehin, J.P., 2005, Late Holocene highstands of Great Salt Lake at Locomotive Springs, Utah [abs.]: Geological Society of America Abstracts with Programs, v. 37, no. 7, p. 335.
- Miller, R.D., 1980, Surficial geologic map along part of the Wasatch Front, Salt Lake Valley, Utah: U.S. Geological Survey Miscellaneous Field Studies Map MF-1198, 13 p., scale 1:100,000.

- Murchison, S.B., 1989, Fluctuation history of Great Salt Lake, Utah, during the last 13,000 years: Salt Lake City, University of Utah, Ph.D. dissertation, 137 p.
- Nelson, A.R., Lowe, M., Personius, S., Bradley, L.A., Forman, S.L., Klauk, R., and Garr, J., 2006, Holocene earthquake history of the northern Weber segment of the Wasatch fault zone, Utah—Paleoseismology of Utah, Volume 13: Utah Geological Survey Miscellaneous Publication 05-8, 39 p., 2 plates, <https://doi.org/10.34191/MP-05-8>.
- Ostenaar, D.A., 1984, Relationships affecting estimates of surface fault displacements based on scarp-derived colluvial deposits [abs.]: Geological Society of America Abstracts with Programs, v. 16, no. 5, p. 327.
- Oviatt, C.G., 2014, The Gilbert episode in the Great Salt Lake basin, Utah: Utah Geological Survey Miscellaneous Publication 14-3, 20 p., <https://doi.org/10.34191/MP-14-3>.
- Oviatt, C.G., 2015, Chronology of Lake Bonneville, 30,000 to 10,000 yr B.P.: Quaternary Science Reviews, v. 110, p. 166–171.
- Oviatt, C.G., and Shroder, J.F., Jr., editors, 2016, Lake Bonneville—a scientific update: Elsevier, Developments in Earth Surface Processes, v. 20, 696 p.
- Oviatt, C.G., Thompson, R.S., Kaufman, D.S., Bright, J., and Forester, R.M., 1999, Reinterpretation of the Burmester core, Bonneville basin, Utah: Quaternary Research, v. 52, p. 180–184.
- Pang, G., Koper, K.D., Mesimeri, M., Pankow, K.L., Baker, B., Farrell, J., Holt, J., Hale, J.M., Roberson, P., Burlacu, R., Pechmann, J.C., Whidden, K., Holt, M.M., Allam, A., and DuRoss, C., 2020, Seismic analysis of the 2020 Magna, Utah, earthquake sequence—evidence for a listric Wasatch fault: Geophysical Research Letters, v. 47, <https://doi.org/10.1029/2020GL089798>.
- Personius, S.F., and Scott, W.E., 1992, Surficial geologic map of the Salt Lake City segment and parts of adjacent segments of the Wasatch fault zone, Davis, Salt Lake, and Utah Counties, Utah: U.S. Geological Survey Miscellaneous Investigations Series Map I-2106, scale 1:50,000. (Digital version published by the Utah Geological Survey, 2009, Map 243DM, <https://doi.org/10.34191/M-243DM>.)
- Prescott, J.R., and Hutton, J.T., 1994, Cosmic ray contributions to dose rates for luminescence and ESR dating—large depths and long-term time variations: Radiation Measurements, v. 23, p. 497–500.
- Puseman, K., and Cummings, L.S., 2005, Separation and identification of charcoal and organics from bulk sediment samples for improved radiocarbon dating and stratigraphic correlations, in Lund, W.R., editor, Western States Seismic Policy Council Proceedings Volume of the Basin and Range Province Seismic Hazards Summit II: Utah Geological Survey Miscellaneous Publication 05-2, 10 p., <https://doi.org/10.34191/MP-05-2>.
- Reimer, P.J., Bard, E., Bayliss, A., Beck, J.W., Blackwell, P.G., Bronk Ramsey, C., Buck, C.E., Cheng, H., Edwards, R.L., Friedrich, M., Grootes, P.M., Guilderson, T.P., Haffidason, H., Hajdas, I., Hatté, C., Heaton, T.J., Hoffmann, D.L., Hogg, A.G., Hughen, K.A., Kaiser, K.F., Kromer, B., Manning, S.W., Niu, M., Reimer, R.W., Richards, D.A., Scott, E.M., Southon, J.R., Staff, R.A., Turney, C.S.M., and van der Plicht, J., 2013, IntCal13 and Marine13 radiocarbon age calibration curves 0–50,000 years cal BP: Radiocarbon, v. 55, no. 4, p. 1869–1887.
- Reitman, N.G., Bennett, S.E.K., Gold, R.D., Briggs, R.W., and DuRoss, C.B., 2015, High-resolution trench photomosaics from image-based modeling—workflow and error analysis: Bulletin of the Seismological Society of America, v. 105, no. 5, p. 2354–2366, <https://doi.org/10.1785/0120150041>.
- Schwartz, D.P., and Coppersmith, K.J., 1984, Fault behavior and characteristic earthquakes—examples from the Wasatch and San Andreas fault zones: Journal of Geophysical Research, v. 89, p. 5681–5698.
- Solomon, B.J., 1998, New evidence for the age of faulting on the West Valley fault zone: Utah Geological Survey, Survey Notes, v. 30, no. 3, p. 8 and 13 <https://doi.org/10.34191/SNT-30-3>.
- Swan, F.H., III, Schwartz, D.P., and Cluff, L.S., 1980, Recurrence of moderate to large magnitude earthquakes produced by surface faulting on the Wasatch fault zone, Utah: Bulletin of the Seismological Society of America, v. 70, p. 1431–1462.
- Toké, N.A., Phillips, J., Langevin, C., Kleber, E., DuRoss, C.B., Hiscock, A.I., McDonald, G.N., Wells, J.D., Carlson, J.K., and Horns, D.M., 2021, The Traverse Ridge paleoseismic site and ruptures crossing the boundary between the Provo and Salt Lake City segments of the Wasatch fault zone, Utah, United States: Frontiers in Earth Science, v. 9, 18 p., <https://doi.org/10.3389/feart.2021.607018>.
- Trumbore, S.E., 2000, Radiocarbon geochronology, in Noller, J.S., Sowers, J.M., and Lettis, W.R., editors, Quaternary geochronology—methods and applications: Washington, D.C., American Geophysical Union, AGU Reference Shelf 4, p. 41–60.
- Utah Geospatial Resource Center (UGRC), 2014a, 2013–2014 Wasatch Front LiDAR elevation data: <https://gis.utah.gov/data/elevation-and-terrain/2013-2014-lidar/>, accessed March 2022.
- Utah Geospatial Resource Center (UGRC), 2014b, 2014 NAIP 1-meter orthophotography: <https://gis.utah.gov/data/aerial-photography/#NAIP>, accessed March 2022.
- Utah Geospatial Resource Center (UGRC), 2018, Hexagon licensed 30-cm aerial imagery: <https://gis.utah.gov/data/aerial-photography/#HEXAGON>, accessed January 2022.

- Van Horn, R., 1982, Surficial geologic map of the Salt Lake City North quadrangle, Davis and Salt Lake Counties, Utah: U.S. Geological Survey Miscellaneous Investigations Series Map I-1404, scale 1:24,000.
- Wheeler, R.L., and Krystinik, K.B., 1992, Persistent and nonpersistent segmentation of the Wasatch fault zone, Utah—statistical analysis for evaluation of seismic hazard, *in* Gori, P.L., and Hays, W.W., editors, Assessment of regional earthquake hazards and risk along the Wasatch front, Utah: U.S. Geological Survey Professional Paper 1500-A-J, p. B1–B47.
- Working Group on Utah Earthquake Probabilities, 2016, Earthquake probabilities for the Wasatch Front region in Utah, Idaho, and Wyoming: Utah Geological Survey Miscellaneous Publication 16-3, 164 p., 5 appendices, <https://doi.org/10.34191/MP-16-3>.
- Zoback, M.L., 1983, Structure and Cenozoic tectonism along the Wasatch fault zone, Utah, *in* Miller, D.M., Todd, V.R., and Howard, K.A., editors, Tectonic and stratigraphic studies in the eastern Great Basin: Geological Society of America Memoir 157, p. 3–27.

## **APPENDICES**

## APPENDIX A

## DESCRIPTION OF STRATIGRAPHIC UNITS EXPOSED IN TRENCHES AT THE AIRPORT EAST SITE

Unit, Genesis <sup>1</sup>	Coordinates (Trench, H [m])	USCS <sup>2</sup>	Texture (%) <sup>3</sup>				Clasts (cm)		Plasticity <sup>4</sup>	Density/Consistency <sup>5</sup>	Cementation	HCl rxn <sup>6</sup>	Clast Angularity	Bedding	Structure	Sorting	Lower Boundary <sup>7</sup>	Color <sup>8</sup>		Notes
			F	S	G	C/B	Largest	Average										Dry	Moist	
17B, S?	S, 26H	Low Plasticity Silt (ML)	100	0	0	0	N/A	N/A	ps	vh	N/A	N/A	N/A	thin	–	well	a,s	10YR 5/1	10YR 4/1	Shell fragments throughout. This is the silty unit at top of hanging wall above prominent burn layer. Weak soil (A horizon, ~20 cm stage I carbonate) formed at surface.
17A, P?	S, 29H	Low Plasticity Clay (CL)	100	0	0	0	N/A	N/A	p	vh	N/A	N/A	N/A	thin	–	well	a,s	10YR 6/1	10YR 5/1	Lowest prominent bed in unit 17, ~10 cm thick, continuous and flat along length of trench (hanging wall). Topped by ~2 cm burn layer. Frequent detrital charcoal.
16B, L?	S, 30.5H	High Plasticity Clay (CH)	100	0	0	0	N/A	N/A	vp	vh	N/A	N/A	N/A	thin	–	well	a,w	10YR 5/1	10YR 5/1	This is clay above blue pins, but below event horizon for P2. Prominent dark A horizon formed in top of unit, 2–7 cm thick. Deformed similarly to unit 15 (soft sediment deformation).
16A, L?	S, 30.5H	High Plasticity Clay (CH)	100	0	0	0	N/A	N/A	p	vh	N/A	N/A	N/A	thin	–	well	a,w		10YR 3/1	Prominent clay on top of marsh deposit. Fills depressions atop soft sediment deformation in unit 15, some charcoal.
15 entire	S, 32H	Interbedded sand, silt, and organic silt	–	–	–	–	–	–	–	–	–	–	–	–	–	–	c	–	–	This is the “Marsh Deposit.” Laterally extensive, thin (typically <2 cm) interbedded black organic silt, yellow/tan sands, and white silt. Entire section shows soft sediment deformation in places. Maximum thickness 15+ cm.
15C, P?	S, 29.5H	Low Plasticity Silt (ML)	100	0	0	0	N/A	N/A	ps	vh	N/A	N/A	N/A	thin	–	well	a	10YR 7/2	10YR 3/3	Very well sorted, “white” (light gray) beds, wispy 2–10 mm near fault zone. Granular and fibrous under hand lens - dolomite?
15B, P?	S, 29.5H	Silty Sand (SM)	50	50	0	0	N/A	N/A	po	h	N/A	N/A	N/A	thin	–	well	a	10YR 6/4	10YR 5/3	Sands in the marsh sequence, primarily two prominent beds, 7+ cm thick, discontinuous, one at base of unit, other at top. Fine/very fine sand plus some other component. Tephra?
15A, P?	S, 29.5H	Low Plasticity Clay (CL)	100	0	0	0	N/A	N/A	ps	vh	N/A	N/A	N/A	thin	–	well	c		10YR 2/1	In 2–10-cm-thick beds. Three main organic-rich beds. Continuous, but obscured by soil development on footwall.
14, S?	S, 39H	Low Plasticity Silt (ML)	100	0	0	0	N/A	N/A	po	eh	N/A	N/A	N/A	N/A	–	well	c		10YR 3/1	More shell fragments than unit 13. Similar to unit 12 in color and texture.
13, S?	S, 39H	Low Plasticity Silt (ML)	100	0	0	0	N/A	N/A	po	eh	N/A	N/A	N/A	N/A	–	well	c		10YR 4/1	Shell fragments throughout, some whole.
12, S	S, 41H	Low Plasticity Silt (ML)	100	0	0	0	N/A	N/A	po	eh	N/A	N/A	N/A	N/A (massive)	massive	well	a, w		10YR 3/2	Frequent charcoal, shelly hash, intact gastropod shells. Lower boundary wavy, abrupt, rip-up clasts or soil processes incorporate beds of unit 11.
11, S?	S, 41H	Low Plasticity Clay (CL)	100	0	0	0	N/A	N/A	ps	vh	N/A	N/A	N/A	thin	blocky where injected by unit 10	well	ne		10YR 5/2	Interbedded grayish brown silty clay and black organic-rich layers 5–10 cm thick. Injected by sand of unit 10 in places.

<sup>1</sup> Units shown on plates 1 and 2. Genesis: **L** - lacustrine, **P** - paludal (marsh), **S** - stream.

<sup>2</sup> Field-based approximation of Unified Soil Classification System (ASTM D2487-17). Textural information may not be representative of entire unit due to vertical and horizontal heterogeneity in units.

<sup>3</sup> Percentages of clast-size fractions (based on area) are field estimates. **F** - fines (silt and clay), **S** - sand, **G** - gravel, **C/B** - cobbles and boulders.

<sup>4</sup> Plasticity: **po** - nonplastic, **ps** - slightly plastic, **p** - plastic, **vp** - very plastic.

<sup>5</sup> Density/consistency (after Birkeland and others, 1991). Wet Density/Consistency: **so** - nonsticky, **ss** - slightly sticky, **s** - sticky, **vs** - very sticky. Dry Density/Consistency: **lo** - loose, **so** - soft, **sh** - slightly hard, **h** - hard, **vh** - very hard, **eh** - extremely hard. Some categories may not be exhibited by units at the site.

<sup>6</sup> Reaction with 10% hydrochloric acid solution.

<sup>7</sup> Lower Boundary (modified from Birkeland and others, 1991). Distinctness: **a** - abrupt (1 mm–2.5 cm), **c** - clear (2.5–6 cm), **g** - gradual (6–12.5 cm), **d** - diffuse (>12.5 cm). Topography: **s** - smooth, **w** - wavy, **i** - irregular, **ne** - base of unit not exposed. Some categories may not be exhibited by units at the site.

<sup>8</sup> Munsell color of matrix (year 2000 - revised version).

N/A = not applicable.

## APPENDIX B

## DESCRIPTION OF SOIL UNITS IN TRENCHES AT THE AIRPORT EAST SITE

Depth	Horizon	Color <sup>1</sup>		Consistency <sup>2</sup>			Texture <sup>3</sup>	Clay Films	Lower Boundary <sup>4</sup>	Plasticity <sup>5</sup>	Structure	Notes
		Dry	Moist	Wet	Moist	Dry						
0–8 cm	A	10YR 3/2	10YR 2/1	ss	fr - f	h	Silt Loam	None	as	ps	Weak, Granular	No obvious O horizon. May have formed as part of colluvial wedge.
8–27 cm	2A	10YR 5.5/1	10YR 2/1	ss	vfr	vh	Silty Clay Loam	None	aw	p	Moderate, Angular Blocky	
27–36 cm	BK1+	10YR 5/1	10YR 2/2	ss	fr	h	Silt Loam	None	cs	p	Angular Blocky	No Bt horizon. B horizon probably does not have primary soil structure development, but has structure from desiccation of parent material.
0–45 cm	A	10YR 3.5/1	10YR 2/1	s	vfr	sh	Silt Loam	None	as	ps	Angular Blocky	Carbonate from layers above it.
4.5–13 cm	BW	10YR 2/1	10YR 2/1	s	fr	sh	Silt Loam	None	aw	p	Angular Blocky	Weak incipient development in clay parent material.

<sup>1</sup> Munsell color of matrix (year 2000 - revised version).

<sup>2</sup> Consistency (after Birkeland and others, 1991). Wet Consistency: **so** - nonsticky, **ss** - slightly sticky, **s** - sticky, **vs** - very sticky. Moist Consistency: **f** - firm, **fr** - friable, **vfr** - very friable. Dry Consistency: **lo** - loose, **so** - soft, **sh** - slightly hard, **h** - hard, **vh** - very hard, **eh** - extremely hard. Some categories may not be exhibited by units at the site.

<sup>3</sup> U.S. Department of Agriculture textural soil classification. Textural information may not be representative of entire unit due to vertical and horizontal heterogeneity in units.

<sup>4</sup> Lower Boundary (modified from Birkeland and others, 1991). Distinctness: **a** - abrupt (1 mm-2.5 cm), **c** - clear (2.5-6 cm), **g** - gradual (6-12.5 cm), **d** - diffuse (>12.5 cm). Topography: **s** - smooth, **w** - wavy, **i** - irregular, **ne** - base of unit not exposed. Some categories may not be exhibited by units at the site.

<sup>5</sup> Plasticity: **ps** - slightly plastic, **p** - plastic.

APPENDIX C

DESCRIPTION OF SCARP-DERIVED COLLUVIUM AND RELATED DEPOSITS IN TRENCHES AT THE AIRPORT EAST SITE

Wedge Unit	Lower Contact Details	Upper Contact Details	Max Thickness (avoiding mini-grabens or wedge heels)	Soil Development Within Wedge?	Soil Development Below Wedge?	Fault Terminations?	Back Rotation/Unconformities?	Other Evidence That Wedge is Related to Scarp/Event Horizon?	Other Notes (14C/OSL samples)/ Evidence Against Wedge Relation to Scarp/Event Horizon?
C1	Indistinct lower contact. Organic-rich colluvium on fine-grained silt/organics (marsh deposits). Contact locally obscured by modern soil development (especially east of h-31 South trench).	N/A (ground surface/modern soil)	~10 cm at h-32.2	Modern soil development apparent throughout wedge, including granular soil peds, organic-rich sediment, and mixing from roots/burrows.	A burn horizon is within unit (17) buried by C1. Charcoal and organic-rich sediment are also present below wedge (above burn horizon).	One in South trench. Clear faulting to base of wedge (5 cm offset).	Unit 16 is highly disturbed in fault zone (near-vertical beds within unit 16 at main FZ) and is unconformably overlain by C1. Unit C2 may be slightly oversteepened by fault drag and buried by C1, in south trench at 32.8H.	Loose organic-rich sediment burying fault scarp in fine-grained sediment. Colluvium is very loose.	<sup>14</sup> C Target: burn horizon. Nothing from C1 (too burrowed/mixed).
C2	Clear. Organic-rich sediment of gray silt/clay.	Clear contact with gray silt that thins onto scarp.	~12 cm at h-32.4	Organics present throughout wedge. No obvious soil development within wedge.	Organics are present at contact between two silt/clay beds.	South trench - upward fault terminations not clear. Differential offset along westernmost fault zone. Evidence for additional event after unit 16 deposition.	Unit 15–16 contact is deformed (steeply dipping) in FZ, compared to unit 16–C2 contact, which is more flat lying.	Organic sediments that thicken on top of deformed sedimentary units. Clay/silt beds below unit 15A are plastically deformed, whereas unit 15A is not.	It is possible that the event horizon for C2 is actually at the blue dot contact (organics between two silt/clay beds) within unit 16. Evidence for this includes possible fault terminations, and soft-sediment deformation of units below, not above this contact (see h-27). <sup>14</sup> C Targets: C2 wedge, organics from blue dot contact.
C3	Clear to indistinct contact within lowermost marsh sequence—interbedded organics and silt(?) that are part of unit 15. Event horizon is above 15a, but below 15b–d, and below organic-rich accumulation of sediment (C3) that is above 15a.	Indistinct contact of very organic-rich marsh sediment with interbedded organics, buff-colored silt, and ash-colored silt in upper marsh sequence (unit 15b–d)	~10 cm at h-32.2	Organics throughout, which likely reflect marsh sedimentation and soil development.	In organic-rich marsh deposits.	None	No, but there is good differential displacement evidence. Unit 15A interbeds are clearly faulted (~15 cm), whereas upper marsh sediments (upper part of unit 15) clearly drape the fault scarp. These sediments were later faulted (likely by AE2) but are only offset a few centimeters.	Organic-rich marsh sediments clearly thicken adjacent to fault (on hanging wall). Unit 15 is ~40 cm thick on hanging wall (at h-32.2), vs. ~30 cm thick in fault zone and on footwall.	<sup>14</sup> C Targets: several marsh interbeds from the C3 wedge.

N/A = not applicable.

**APPENDIX D****PROCESSING AND ANALYSIS OF RADIOCARBON SAMPLE MATERIAL FROM  
THE AIRPORT EAST SITE BY PALEORESEARCH INSTITUTE**

CHARCOAL/WOOD IDENTIFICATION AND EXAMINATION OF BULK SOIL SAMPLES  
FOR POTENTIAL RADIOCARBON Datable MATERIAL FROM  
THE AIRPORT EAST TRENCH SITE, TAYLORSVILLE FAULT, SALT LAKE CITY, UTAH

By

Peter Kováčik

PaleoResearch Institute, Inc.  
Golden, Colorado

PaleoResearch Institute Technical Report 2015-090

Prepared for

Utah Geological Survey  
Salt Lake City, Utah

December 2015

## INTRODUCTION

The Airport East trench site is located east of Salt Lake City International Airport in Salt Lake City, Utah. Two paleoseismic trenches, South and North, were excavated across the Taylorsville Fault of the West Valley fault zone (WVFZ)(Michael Hylland and Adam Hiscock, personal communication October 2, 2015). Eleven bulk soil samples, ten charcoal samples, and one wood sample, collected from the south wall of the South Trench were submitted to recover and identify material suitable for AMS radiocarbon age determination.

## METHODS

### Macrofloral

The bulk samples were floated using a modification of the procedures outlined by Matthews (1979). Each sample was added to approximately three gallons of water, then stirred until a strong vortex formed. The floating material (light fraction) was poured through a 250-micron mesh sieve. All material that passed through the screen was retained for possible microcharcoal, particulate soil organics, and/or humate extraction. Additional water was added and the process repeated until all floating material was removed from the sample (a minimum of five times). The material that remained in the bottom (heavy fraction) was poured through a 0.5-mm mesh screen. The floated portions were allowed to dry. Some of the charcoal samples were water-screened through a 250-micron mesh sieve and allowed to dry prior to identification.

The light fractions were weighed, then passed through a series of graduated screens (US Standard Sieves with 4-mm, 2-mm, 1-mm, 0.5-mm, and 0.25-mm openings) to separate charcoal debris and to initially sort the remains. The contents of each screen then were examined. Charcoal pieces larger than 0.5 mm, or 0.25 mm in diameter were separated from the rest of the light fraction, and the total charcoal was weighed. Charcoal pieces in a representative sample were broken to expose fresh cross, radial, and tangential sections, then examined under a binocular microscope at a magnification of 70x and under a Nikon Optiphot 66 microscope at magnifications of 320–800x. The weights of each charcoal type within the representative sample were recorded. The material that remained in the 4-mm, 2-mm, 1-mm, 0.5-mm, and 0.25-mm sieves was scanned under a binocular stereo microscope at a magnification of 10x, with some identifications requiring magnifications of up to 70x. The material that passed through the 0.25-mm screen was not examined. The heavy fractions were scanned at a magnification of 2x for the presence of botanic remains. The term "seed" is used to represent seeds, achenes, caryopses, and other disseminules. Remains from the light and heavy fractions were recorded as charred and/or uncharred, whole and/or fragments. Macrofloral remains, including charcoal, were identified using manuals (Carlquist 2001; Hoadley 1990; Martin and Barkley 1961; Musil 1963; Schopmeyer 1974; Schweingruber, et al. 2011; Schweingruber, et al. 2013) and by comparison with modern and archaeological references. Clean laboratory conditions were used during flotation and identification to avoid contamination of charcoal and botanic remains to be submitted for radiocarbon dating. All instruments were washed between samples, and the samples were protected from contact with modern charcoal.

## DISCUSSION

Situated on the Taylorsville Fault of the West Valley fault zone (WVFZ) in Salt Lake City, Utah, two trench exposures at the Airport East trench site display possible paleo-Jordan River floodplain deposits, marshy wetland deposits, and fault-scarp-derived colluvium. Local vegetation modified by modern activities is limited to grass (*Poaceae*) cover. The South and North paleoseismic trenches were exposed across one of the Taylorsville Fault strands, just east of the Salt Lake City International Airport, at an elevation of 4210–4213 ft (Michael Hylland and Adam Hiscock, personal communication October 2, 2015). Macrofloral remains including charcoal/wood, recovered in 11 bulk soil samples, one wood, and 10 charcoal samples (Table 1) from the south wall of South Trench were identified, and charred materials appropriate for AMS radiocarbon analysis were isolated.

### Unit 11

A single sample, AE-S-RC24, collected from the upper organic-rich interbed in unit 11 at a depth of 2.18 mad did not contain any charred floral remains (Table 2).

### Unit 12

Charcoal sample AE-S-RC20, collected from the top of unit 12 (2.18 mad), yielded 14 vitrified probable rhizome/tuber fragments from an unspecified monocotyledonous plant (Tables 2 and 3). Although the fragments' mass (0.0519 g) is sufficient, rhizomes, similarly to roots, probably grew into older units introducing younger material. Due to this fact they are usually not recommended for AMS radiocarbon dating.

### Unit 12A

Two samples (AE-S-RC18 and AE-S-RC15) were collected from the soil developed on unit 12. Sample AE-S-RC18 (2.28 mad) from the base of unit 12A contained numerous charred and very friable organic fragments (0.0209 g) with no specific structure and ash clumps (0.0782 g). Although both items are large enough for radiocarbon dating, they probably will dissolve during chemical pretreatment, making them poor choices for dating.

Ten vitrified probable monocot stem or root fragments, weighing 0.0313 g, represent the only charred remains suitable for AMS radiocarbon dating recovered in bulk soil sample AE-S-RC15 (top of unit 12A, 2.5 mad). Uncharred floral remains include few rootlets. Recovery of moderate quantities of uncharred *Chara* oogonia indicate stonewort, a submerged algae found mostly in hard-water or alkaline lakes and slowly flowing streams with abundant calcium. Additionally, similar conditions are suggested by a significant presence of ostracod shell, representing small, bivalved crustaceans. Uncharred snail shells, both depressed and oblong, also were noted. Stonewort, ostracod, and snail shells suggest an aquatic environment supporting the assumption that this area probably represented a flood plain and a marshy wetland. Six small uncharred bone fragments also were noted.

### **Unit 13**

An uncharred *Chara* oogonium and a few ostracods also were present in sample AE-S-RC21 (2.63 mad) from the middle of unit 13. One tiny unidentifiable charcoal fragment too small for further identification is insufficient (less than 0.0001 g) for radiocarbon analysis.

### **Unit 14**

One bulk soil sediment (AE-S-RC1) and one charcoal sample (AE-S-RC22) were collected from the top of unit 14 at depths of 2.10 mad and 2.62 mad, respectively. Sample AE-S-RC1 yielded one charred *Scirpus*-type seed fragment, weighing less than 0.0001 g, reflecting bulrush (Tables 2 and 3). In addition, 21 vitrified monocot stem fragments were recovered, indicating grasses (Poaceae), sedges (Cyperaceae), and lilies (Liliaceae). Presence of charred seed from bulrush, a member of the sedge family, suggests the monocot stem fragments could represent the same genus. Vitrified monocot stem fragments yielded a mass of 0.0138 g and can be submitted for radiocarbon analysis. A few uncharred roots/rootlets and numerous uncharred *Chara* oogonia also were noted. Uncharred non-floral remains include numerous ostracods and snail shell fragments (depressed and oblong). Both floral (bulrush, monocot, stonewort) and non-floral remains (ostracod and snail shells) are typical of wetlands.

Sample AE-S-RC22 contained unidentified organic material too vitrified for further identification weighing 0.0033 g. These fragments can be used for AMS radiocarbon age determination. A few uncharred ostracod and snail shell fragments also were noted.

### **Unit 15**

Two bulk soil samples (AE-S-RC2 and AE-S-RC6) were collected from unit 15, a marsh deposit. In addition, sediment samples AE-S-RC4 and AE-S-RC5 were removed from the C3 colluvial wedge, contained within the same unit.

#### **Base of Unit 15**

Sample AE-S-RC2 was collected below a silty interbed at the base of unit 15. Charred floral remains recovered in this sample include several *Scirpus*-type seed fragments (0.0004 g) and few unidentified seeds (0.0002 g). One parenchymous tissue fragment weighing less than 0.0001 g also was noted. Parenchyma is the botanical term for relatively undifferentiated tissue composed of many similar cells with thin primary walls. Parenchyma occurs in many different plant tissues in varying amounts, especially large fleshy organs such as roots and stems, but also in fruits, seeds, cones, periderm (bark), leaves, needles, etc. (Hather 2000:1; Mauseth 1988). The charcoal record yielded 14 unidentifiable fragments (0.0001 g) too small and too vitrified for further identification. None of the recovered charred plant types yielded sufficient mass for AMS radiocarbon dating. The presence of macroscopic charred remains notes the potential for this sample to contain charred microscopic fragments (microscopic charcoal). Microscopic charcoal can be extracted from the sediment that passed through the 250-micron mesh sieve during the flotation procedure and has been retained. Retention of sediments for possible microscopic charcoal, particulate soil organics, and/or humate extraction is part of our policy to provide additional options when sediments yield insufficient mass or lacks any

macroscopic charred remains for AMS radiocarbon dating. Uncharred floral and non-floral remains include a few rootlets, several bone fragments, and moderate quantities of ostracods and snail shells (depressed and oblong).

### **C3 Colluvial Wedge**

Bulk soil sample AE-S-RC4, collected from the lower portion of the C3 colluvial wedge at a depth of 2.26 mad, yielded 13 monocot stem fragments (0.0052 g) and 10 *Scirpus*-type (bulrush) seed fragments (0.0004 g). The charcoal record includes one unidentified hardwood fragment (0.0002 g) and 35 unidentifiable fragments (0.0031 g), too small and too vitrified for further identification. Charred monocot stem fragments and unidentifiable charcoal fragments yielded a mass suitable for radiocarbon analysis. Uncharred floral remains include few *Chara* (stonewort) oogonia and roots/rootlets.

Thirty-six charred *Scirpus*-type (bulrush) seed fragments, weighing 0.0009 g, represent the only charred remains recovered in sample AE-S-RC5 (2.3 mad) from the upper part of the C3 colluvial wedge. Although, these fragments are minimally sufficient to obtain a date, it is possible that extraction of microscopic charcoal from retained sediments can increase the quantity of charred particles for AMS radiocarbon dating. Few uncharred roots and rootlets also were noted in the sample.

### **Top of Unit 15**

Charred floral remains also were present in bulk soil sample AE-S-RC6 (2.41 mad) collected at the top of unit 15. They include 35 vitrified monocot stem fragments (0.0789 g), six vitrified monocot/herbaceous dicot stem fragments (0.0306 g), six *Scirpus*-type (bulrush) seed fragments (0.0005 g), several *Scirpus*-type endosperms and endosperm fragments (0.0092 g), and one unidentified seed (less than 0.0001 g). Presence of bulrush seeds suggests that the monocot stems could represent sedges, such as bulrush, rather than grasses. Charred stems as well as bulrush endosperms can be submitted for radiocarbon age determination. Uncharred floral remains include roots and rootlets.

### **Unit 16**

Two soil samples (AE-S-RC7 and AE-S-RC8) collected below the C2 colluvial wedge, one charred botanic sample (AE-S-RC19) recovered from a hanging wall, and one wood sample (AE-S-RC23) removed from a 3 meter deep auger hole, represent unit 16. The auger hole sample, AE-S-RC23 (0.10 mbd), contained eight unidentified root fragments (0.3338 g). These pieces are compressed and appear to be lignified, suggesting a long period of exposure to anaerobic conditions and degradation by microorganisms.

One charred and friable organic fragment was recovered in sample AE-S-RC19 (2.3 mad) collected from the base of unit 16 in a hanging wall. This fragment, too small for further identification, yielded an insufficient weight of 0.0002 g to obtain a radiocarbon date.

Bulk soil sample AE-S-RC7, removed from the top of the lower clay deposit in unit 16 at a depth of 2.49 mad, contained three different types of charred remains. Eleven monocot stem fragments (0.0009 g) and several *Scirpus*-type (bulrush) seeds (0.0011 g) are minimally

sufficient, while a large number of tiny unidentifiable charcoal fragments, weighing 0.0032 g, can be submitted for AMS radiocarbon age determination. Uncharred remains identified in the sample include a few rootlets and one ostracod.

The top of unit 16, directly below the C2 colluvial wedge, also was sampled (AE-S-RC8). Charred floral remains recovered in this sample include five monocot stem fragments (0.0006 g), one *Typha* (cattail) seed (less than 0.0001 g), and numerous unidentifiable charcoal fragments (0.0031 g). One uncharred *Chara* (stonewort) oogonia, two uncharred *Typha* seeds, and a few uncharred roots/rootlets also were noted. Uncharred non-floral remains include one ostracod and few snail shell fragments.

Unidentifiable charcoal from samples AE-S-RC7 and AE-S-RC8 consists of numerous extremely small charcoal fragments that expose more surface area to chemical pre-treatment, which can result in greater mass loss during that process.

### **C2 Colluvial Wedge**

Bulk soil sample AE-S-RC10 and a botanic sample were collected from the C2 colluvial wedge at depths of 2.66 mad and 2.72 mad, respectively. Sample AE-S-RC10 yielded various charred floral remains, including 61 monocot stem fragments (0.0094 g), one Poaceae A caryopsis (less than 0.0001 g), several *Scirpus*-type seeds and seed fragments (0.0079 g), one *Typha* seed (less than 0.0001 g), and two unidentified seed fragments (0.0001 g), reflecting monocots including grasses, sedges (bulrush), cattail, and possibly other taxa. Forty-three tiny unidentifiable charcoal fragments (0.0068 g), too small and vitrified for further identification, also were recovered. Charred stems, bulrush seeds, or charcoal fragments provide suitable mass for radiocarbon analysis. Uncharred *Chara* (stonewort) oogonia, *Typha* (cattail) seeds, and an ostracod indicate an aquatic environment. Uncharred rootlets and two sclerotia also were noted in the sample. Sclerotia are commonly called "carbon balls." They are small, black, solid or hollow spheres that can be smooth or lightly sculpted. These forms range from 0.5 to 4 mm in size. Sclerotia are the resting structures of mycorrhizae fungi, such as *Cenococcum graniforme*, that have a mutualistic relationship with tree roots. Many trees are noted to depend heavily on mycorrhizae and might not be successful without them. "The mycelial strands of these fungi grow into the roots and take some of the sugary compounds produced by the tree during photosynthesis. However, mycorrhizal fungi benefit the tree because they take in minerals from the soil, which are then used by the tree" (Kricher and Morrison 1988:285). Sclerotia appear to be ubiquitous and are found with coniferous and deciduous trees including *Abies* (fir), *Juniperus communis* (common juniper), *Larix* (larch), *Picea* (spruce), *Pinus* (pine), *Pseudotsuga* (Douglas fir), *Alnus* (alder), *Betula* (birch), *Populus* (poplar, cottonwood, aspen), *Quercus* (oak), and *Salix* (willow). These forms originally were identified by Dr. Kristiina Vogt, Professor of Ecology in the School of Forestry and Environmental Studies at Yale University (McWeeney 1989:229-230; Trappe 1962).

Fifteen charred monocot stem fragments (0.0013 g) recovered in sample AE-S-RC9 are minimally sufficient for AMS radiocarbon dating. In addition, a single *Scirpus*-type (0.00) seed, weighing only 0.0002 g, was recovered.

### Unit 17

Bulk soil sample AE-S-RC12, collected from a burn horizon (unit 17) at a depth of 2.7 mad, contained 36 monocot stem fragments (0.0067 g) suitable for AMS radiocarbon analysis. A few charred (0.0005 g) and uncharred *Scirpus*-type (bulrush) seeds also were recovered. In addition, a few uncharred rootlets and a single depressed snail shell were noted.

### Unit 17b

Three botanic samples were collected from unit 17b, situated above the burn horizon (unit 17). All three samples, AE-S-RC13 (2.76 mad), AE-S-RC11 (2.79 mad), and AE-S-RC14 (2.8 mad), contained charred/vitrified fragments of monocot rhizome/tubers. These fragments most resemble Cyperaceae rhizome/tubers, including bulrush. Although charred rhizome/tuber fragments from these samples yielded weights of 0.2531 g (AE-S-RC13), 0.0201 g (AE-S-RC11), and 0.6526 g (AE-S-RC14), and, as charred remains, would be suitable for AMS radiocarbon analysis, the fact that they represent roots indicates other factors must be considered. Roots are intrusive into older units. If they were burned *in situ* they might not accurately reflect the stratum age. This portion of the determination of suitability for dating should be made based on geological information and observations at the site.

### C1 Colluvial Wedge

Bulk soil sample AE-S-RC17 represents the upper most sample (2.91 mad) collected from the C1 colluvial wedge, an intact sediment block containing charcoal. This sample yielded 46 monocot stem fragments (0.0398 g) suitable for radiocarbon age determination. Other charred remains include four *Scirpus*-type (bulrush) seed fragments (0.0003 g), and several unidentified seeds and seed fragments representing at least two different plants (0.0004 g and 0.0013 g). Uncharred floral remains noted in the sample include numerous *Chara* oogonia, moderate quantities of probable *Portulaca* seeds (purslane), a few *Scirpus*-type seeds, and roots/rootlets. Six uncharred small fish bone fragments, an ostracod, and several snail shells (depressed- and oblong-shaped) suggest a wetland environment.

## **SUMMARY AND CONCLUSIONS**

Examination of 11 bulk soil samples, 10 charred botanic/charcoal samples, and one wood sample from South Trench across the Taylorsville Fault at the Airport East trench site, Salt Lake City, Utah, resulted in recovery of various charred botanic remains including charcoal, in sufficient quantities for AMS radiocarbon age determination.

The macrofloral record is dominated by charred monocot plant parts including sedges (rhizomes/tubers) such as bulrush (seeds and endosperms), cattail (seeds), and grasses (caryopsis). These plants, recovered in multiple deposits in the South Trench, suggest a wetland environment. In addition, the presence of stonewort (*Chara*) algae, ostracods, various snails, and fish bone fragments confirms the assumption that the sampled units represent possible paleo-Jordan River floodplain and marshy wetland deposits.

Wood sample AE-S-RC23 from unit 16 yielded several uncharred, compressed, and lignified root fragments. Compression suggests these fragments were deposited for a long period. Sample AE-S-RC24 from unit 11 did not contain any charred floral remains. Charred remains were present in the majority of samples; however, often in quantities not sufficient for AMS radiocarbon analysis. Charcoal fragments, noted only in six samples (AE-S-RC10, 8, 7, 4, 2, and 21), were extremely small and too vitrified for identification to a genus or a family level (Table 4). Unidentified hardwood (AE-S-RC4) and unidentifiable (AE-S-RC2 and AE-S-RC21) charcoal yielded insufficient mass for radiocarbon analysis. Although samples AE-S-RC8, 7, and 4 yielded unidentifiable charcoal weighing approximately 0.0030 g, they consist of numerous and very small fragments, which exposes more surface area to chemical pre-treatment, usually resulting in a greater mass loss during processing.

Charred bulrush (*Scirpus*-type) seeds from samples AE-S-RC17, 12, 9, 7, 6, 5, 2, and 1 are either too small or minimally sufficient for radiocarbon dating. However, bulrush seeds from sample AE-S-RC10 and bulrush endosperms from sample AE-S-RC6 have a greater probability to return a radiocarbon date. Charred monocot stems from samples AE-S-RC17, 12, 10, 6, 4, 1, and 15 are suitable for AMS radiocarbon age determination, while those from samples AE-S-RC9, 8, and 7 are insufficient. Other charred floral remains including cattail (*Typha*) seeds (AE-S-RC10 and AE-S-RC7), unidentified seeds (AE-S-RC17, 10, 6, and 2), large grass (Poaceae A) caryopsis (AE-S-RC10), parenchymous tissue (AE-S-RC2), and unidentified organic material (AE-S-RC19) are too small for radiocarbon analysis. Charred organic material from samples AE-S-RC22 and AE-S-RC18 yielded masses sufficient for AMS radiocarbon dating. Charred monocot (AE-S-RC20), including probable sedge (AE-S-RC14, 11, and 13), rhizomes/tubers usually are not recommended for radiocarbon analysis because they often do not represent deposition of burned material with sediments. Rather, they indicate younger organic material that grew into older units and burned in situ. The final determination of their suitability should be made based on field observations and geology.

TABLE 1  
 PROVENIENCE DATA FOR SAMPLES FROM THE AIRPORT EAST TRENCH SITE,  
 TAYLORSVILLE FAULT, SALT LAKE CITY, UTAH

Sample No.	Unit	Colluvial wedge	Horizontal location (m)	Vertical location (mad)	Provenience/ Description	Analysis
AE-S-RC17		C1	31.85	2.91	Bulk soil sample from P1 colluvium; contains charcoal; minimum age of P1	Macrofloral
AE-S-RC14	17b		31.56	2.8	Macrocharcoal sample from above burn horizon and below P1 colluvium; maximum age of P1 surface-faulting earthquake	Botanical ID
AE-S-RC11			32.18	2.79	Macrocharcoal sample from above burn horizon and below P1 colluvium; maximum age of P1 surface-faulting earthquake	Botanical ID
AE-S-RC13			30.64	2.76	Macrocharcoal sample from above burn horizon	Botanical ID
AE-S-RC12	17		30.54	2.7	Bulk soil sample from burn horizon; age of burn horizon unit 17	Macrofloral
AE-S-RC9		C2	32.23	2.72	Macrocharcoal sample from P2 colluvium; minimum age of P2 surface-faulting earthquake	Botanical ID
AE-S-RC10			32.15	2.66	Bulk soil sample from P2 colluvium; minimum age of P2 surface-faulting earthquake	Macrofloral
AE-S-RC8	16		32.21	2.65	Bulk soil sample from top of clay deposit directly below P2 colluvium; maximum age of P2 surface-faulting earthquake	Macrofloral
AE-S-RC7			32.02	2.49	Bulk soil sample from top of lower clay deposit; maximum age of P2 surface-faulting earthquake	Macrofloral
AE-S-RC19			29.86	2.3	Macrocharcoal sample from base of unit 16 in hanging wall	Botanical ID
AE-S-RC23			30	-0.1	Wood sample from 3m deep auger hole	Botanical ID

TABLE 1 (Continued)

Sample No.	Unit	Colluvial wedge	Horizontal location (m)	Vertical location (mad)	Provenience/ Description	Analysis
AE-S-RC6	15		31.87	2.41	Bulk soil sample from near top of marshy deposit (unit 15); age control on OSL sample L2	Macrofloral
AE-S-RC5		C3	31.9	2.3	Bulk soil sample from upper P3 colluvium; minimum age for P3 surface-faulting earthquake	Macrofloral
AE-S-RC4			31.9	2.26	Bulk soil sample from lower P3 colluvium; minimum age for P3 surface-faulting earthquake	Macrofloral
AE-S-RC2			31.69	2.19	Bulk soil sample from base of unit and below silty interbed; maximum age for P3 surface-faulting earthquake	Macrofloral
AE-S-RC22	14		55.3	2.62	Macrocharcoal sample from top of unit	Botanical ID
AE-S-RC1			31.79	2.10	Bulk soil sample from top of unit; maximum age for P3 surface-faulting earthquake	Macrofloral
AE-S-RC21	13		42.94	2.63	Macrocharcoal sample from middle of unit	Botanical ID
AE-S-RC15	12A		35.75	2.5	Bulk soil sample from top of soil developed on unit 12	Macrofloral
AE-S-RC18			34.56	2.28	Macrocharcoal sample from base of soil developed on unit 12	Botanical ID
AE-S-RC20	12		47.52	2.18	Macrocharcoal sample from top of unit	Botanical ID
AE-S-RC24	11		36.88	2.18	Macrocharcoal sample from upper organic-rich interbed in unit 11; maximum age of liquefaction event	Botanical ID

TABLE 2  
 MACROFLORAL REMAINS FROM THE AIRPORT EAST TRENCH SITE,  
 TAYLORSVILLE FAULT, SALT LAKE CITY, UTAH

Sample No.	Identification	Part	Charred		Uncharred		Weights/ Comments
			W	F	W	F	
AE-S-RC17	Volume Floated						170.0 ml
C1 2.91 mad	Light Fraction Weight						0.882 g
	FLORAL REMAINS:						
	Monocot	Stem		46			0.0398 g
	<i>Scirpus</i> -type	Seed		4			0.0003 g
	Unidentified S	Seed	5				0.0004 g
	Unidentified L	Seed		3			0.0013 g
	<i>Chara</i>	Oogonia			X	X	Numerous
	cf. <i>Portulaca</i>	Seed			X	X	Moderate
	<i>Scirpus</i> -type	Seed			4	1	
	Roots					X	Few
	Rootlets					X	Moderate
	NON-FLORAL REMAINS:						
	Fish bone					6	0.0018 g
	Ostracod	Shell				1	
Snail shell					X	Moderate	
Snail shell - depressed				X	X	Few	
Snail shell - oblong				X	X	Few	
AE-S-RC14	Sample Weight						0.779 g
Unit 17b	FLORAL REMAINS:						
2.8 mad	cf. Cyperaceae	Rhizome/ Tuber		2			0.6526 g
AE-S-RC11	Volume Water-screened						1.0 ml
Unit 17b	Water-screened Sample Weight						0.085 g
2.79 mad	FLORAL REMAINS:						
	Monocot, cf. Cyperaceae - vitrified	Rhizome/ Tuber		2			0.201 g
AE-S-RC13	Sample Weight						0.493 g
Unit 17b	FLORAL REMAINS:						
2.76 mad	Monocot, cf. Cyperaceae - vitrified	Rhizome/ Tuber		4			0.2531 g

TABLE 2 (Continued)

Sample No.	Identification	Part	Charred		Uncharred		Weights/ Comments
			W	F	W	F	
AE-S-RC12	Volume Floated						10.0 ml
Unit 17 2.7 mad	Light Fraction Weight						0.057 g
	FLORAL REMAINS:						
	Monocot/Herbaceous Dicot	Stem		36			0.0067 g
	<i>Scirpus</i> -type	Seed	1	2			0.0005 g
	<i>Scirpus</i> -type	Seed			2	8	
	Rootlets					X	Few
NON-FLORAL REMAINS:							
	Snail shell - depressed					1	
AE-S-RC9	Volume Water-screened						3.0 ml
C2 2.72 mad	Water-screened Sample Weight						0.085 g
	FLORAL REMAINS:						
	Monocot	Stem		15			0.0013 g
	<i>Scirpus</i> -type	Seed	1				0.0002 g
AE-S-RC10	Volume Floated						50.0 ml
C2 2.66 mad	Light Fraction Weight						0.240 g
	FLORAL REMAINS:						
	Monocot	Stem		61			0.0094 g
	Poaceae C	Caryopsis	1				< 0.0001 g
	<i>Scirpus</i> -type	Seed	6	44			0.0079 g
	<i>Typha</i>	Seed	1				< 0.0001 g
	Unidentified	Seed		2			0.0001 g
	<i>Chara</i>	Oogonia			X	X	Few
	<i>Typha</i>	Seed			3		
	Rootlets					X	Moderate
	Sclerotia				2		
	CHARCOAL/WOOD:						
	Total charcoal $\geq$ 0.5 mm						0.0068 g
	Unidentifiable - small, vitrified	Charcoal		43			0.0068 g
NON-FLORAL REMAINS:							
	Ostracod					1	

TABLE 2 (Continued)

Sample No.	Identification	Part	Charred		Uncharred		Weights/ Comments
			W	F	W	F	
AE-S-RC8	Volume Floated						100.0 ml
Unit 16 2.65 mad	Light Fraction Weight						0.174 g
	FLORAL REMAINS:						
	Monocot	Stem		5			0.0006 g
	<i>Typha</i>	Seed	1				< 0.0001 g
	<i>Chara</i>	Oogonia				1	
	<i>Typha</i>	Seed			2		
	Roots					X	Few
	Rootlets					X	Few
	CHARCOAL/WOOD:						
	Total charcoal $\geq$ 0.25 mm						0.0031 g
	Unidentifiable - small, vitrified	Charcoal		X			0.0031 g
	NON-FLORAL REMAINS:						
	Ostracod					1	
	Snail shell					X	Few
AE-S-RC7	Volume Floated						125.0 ml
Unit 16 2.49 mad	Light Fraction Weight						0.343 g
	FLORAL REMAINS:						
	Monocot	Stem		11			0.0009 g
	<i>Scirpus</i> -type	Seed	1	16			0.0011 g
	Rootlets					X	Few
	CHARCOAL/WOOD:						
	Total charcoal $\geq$ 0.25 mm						0.0032 g
	Unidentifiable - small, vitrified	Charcoal		X			0.0032 g
	NON-FLORAL REMAINS:						
	Ostracod					1	
AE-S-RC19	Volume Water-screened						1.0 ml
Unit 16 2.3 mad	Water-screened Sample Weight						0.005 g
	FLORAL REMAINS:						
	Organic material - small			1			0.0002 g
AE-S-RC23	Sample Weight						0.484 g
Unit 16 -0.1 mad	FLORAL REMAINS:						
	Unidentified - lignified, compressed	Root				8	0.3338 g

TABLE 2 (Continued)

Sample No.	Identification	Part	Charred		Uncharred		Weights/Comments
			W	F	W	F	
AE-S-RC6	Volume Floated						125.0 ml
Unit 15	Light Fraction Weight						0.864 g
2.41 mad	FLORAL REMAINS:						
	Monocot - vitrified	Stem		35			0.0789 g
	Monocot/Herbaceous Dicot - vitrified	Stem/Root		6			0.0306 g
	<i>Scirpus</i> -type	Seed		6			0.0005 g
	<i>Scirpus</i> -type	Endosperm	36	27			0.0092 g
	Unidentified	Seed	1				< 0.0001 g
	Roots					X	Few
	Rootlets					X	Moderate
	NON-FLORAL REMAINS:						
	Sand					X	Few
AE-S-RC5	Volume Floated						100.0 ml
Unit 15	Light Fraction Weight						0.155 g
C3	FLORAL REMAINS:						
2.3 mad	<i>Scirpus</i> -type	Seed		36			0.0009 g
	Roots					X	Few
	Rootlets					X	Few
AE-S-RC4	Volume Floated						125.0 ml
Unit 15	Light Fraction Weight						0.088 g
C3	FLORAL REMAINS:						
2.26 mad	Monocot	Stem		13			0.0052 g
	<i>Scirpus</i> -type	Seed		10			0.0004 g
	<i>Chara</i>	Oogonia			X	X	Few
	Roots					X	Few
	Rootlets					X	Few
	CHARCOAL/WOOD:						
	Total charcoal $\geq$ 0.25 mm						0.0033 g
	Unidentified hardwood - small, vitrified	Charcoal		1			0.0002 g
	Unidentifiable - small, vitrified	Charcoal		35			0.0031 g

TABLE 2 (Continued)

Sample No.	Identification	Part	Charred		Uncharred		Weights/Comments
			W	F	W	F	
AE-S-RC2	Volume Floated						200 ml
Unit 15	Light Fraction Weight						0.044 g
2.19 mad	FLORAL REMAINS:						
	<i>Scirpus</i> -type	Seed		17			0.0004 g
	Parenchymous tissue			1			< 0.0001 g
	Unidentified	Seed	1	5			0.0002 g
	Rootlets					X	Few
	CHARCOAL/WOOD:						
	Total charcoal $\geq$ 0.25 mm						0.0001 g
	Unidentifiable - small, vitrified	Charcoal		14			0.0001 g
	NON-FLORAL REMAINS:						
	Bone < 2 mm					19	0.0094 g
Ostracod				X	X	Moderate	
Snail shell					X	Moderate	
Snail shell - depressed				X	X	Moderate	
Snail shell - oblong				X	X	Few	
AE-S-RC22	Volume Water-screened						1.0 ml
Unit 14	Water-screened Sample Weight						0.027 g
2.62 mad	FLORAL REMAINS:						
	Organic material - vitrified			4			0.0033 g
	NON-FLORAL REMAINS:						
	Ostracod					X	Few
	Snail shell					X	Few
AE-S-RC1	Volume Floated						550.0 ml
Unit 14	Light Fraction Weight						0.851 g
2.10 mad	FLORAL REMAINS:						
	Monocot - vitrified	Stem		21			0.0138 g
	<i>Scirpus</i> -type	Seed		1			< 0.0001 g
	<i>Chara</i>	Oogonia			X	X	Numerous
	Roots					X	Few
	Rootlets					X	Few
	NON-FLORAL REMAINS:						
	Ostracod				X	X	Numerous
	Snail shell					X	Numerous
	Snail shell - depressed				X	X	Numerous
Snail shell - oblong				X	X	Moderate	

TABLE 2 (Continued)

Sample No.	Identification	Part	Charred		Uncharred		Weights/Comments
			W	F	W	F	
AE-S-RC21	Volume Water-screened						1.0 ml
Unit 13 2.63 mad	Water-screened Sample Weight						0.015 g
	FLORAL REMAINS:						
	<i>Chara</i>	Oogonia			1		
	CHARCOAL/WOOD:						
	Total charcoal < 0.25 mm						< 0.0001 g
	Unidentifiable - small, vitrified	Charcoal		1			0.0001 g
	NON-FLORAL REMAINS:						
Ostracod				X	X	Few	
Sediment					X	Few	
AE-S-RC15	Volume Floated						450.0 ml
Unit 12A 2.5 mad	Light Fraction Weight						0.648 g
	FLORAL REMAINS:						
	cf. Monocot - vitrified	Stem/Root		10			0.0313 g
	<i>Chara</i>	Oogonia			X	X	Moderate
	Rootlets					X	Few
	NON-FLORAL REMAINS:						
	Bone					6	0.0107 g
Ostracod				X	X	Moderate	
Snail shell					X	Numerous	
Snail shell - depressed				X	X	Numerous	
Snail shell - oblong				X	X	Few	
AE-S-RC18	Sample Weight						0.779 g
Unit 12A 2.28 mad	FLORAL REMAINS:						
	Organic material - small, friable			X			0.0209 g
	Ash			X			0.0782 g
	NON-FLORAL REMAINS:						
	Sediment and ash				X	Few	

TABLE 2 (Continued)

Sample No.	Identification	Part	Charred		Uncharred		Weights/ Comments
			W	F	W	F	
AE-S-RC20	Volume Water-screened						3.0 ml
Unit 12	Water-screened Sample Weight						0.079 g
2.18 mad	FLORAL REMAINS:						
	Monocot - vitrified	cf. Rhizome/ Tuber		14			0.0519 g
	NON-FLORAL REMAINS:						
	Snail shell					X	Few
	Snail shell - depressed				X	X	Few
AE-S-RC24	Volume Water-screened						1.0 ml
Unit 11	Water-screened Sample Weight						0.083 g
2.18 mad	FLORAL REMAINS:						
	Sediment					X	Few

W = Whole  
 F = Fragment  
 X = Presence noted in sample  
 ml = milliliter  
 g = grams  
 mm = millimeters

TABLE 3  
 INDEX OF MACROFLORAL REMAINS RECOVERED FROM THE AIRPORT EAST TRENCH SITE,  
 TAYLORSVILLE FAULT, SALT LAKE CITY, UTAH

Scientific Name	Common Name
FLORAL REMAINS:	
<i>Chara</i>	Stonewort - a submerged algae found mostly in hard-water or alkaline lakes and slowly flowing streams with abundant calcium
Cyperaceae	Sedge family
<i>Scirpus</i> -type (includes <i>Amphiscirpus</i> , <i>Bolboshoenus</i> , <i>Isolepis</i> , <i>Shoenoplectus</i> , and <i>Scirpus</i> )	Bulrush
Monocot	A member of the Monocotyledonae class of Angiosperms, which include grasses, sedges, lilies, and palms
Monocot/Herbaceous dicot	A member of the Monocotyledonae class of Angiosperms, which include grasses, sedges, members of the agave family, lilies, and palms/ A non-woody member of the Dicotyledonae class of Angiosperms
Poaceae C	Members of the grass family with small caryopses, such as <i>Agrostis</i> (bentgrass), <i>Muhlenbergia</i> (muhly grass), <i>Poa</i> (bluegrass), etc.
<i>Portulaca</i>	Purslane
<i>Typha</i>	Cattail
Parenchymous tissue	Relatively undifferentiated tissue composed of many similar cells with thin primary walls—occurs in different plant organs in varying amounts, especially large fleshy organs such as roots and stems, but also fruits, seeds, cones, periderm (bark), leaves, needles, etc.
Sclerotia	Resting structures of mycorrhizae fungi

TABLE 3 (Continued)

Scientific Name	Common Name
CHARCOAL/WOOD:	
Unidentified hardwood - small	Wood from a broad-leaved flowering tree or shrub, fragments too small for further identification
Unidentified hardwood - vitrified	Wood from a broad-leaved flowering tree or shrub, exhibiting a shiny, glassy appearance due to fusion by heat
Unidentified hardwood - lignified	Wood from a broad-leaved flowering tree or shrub that was exposed for a long time to anaerobic conditions and degraded by microorganisms
Unidentifiable - small	Charcoal fragments too small for further identification
Unidentifiable - vitrified	Charcoal exhibiting a shiny, glassy appearance due to fusion by heat
Ostracod	Small, bivalved crustaceans widely distributed in fresh and saline water, normally under well oxygenated conditions in lakes, ponds, springs, and streams
Snail shell - depressed	Snail shell with a depressed (flat) shape where the width is much bigger than the height
Snail shell - oblong	Snail shell with an oblong shape where the height is much bigger than the width

TABLE 4  
SUMMARY OF CHARRED REMAINS FROM THE AIRPORT EAST TRENCH SITE, TAYLORSVILLE FAULT, SALT LAKE CITY, UTAH

Sample No.	Unit	Colluvial Wedge	Charred remains	Part	Size	Weight
AE-S-RC17		C1	Monocot** <i>Scirpus</i> -type Unidentified S Unidentified L	Stem Seed Seed Seed		0.0398 g 0.0003 g 0.0004 g 0.0013 g
AE-S-RC14	17b		cf. Cyperaceae**	Rhizome/ Tuber		0.6526 g
AE-S-RC11			Monocot, cf. Cyperaceae - vitrified**	Rhizome/ Tuber		0.201 g
AE-S-RC13			Monocot, cf. Cyperaceae - vitrified**	Rhizome/ Tuber		0.2531 g
AE-S-RC12	17		Monocot/Herbaceous Dicot** <i>Scirpus</i> -type	Stem Seed		0.0067 g 0.0005 g
AE-S-RC9		C2	Monocot** <i>Scirpus</i> -type	Stem Seed		0.0013 g 0.0002 g
AE-S-RC10			Monocot** Poaceae C <i>Scirpus</i> -type** <i>Typha</i> Unidentified Unidentifiable - small, vitrified**	Stem Caryopsis Seed Seed Seed Charcoal		0.0094 g < 0.0001 g 0.0079 g < 0.0001 g 0.0001 g 0.0068 g
AE-S-RC8	16		Monocot <i>Typha</i> Unidentifiable - small, vitrified**	Stem Seed Charcoal		0.0006 g < 0.0001 g 0.0031 g
AE-S-RC7			Monocot <i>Scirpus</i> -type Unidentifiable - small, vitrified**	Stem Seed Charcoal		0.0009 g 0.0011 g 0.0032 g

TABLE 4 (Continued)

Sample No.	Unit	Colluvial Wedge	Charred remains	Part	Size	Weight	
AE-S-RC19	16		Organic material - small			0.0002 g	
AE-S-RC23			Uncharred: Unidentified - lignified, compressed**	Root		0.3338 g	
AE-S-RC6	15		Monocot - vitrified**	Stem		0.0789 g	
			Monocot/Herbaceous Dicot - vitrified**	Stem/Root		0.0306 g	
			<i>Scirpus</i> -type	Seed		0.0005 g	
			<i>Scirpus</i> -type**	Endosperm		0.0092 g	
			Unidentified	Seed		< 0.0001 g	
AE-S-RC5		C3		<i>Scirpus</i> -type	Seed		0.0009 g
AE-S-RC4				Monocot**	Stem		0.0052 g
				<i>Scirpus</i> -type	Seed		0.0004 g
				Unidentified hardwood - small, vitrified	Charcoal		0.0002 g
			Unidentifiable - small, vitrified**	Charcoal	≥ 0.25 mm	0.0031 g	
AE-S-RC2			<i>Scirpus</i> -type	Seed		0.0004 g	
			Parenchymous tissue			< 0.0001 g	
			Unidentified	Seed	≥ 0.25 mm	0.0002 g	
			Unidentifiable - small, vitrified	Charcoal	≥ 0.25 mm	0.0001 g	
AE-S-RC22	14		Organic material - vitrified**			0.0033 g	
AE-S-RC1				Monocot - vitrified**	Stem		0.0138 g
			<i>Scirpus</i> -type	Seed		< 0.0001 g	
AE-S-RC21	13		Unidentifiable - small, vitrified	Charcoal	< 0.25 mm	< 0.0001 g	
AE-S-RC15	12A		cf. Monocot - vitrified**	Stem/Root		0.0313 g	
AE-S-RC18				Organic material - small, friable**			0.0209 g
			Ash**			0.0782 g	
AE-S-RC20	12		Monocot - vitrified**	cf. Rhizome/ Tuber		0.0519 g	

g = grams

mm = millimeters

\*\* = suitable for AMS radiocarbon age determination

## REFERENCES CITED

- Carlquist, Sherwin  
2001 *Comparative Wood Anatomy: Systematic, Ecological, and Evolutionary Aspects of Dicotyledon Wood*. 2nd ed. Springer Series in Wood Science. Springer, Berlin.
- Hather, Jon G.  
2000 *Archaeological Parenchyma*. Archetype Publications Ltd., London.
- Hoadley, Bruce  
1990 *Identifying Wood: Accurate Results with Simple Tools*. The Taunton Press, Inc., Newtown.
- Kricher, John C. and Gordon Morrison  
1988 *A Field Guide to Ecology of Eastern Forests*. The Peterson Field Guide Series. Houghton Mifflin Company, Boston and New York.
- Martin, Alexander C. and William D. Barkley  
1961 *Seed Identification Manual*. University of California, Berkeley.
- Matthews, Meredith H.  
1979 Soil Sample Analysis of 5MT2148: Dominguez Ruin, Dolores, Colorado. Appendix B. In *The Dominguez Ruin: A McElmo Phase Pueblo in Southwestern Colorado*, edited by A. D. Reed. Cultural Resource Series No. 7. Bureau of Land Management, Denver.
- Mauseth, James D.  
1988 Parenchyma. Chapter 3. In *Plant Anatomy*, pp. 43-51. The Benjamin/Cummings Publishing Company, Inc., Menlo Park, California.
- McWeeney, Lucinda  
1989 What Lies Lurking Below the Soil: Beyond the Archaeobotanical View of Flotation Samples. *North American Archaeologist* 10(3):227-230.
- Musil, Albina F.  
1963 *Identification of Crop and Weed Seeds*. Agricultural Handbook no. 219. U.S. Department of Agriculture, Washington, D.C.
- Schopmeyer, C. S.  
1974 *Seeds of Woody Plants in the United States*. Agricultural Handbook No. 450. United States Department of Agriculture, Washington, D.C.
- Schweingruber, Fritz H., Annett Borner and Ernst-Detlef Schulze  
2011 *Atlas of Stem Anatomy in Herbs, Shrubs and Trees* Vol I. Springer-Verlag, Berlin Heidelberg.  
  
2013 *Atlas of Stem Anatomy in Herbs, Shrubs and Trees* Vol. II. Springer-Verlag, Berlin Heidelberg.

Trappe, James M.

1962 Fungus Associates of Ectotrophic Mycorrhizae. In *The Botanical Review*. U.S. Department of Agriculture, Washington D.C.

## APPENDIX E

## SUMMARY OF RADIOCARBON DATING AT THE AIRPORT EAST SITE

Sample No. <sup>1</sup>	NOSAMS <sup>2</sup> Accession No.	Unit <sup>3</sup>	Sample Description <sup>4</sup>	Sample wt. (mg)	Lab Age <sup>5</sup> ( <sup>14</sup> C yr B.P.) (mean, ±1σ)		D <sup>13</sup> C (if measured)	Calibrated Age (cal yr B.P.) (95% range)		Calibrated Age <sup>6</sup> (cal yr B.P.) (mean, ±1σ)		Calibrated Age <sup>7</sup> (103 cal yr B.P.) (mean, ±2σ)	
AE-S-RC1	OS-124540	14	Charred Monocot Stems	13.8	2540	20	-23.74	2745	2505	2666	78	2.7	0.2
AE-S-RC2a	OS-124722	15	Charred Unidentified Seeds	0.6	2290	50	-25.44	2420	2150	2278	74	2.3	0.1
AE-S-RC4a	OS-124541	C3	Charred Monocot Stems	5.2	1850	15	-24.61	1860	1720	1780	33	1.8	0.1
AE-S-RC6a	OS-124586	15	Charred Monocot Stems	30.5	1170	15	-22.48	1175	1010	1105	44	1.1	0.1
AE-S-RC7a	OS-124542	16	Charred Monocot Stems/Seeds	2.0	885	15	-26.03	901	737	802	49	0.8	0.1
AE-S-RC8a	OS-124610	16	Unidentified Charcoal	3.1	890	15	-25.73	903	741	818	51	0.8	0.1
AE-S-RC10a	OS-124543	C2	Charred Monocot Stems	9.4	535	15	-23.16	621	520	543	22	0.5	0.04
AE-S-RC11	OS-124544	17	Charred Monocot Tuber	20.1	450	15	-26.94	522	497	509	6	0.5	0.01
AE-S-RC12a	OS-124545	17-burn horizon	Charred Monocot Stems	6.7	375	15	-24.18	500	331	435	57	0.4	0.1
AE-S-RC15	OS-124546	12	Charred Monocot Stem/Tuber	31.3	4390	25	-23.36	5039	4868	4947	53	4.9	0.1
AE-S-RC17a	OS-124448	C1	Charred Monocot Stems	14.3	175	15	-24.33	284	141	168	86	0.2	0.2
AE-S-RC17b	OS-124449	C1	Charred Scirpus-type Seeds	2.0	470	15	-26.10	528	503	515	6	0.5	0.01
AE-S-RC20	OS-124547	12	Charred Monocot Tuber	33.4	4370	20	-22.80	5029	4863	4924	38	4.9	0.1
AE-S-RC23	OS-124548	10	Unidentified Root Material	118.7	5500	25	-27.57	6394	6218	6299	28	6.3	0.1

<sup>1</sup> AE: Airport East; S: South Trench; RC: Radiocarbon.

<sup>2</sup> National Ocean Sciences Accelerator Mass Spectrometry Facility, Woods Hole Oceanographic Institution (Woods Hole, Massachusetts).

<sup>3</sup> Units correspond to plates 1 and 2.

<sup>4</sup> Charcoal separation and identification by PaleoResearch Institute (Golden, Colorado); see appendix D.

<sup>5</sup> Laboratory-reported radiocarbon age with one standard deviation (1σ) uncertainty. B.P. is before present (1950 CE).

<sup>6</sup> Mean calendar-calibrated age and 1σ uncertainty, determined using OxCal calibration software (v. 4.2; Bronk Ramsey, 1995, 2001) and the IntCal13 atmospheric data set (Reimer and others, 2013).

<sup>7</sup> Mean age rounded to nearest century, in thousands of years B.P.; 2σ uncertainty.

## APPENDIX F

## SUMMARY OF LUMINESCENCE DATING AT THE AIRPORT EAST SITE

Sample No.	Water Content <sup>1</sup> (%)	Saturation History <sup>2</sup> (%)	K (%) <sup>3</sup>	U (ppm) <sup>3</sup>	Th (ppm) <sup>3</sup>	Total Dose (Gy/ka) <sup>4</sup>	Equivalent Dose (Gy)	N <sup>5</sup>	Scatter <sup>6</sup>	Age (yrs) <sup>7</sup>
AE-S-L1	14 (38)	90	1.88 ± 0.03	3.57 ± 0.29	9.97 ± 0.46	2.72 ± 0.08	13.6 ± 0.15	30 (32)	39%	4980 ± 270
AE-S-L2	8 (55)	90	1.98 ± 0.03	4.87 ± 0.27	8.50 ± 0.37	2.65 ± 0.07	5.45 ± 0.32*	5 (6)	39%	1940 ± 200
AE-N-L3 (sand) <sup>8</sup>	10 (29)	50	2.30 ± 0.04	3.40 ± 0.36	9.40 ± 0.40	3.53 ± 0.11	45.3 ± 2.9	11 (12)	17%	12,830 ± 910
AE-N-L3 (silt) <sup>8</sup>	10 (29)	90	2.30 ± 0.04	3.40 ± 0.36	9.40 ± 0.40	3.18 ± 0.10	13.8 ± 0.71	30 (32)	25%	4340 ± 260

<sup>1</sup> Field moisture, with figures in parentheses indicating the complete sample saturation %. Ages calculated using complete sample saturation adjusted per saturation history % (e.g., 14 (38) = 38\*0.90 = 34).

<sup>2</sup> Estimated water saturation history (i.e., time below water table) of sampled material.

<sup>3</sup> Analyses obtained using high-resolution gamma spectrometry (high purity Ge detector).

<sup>4</sup> Includes cosmic doses and attenuation with depth calculated using the methods of Prescott and Hutton (1994). Cosmic doses were all at 0.25 Gy/ka.

<sup>5</sup> Number of replicated equivalent dose (DE) estimates used to calculate the equivalent dose. Figures in parentheses indicate total number of measurements included in calculating the represented DE and age using the central age model (CAM) or weighted mean dependent on scatter; analyzed via single aliquot regeneration on quartz grains.

<sup>6</sup> Defined as “over-dispersion” of the DE values. Obtained by the “R” factor program. Values >35% are considered to be poorly bleached sediments.

<sup>7</sup> Dose rate and age for fine-grained 250–90-micron-sized quartz. Exponential + linear fit used on equivalent dose, errors to one sigma.

<sup>8</sup> AE-N-L3 was collected as a single sample comprising liquefied sand that had been injected into silty host sediment; the sand and silt fractions were separated in the laboratory and dated individually.

\* Equivalent dose generated using the minimum age model (MAM).

## APPENDIX G

### OXCAL MODEL FOR THE TAYLORSVILLE FAULT AT THE AIRPORT EAST SITE

An OxCal model for the Taylorsville fault at the Airport East site was created using OxCal calibration and analysis software (version 4.3; Bronk Ramsey, 2009) and the IntCal13 radiocarbon calibration curve (Reimer and others, 2013). The models include *C\_Date* for luminescence ages, *R\_Date* for radiocarbon ages, and *Boundary* for undated events (paleoearthquakes). These components are arranged into ordered sequences based on the relative stratigraphic positions of the samples. The sequences may contain phases, or groups where the relative stratigraphic ordering information for the individual radiocarbon ages is unknown. The model is presented here in reverse stratigraphic order, following the order in which the ages and events are evaluated in OxCal.

**Model Input**

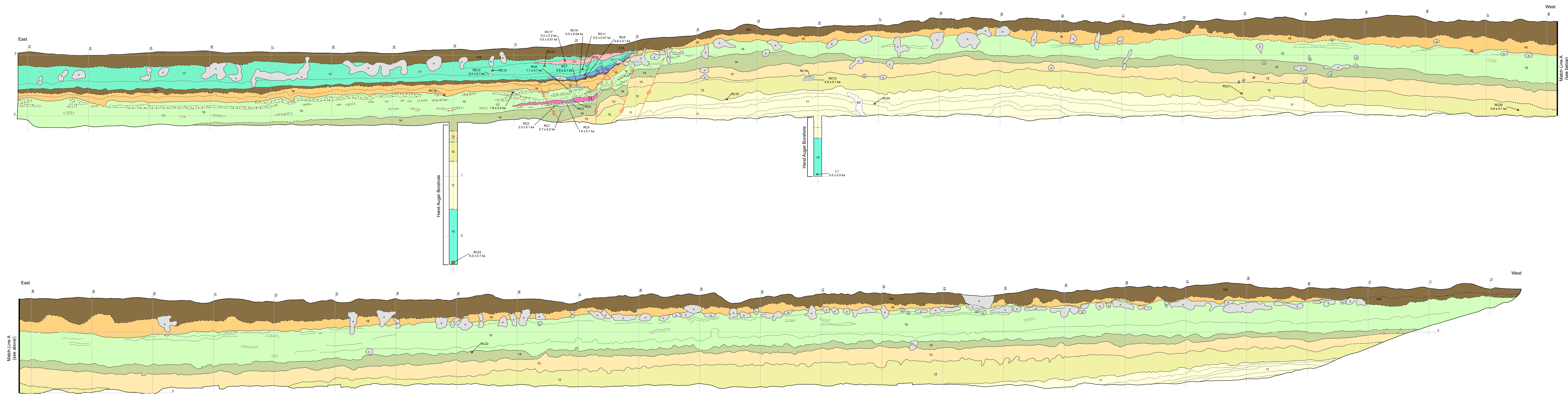
```

Plot()
{
Sequence("Airport East, full chronology")
{
Boundary("Start");
Phase("Unit 10, Alluvial Sand");
{
R_Date("AE-S-RC23, C14 5500+/-25", 5500,25);
C_Date("AE-S-L1, OSL 4980+/-270", -2964,270);
}
Boundary("LE1");
Phase("Unit 12, Alluvial Silt");
{
R_Date("AE-S-RC20, C14 4370+/-20", 4370,20);
R_Date("AE-S-RC15, C14 4390+/-25", 4390,25);
};
R_Date("AE-S-RC1, C14 2540+/-20", 2540,20);
R_Date("AE-S-RC2a, C14 2290+/-50", 2290,50);
Boundary("AE3");
R_Date("AE-S-RC4a, C14 1850+/-15", 1850,15);
Phase("Unit 15, Marsh Deposits");
{
C_Date("AE-S-L2, OSL 1940+/-200", 76,200);
R_Date("AE-S-6a, C14 1170+/-15", 1170,15);
};
R_Date("AE-S-7a, C14 885+/-15", 885,15);
R_Date("AE-S-8a, C14 890+/-15", 890,15);
Boundary("AE2");
R_Date("AE-S-RC10a, C14 535+/-15", 535,15);
R_Date("AE-S-RC11, C14 450+/-15", 450,15);
Boundary("AE1");
R_Date("AE-S-17a, C14 175+/-15", 175,15);
Boundary("Begin Historical Record", 1847 AD);
};
};
};

```

### Model Output

Airport East Full Chronology	Unmodelled (BP)		Modelled (BP)		Agreement
	mean	sigma	mean	sigma	
Boundary Start			6798	438	
Phase Unit 10, Alluvial Sand					
R_Date AE-S-RC23, C14 5500 ± 25	6299	28	6298	27	99.7
C_Date AE-S-L1, OSL 4980 ± 270	4915	270	5271	177	66.5
<b>Boundary LE1</b>			<b>5108</b>	<b>145</b>	
Phase Unit 12, Alluvial Silt					
R_Date AE-S-RC20, C14 4370 ± 20	4924	38	4942	34	98
R_Date AE-S-RC15, C14 4390 ± 25	4947	53	4905	27	107.2
R_Date AE-S-RC1, C14 2540 ± 20	2666	78	2666	78	98.9
R_Date AE-S-RC2a, C14 2290 ± 50	2278	74	2284	73	101
<b>Boundary AE3</b>			<b>1984</b>	<b>147</b>	
R_Date AE-S-RC4a, C14 1850 ± 15	1780	33	1783	33	99.4
Phase Unit 15, Marsh Deposits					
C_Date AE-S-L2, OSL 1940 ± 200	1875	200	1652	107	79.5
R_Date AE-S-6a, C14 1170 ± 15	1105	44	1105	43	97.9
R_Date AE-S-7a, C14 885 ± 15	802	49	838	50	89.1
R_Date AE-S-8a, C14 890 ± 15	818	51	788	39	95
<b>Boundary AE2</b>			<b>633</b>	<b>78</b>	
R_Date AE-S-RC10a, C14 535 ± 15	543	22	539	16	100.4
R_Date AE-S-RC11, C14 450 ± 15	509	6	509	6	94.7
<b>Boundary AE1</b>			<b>393</b>	<b>99</b>	
R_Date AE-S-17a, C14 175 ± 15	168	86	201	41	98.3
Boundary Begin historical record, 1847	104	0	104	0	100



**Scarp-Derived Colluvium and Related Deposits**

- C1** Units C1-C3: Scarp-derived colluvium and associated marsh sediments in wedge-shaped deposits that formed on the hanging wall in response to surface-faulting earthquakes.
- C2**
- C3**

**Soil A Horizon**

- 16A** Soil A Horizon, named after unit formed on. Example - soil formed on unit 16 is "16A."

**Fluvial Overbank, Marsh, and Lacustrine Deposits**

- 17** Unit 17: Dark-gray silty clay capped by modern soil. Lower part contains 2-cm-thick burn layer.
- 16** Unit 16: Gray clay capped by a weakly developed soil A horizon.
- 15** Unit 15: Black silty clay containing yellowish-brown silt and fine sand interbeds. Very organic rich.
- 14**
- 13** Units 12, 13, and 14: Dark clayey silt units deposited on paleo-Jordan River floodplain. Abundant gastropod and ostracode shell fragments.
- 12**

**Wetland and Fluvial Channel Deposits**

- 11** Unit 11: Silty clay containing two thin, dark, organic-rich layers. Unit deformed by broad folding. Angular unconformity at top contact with unit 12.
- 10** Unit 10: Fine, mica-rich quartz sand exposed in auger holes in trench floor. Fines upward.

**Explanation**

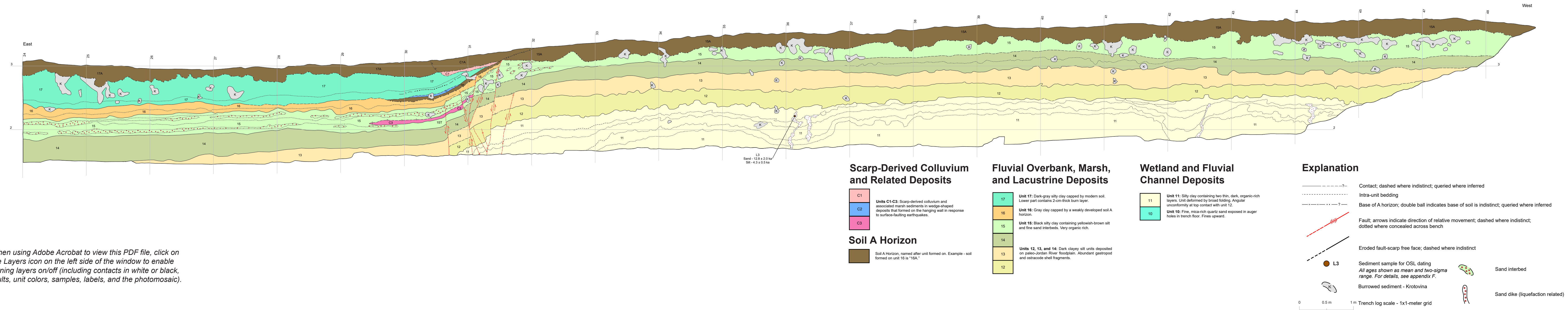
- Contact; dashed where indistinct; queried where inferred
- - - - - Intra-unit bedding
- · - · - · - Base of A horizon; double ball indicates base of soil is indistinct; queried where inferred
- - - - - Approximate groundwater elevation in boreholes at time of trenching
- Fault; arrows indicate direction of relative movement; dashed where indistinct
- Eroded fault-scarp free face; dashed where indistinct
- ▲ RC11 Macro charcoal sample for C-14 dating
- RC10 Bulk-soil sediment sample for C-14 dating
- RC23 Wood sample for C-14 dating
- L1 Sediment sample for OSL dating  
All ages shown as mean and two-sigma range.  
For details, see appendix E (C-14) and appendix F (OSL).
- Sand interbed
- Sand dike (liquefaction related)
- Burrowed sediment - Krotovina



When using Adobe Acrobat to view this PDF file, click on the Layers icon on the left side of the window to enable turning layers on/off (including contacts in white or black, faults, unit colors, samples, labels, and the photomosaic).

Although this product represents the work of professional scientists, the Utah Department of Natural Resources, Utah Geological Survey, makes no warranty, expressed or implied, regarding its suitability for a particular use. The Utah Department of Natural Resources, Utah Geological Survey, shall not be liable under any circumstances for any direct, indirect, special, incidental, or consequential damages with respect to claims by users of this product.

**STRATIGRAPHIC AND STRUCTURAL RELATIONS IN THE SOUTH TRENCH AT THE AIRPORT EAST TRENCH SITE**



When using Adobe Acrobat to view this PDF file, click on the Layers icon on the left side of the window to enable turning layers on/off (including contacts in white or black, faults, unit colors, samples, labels, and the photomosaic).

Although this product represents the work of professional scientists, the Utah Department of Natural Resources, Utah Geological Survey, makes no warranty, expressed or implied, regarding its suitability for a particular use. The Utah Department of Natural Resources, Utah Geological Survey, shall not be liable under any circumstances for any direct, indirect, special, incidental, or consequential damages with respect to claims by users of this product.

## STRATIGRAPHIC AND STRUCTURAL RELATIONS IN THE NORTH TRENCH AT THE AIRPORT EAST TRENCH SITE